The University Of Sheffield.

Optimisation of a flexible polyurethane foam formulation for use as soilless growing media

Harry Charles Wright

A thesis submitted in partial fulfilment of the requirements for the degree of Doctor of Philosophy

The University of Sheffield
Faculty of Chemistry
Department/School of Science

September 2020

Abstract

Increasing pressure for controlled environmental agriculture (CEA) using hydroponic techniques to reduce their environmental impact as well as the rapid growth of this sector has led to research into more environmentally friendly growing media. Flexible polyurethane foams (fPUF) are a possible alternative to current growing media, however there is little literature reporting the development and optimisation of fPUF for horticultural applications. The aim of this thesis is to use design of experiment (DoE) techniques to understand the influence of the fPUF formulation on select physical and chemical foam properties and optimise these properties for plant growth using hydroponic techniques.

Fast, easy to measure techniques were developed or adapted from literature for screening select foam physical properties (density, cell size, water holding capacity, water drop penetration and airflow) and chemical properties (cation exchange capacity) to allow for rapid formulation development. Complete conversion of isocyanate was ensured by using adiabatic temperature rise techniques during the foam reaction.

A combination of polyols with a high ethylene oxide polyol composition (58.2 %) composed of a 75:25 ratio of Voranol 1447: Voranol 3322 was selected to make hydrophilic foams. 30 part per hundred polyol (PPHP) of sodium bentonite was used to increase the water holding capacity of the foam. Carefully selected reactive catalysts, dimethylethanolamine (DMEA) and Specflex Activ 2306, a catalytically active polyol reduced the likelihood of reagents leaching out of the foam. Models for fPUF physical properties and reaction responses were developed and verified using DoE techniques. These models used the catalyst and surfactant loadings as factors influencing the responses. Spring onions (*Allium cepa*) were grown in a set of foams with varying physical properties and growth and nutrition responses were modelled. Cell size and water holding capacity were the most important factors in predicting plant growth and nutrient uptake, with a small cell size and high water holding capacity preferred. An optimised set of physical properties was predicted using these models

and an optimum foam formulation was selected. This foam was made its physical properties matched the predicted optimum properties.

Declaration

The work described in the present thesis was undertaken at the University of Sheffield between October 2016 and September 2020, under the supervision of Professor Anthony J. Ryan and Professor Duncan D. Cameron. Unless otherwise stated, it is the work of the author and has not been submitted in whole or in any part for any other degree at this or any other Institute. Some research reported in this manuscript has been published in a peer reviewed articles referenced below.

Publications of work presented in this thesis

Wright, H.C., Zhu, J., Cameron, D.D. and Ryan A.J. (in press). Flexible polyurethane foam with sodium bentonite: Improving the properties of foams for use as a synthetic growing media. *Acta Hortic*, 2020.

Al Meselmani, M.A., Wright, H.C., Cameron, D.D. and Ryan A.J. How scientists and refugees brought green to the Desert Garden. *Nat Rev Earth Environ* **1,** 439 (2020).

Harry C Wright
Department of Chemistry
University of Sheffield
September 2020

Acknowledgments

First of all I would like to thank my co-supervisors Prof Tony Ryan and Prof Duncan Cameron for the opportunity to carry out this PhD in your respective research groups. Your endless knowledge and enthusiasm for this work made every difficultly encountered easy. Your care for your students' wellbeing goes beyond what could ever be expected of you and I am deeply grateful to you both.

I would like to thank the Grantham Centre for Sustainable Futures for providing the funding for this project, as well as all the invaluable training received as part of the PhD. I would specifically like to thank Deborah Beck and Eva Vichova for all the guidance and help along the way.

Without all the valuable training on equipment, teaching of techniques and use of shared equipment this project would not have been possible. Thank you to Andy Pryke and the Farapack group all the shared equipment and help along the way. Thanks to Rob Hanson for training on the spectrophotometer, DSC and TGA. Thanks to all those in the SMALL lab for patiently teaching me the SAXS basics, even though it never made it into this thesis. Thanks Garry Taylor for the help with the design and building of the airflow meter. Thanks to Chris Holland for use of his universal tester and to Andreas Koeppel for making a custom mount and training on the equipment. Thanks to Maggi Killion and Dale Bavastock up at AWEC for training in the controlled environments. A special thank you to Irene Johnson for her patience in teaching me several plant analysis techniques.

An often overlooked work life balance is required to complete a PhD, and without all the friends made along the way I'd never have had that balance. To the e floor office group, the early morning breakfast club and Friday afternoon drinks were always welcome. The late afternoon cycles were a fantastic way to keep my mind off the PhD. To all my fellow Grantham Scholars, thank you for every distraction along the way, whether it was a beer and cider festival, an evening playing VR Playstation or an evening of DnD it was greatly appreciated.

I owe a great deal to my family, your ongoing support and love kept me going. I am perpetually grateful to you.

Finally, to Sonette, the catalyst for all that is good in my life, without you nothing is possible.

Glossary of Symbols and Acronyms

Acronym	Description
AEC	anion exchange capacity
ANOVA	analysis of variance
AMF	arbuscular mycorrhizal fungi
ATR	adiabatic temperature rise
AUC	area under curve
AWEC	Arthur Willis Environmental Centre
CEA	controlled environment agriculture
CEC	cation exchange capacity
CFC	chlorofluorocarbons
CFD	compression force deflection
DMF	dimethylformamide
DMEA	dimethyl ethanol amine
DoE	design of experiments
EO	ethylene oxide content
ExG	excess green
ExR	excess red
fPUF	flexible polyurethane foam
HDI	hexamethyl diisocyanate
HS	polyurethane hard segment
ICP-OES	inductively coupled plasma - optical emission spectrometry
IMDA	imidazole
IPDI	isophorone diisocyanate
KOH	potassium hydroxide
LDH	layered double hydroxide
LECA	lightweight expanded clay aggregate
MDI	methylene diphenyl diisocyanate
-NCO	isocyanate group
NMR	nuclear magnetic resonance spectroscopy
-OH	hydroxyl group
PEG	polyethylene glycol

PET	polyethylene terephthalate
PGPB	plant growth promoting bacteria
PMDA	pyromellitic dianhydride
PO	propylene oxide content
PPHP	parts per hundred polyol
PU	polyurethane
PUF	polyurethane foam
PVC	polyvinyl chloride
RGB	red, green, blue colour bands
RPi	Raspberry Pi
SEM	scanning electron microscopy
SPAD	soil plant analysis development
SS	polyurethane soft segment
TDI	toluene diisocyanate
TEDA	triethylenediamine
TOF	time of flight
UV	ultraviolet
VOC	volatile organic compound
WHC	water holding capacity

Symbol	**Description**
A	cross sectional area
A_{663}	spectrophotometer absorption at 663 nm
β	fitting constant
CC_{corr}	corrected colour channel
CFD_{50}	compression force deflection
C_0	initial $[Cu(Trien)]^{2+}$ concentration
C_a	chlorophyll A
C_b	chlorophyll B
C_s	$[Cu(Trien)]^{2+}$ concentration
C_t	total chlorophyll
C_{x+c}	total carotenoids
c_p	heat capacity

d	cell diameter
E_n	equivalent weight
ε	error
F	force
ΔH	heat of formation
h	plant height
h_f	final foam height
h_{max}	maximum foam height
k_1	rate of formation
L	component loading
M	HCl molarity
M_n	molecular mass
m	mass
m_d	plant shoot dry mass
m_{dry}	dry foam mass
m_f	final foam mass
m_{max}	initial reactant mass
m_{raw}	raw mass reading
m_s	mass sample
m_t	mass of reacted foam
m_{wet}	mass of wet foam
N	nitrogen content
N_{closed}	number of closed cells
N_{open}	number of open cells
N_{part}	number of partially open cells
N_{pin}	number of cells with pin holes
P	phosphorus content
P_{eff}	effective number of open cells
Φ	air filled porosity
P_{NCO}	isocyanate conversion
ρ	density
R, G, B	red, green and blue colour bands
r, g, b	normalised RGB colour bands

r	stoichiometric ratio isocyanate
r_1	rate of reaction
T_{ad}	adiabatic temperature
T_{amb}	ambient temperature
T_{exp}	reaction temperature
T_{max}	maximum reaction temperature
$T_{maxcalc}$	maximum theoretic temperature
t_{hmax}	time of maximum foam height
t_{Tmax}	time of maximum reaction temperature
U	global heat transfer coefficient
U'	overall heat transfer coefficient
V	volume

Contents

Chapter 1:
Introduction

1.1. Project Background

The global food production system is currently under pressure from stressors related to both non climate change (urbanisation, population, income growth) and climate change[1] with the increase in global population, expected to reach 9.7 billion by 2050[2], the primary stressor for the required increase in food production. These stressors are leading to a further intensification of the conventional agriculture system. This intensification of agricultural practices is adding to the food production problem, with highly intense agricultural practices causing soil degradation (loss of organic matter, erosion, contamination, loss of biodiversity) at an unsustainable rate[3]. Controlled environmental agriculture (CEA) and the use of soilless growing techniques, such as hydroponics can add significant contributions to supplying fresh fruits and vegetables, especially in urban areas, using artificial lighting and optimised growing conditions in urban greenhouses[4].

A controlled environment, in agriculture, is at minimum an environment which protects crops from the elements (wind, rain snow etc), although is more likely to have some level of temperature control. Many modern controlled environments offer more complete control, including light, atmospheric composition, as well as the rooting medium[5]. Professor Dickson Despommier has been paramount in raising public interest into CEA and his book on the subject lists several benefits of this kind of intensive agriculture. These advantages include maximising yield in small spaces, year round growing, reduction in water use, reduction in fertiliser use, reduction in pesticide use, increased availability of locally produced healthy food and the use of non-arable regions for agriculture[6]. The two main drawbacks of CEA is the high startup cost, requiring careful economic feasibility studies before setting up greenhouses[7] and the high energy costs for artificial lighting required for year round production[8]. Hydroponics is the primary growing technique used in CEA greenhouses, as hydroponics offer a higher level of control and automation of water, nutrients and gasses to the root zone of the crops[4].

Hydroponics is a growing technology where plants are grown in nutrient solutions (water with fertiliser) in the absence of conventional soil. This can be done with or

without the use of a growing media to provide mechanical support for the plants. Hydroponics can further be sub categorised into open and closed hydroponic systems. Open systems do not reuse nutrient solution and closed systems recover excess nutrient solution and reuse it in the system[9]. There are several different methods for supplying nutrients to plants in hydroponics including but not limited to drip irrigation, flood and drain systems, deep water systems (where plant roots are submerged in an aerated nutrient solution) and nutrient film technique (where a thin layer of nutrient continuously flows whilst in contact with some of the roots). For high value crops such as tomatoes, cucumbers and peppers open or closed hydroponics systems with dripper feeds and plants supported by a growing media, normally rockwool, are the norm.

Rockwool is a chemically inert growing media, made from volcanic rock that is melted in a furnace at high temperature and spun into a fibre. It has incredibly high porosity (96%) and is well suited to hydroponic growth techniques[10]. However there are some environmental worries about rockwool as a growing media, due to the high amount of CO_2 produced during its production (167 kg of CO_2 into the environment per cubic meter produced)[11] as well as the end of life disposal of rockwool, which has historically been disposed of at landfill. More recently countries like the Netherlands and the United Kingdom have taken to recycling a large portion of agricultural rockwool[12]. These environmental drawbacks of current media as well as the continued expansion of CEA (with a report projecting a 9.2 % increase in value in USA between 2020-2025[13]) means that there is a market gap for novel innovative growing media.

This thesis looks at the setting out a framework for developing a novel flexible polyurethane based soilless growing media for the growth of high value crops in hydroponic systems. The remainder of this chapter focusses initially on soilless growing media and their properties and is followed by an introduction to polyurethanes as well as the chemistry and components required for making a flexible polyurethane foam.

1.2. An Introduction to Soilless Growing Media

The horticultural industry relies heavily on growing media for raising small plants and for the growth of ornamentals. Growing media is defined as any substrate which allows a plants roots to grow, whilst extracting water and nutrients[14]. These growing media are made up of several components and are generally a mixture of natural soil materials (loam, clay, sand, peat), compost and other mineral or organic materials (perlite, wood, moss).

In soilless growing (hydroponics), a soilless growing media is generally used. Soilless growing media are growing media as defined above, however without the natural soil material. These natural soil materials are omitted in hydroponic media as they are highly variable and can introduce a range of unknown bacteria and fungi into a system. For the remainder of this discussion soilless growing media and substrate are used interchangeably.

1.2.1. Properties of Soilless Growing Media

Soilless growing media properties can be broken down into three important categories, physical, chemical and biological properties.

1.2.1.1. Physical Properties

Any growing substrate is formed of three phases, which all have important roles to play. The solid phase, ensuring that the growing media has sufficient mechanical strength to anchor the plant and hold it upright. The liquid phase, which ensures that the plant gets water and nutrients that are dissolved in the water solution and the gas phase which allows for oxygen and carbon dioxide gas to transfer between the surrounding air and plants roots[15].

Of these three phases the liquid and gas phases are the most complex to recreate. The difficulty lies in the fact that there are no globally accepted standards for the physical characteristics of soilless growing media. There are however suggested

ranges given for some of the important physical properties of growing media. These ranges are given in Table 1.1[16].

These physical properties include the porosity of the media, which is defined as the volume of a media not occupied by solid particles. This can be calculated by taking the ratio of the bulk density of the media, and dividing it by the actual density of the solid particles. This open area within a media can either be filled with air or with water. The fraction filled with air is called the air space and the fraction filled with water is called the water-filled porosity. The water holding capacity (WHC) is defined as the maximum amount of water that a growing media can hold.

Table 1.1: Suggested ranges for select physical properties of growing media[16].

Physical Property	Suggested Range
Total porosity	50 – 85 %
Air space	10 – 30 %
Water Holding Capacity	450 – 600 $g_{H2O}.l^{-1}_{substrate}$
Bulk density	0.19 – 0.7 $kg.l^{-1}_{substrate}$

For many agricultural practices, this is where the design of substrates stops, they ensure that the physical properties are suitable and that the media is chemically inert, however the media can be improved by including the chemical and biochemical properties in the design.

1.2.1.2. Chemical Properties

The first and most important chemical characteristic of a growing media is its pH. Nutrients become available to plants at different pH's and many plants can only grow in media that has a certain pH. A pH between 6 and 7 is often seen as optimum for nutrient uptake[17]. pH can have an effect on many other properties of a growing media, such as microbial activity and well as changing the ion exchange capacity of certain clays[18].

In addition to pH the ability for a media to exchange ions can also be important in soilless growing media. This exchange can be expanded to the cation exchange

capacity (CEC) and the anion exchange capacity (AEC). This exchange of ions is important as they can affect the ionic composition of the nutrient solution. The cation exchange capacity of several common organic and inorganic growing media is shown in Table 1.2[19]. From Table 1.2 it is clear that many of the inorganic rock based media (Perlite, rockwool, tuff) have much lower CEC when compared to the organic natural media (coir, peat, bark).

Table 1.2: The cation exchange capacity (CEC) for select soilless growing media[19]*.*

Media	CEC /cmol.kg^{-1}
Perlite	25 - 35
Rockwool	34
Tuff	10 - 60
Zeolite	200 - 400
Coconut Coir	39 - 60
Peat	90 - 140
Pine Bark	98
Compost	160 - 180

CEC of growing media can also be changed by the addition of additives. The addition of negatively charged clays, such as bentonite and montmorillonite, to soilless growing media has shown increased CEC, water retention and has led to more efficient use of nutrients[20].

Anion exchange capacity of growing media is generally low as there are few positively charged surfaces or colloids in growing media. There is little literature on AEC of growing media and its effect on plant growth, however there has been research into the addition of layered double hydroxides, a positively charged clay with high AEC value to soil. These clays acted as a slow release nitrogen fertiliser, reducing the amount of nitrate that leached from the soil[21]. Worries about pollution in soilless horticulture due to excess fertilisation has led to efforts to control the amount of nutrient available in the root zone and to the development of substrates that contribute nutrients to the crop. One way of doing this is by pre-charging the substrate with nutrients that will then act as a slow release fertiliser during the growing cycle. For this to be achievable the substrate would need to have a high CEC and AEC[19].

Designing a growing media with high anion exchange will may have important benefits, making more nutrients available to the plants as well as increasing the efficiency of fertilisers which may otherwise leach out of the growing media, this would be more important in open hydroponic systems where excess nutrient solution is not captured.

1.2.1.3. Biological Properties

One of the factors that led to the development of soilless growing techniques was the prevention of soil-pathogenic microorganisms[22]. Although this has been relatively successful, microbial contamination can still occur from a variety of sources (water, plant material, growing media) and losses from pathogen contamination in soilless cultivation can be greater than soil grown crops. Furthermore once introduced these pathogens are generally favoured for several reasons. There is an abundant amount of genetically uniform plants, a controlled environment with ideal temperature and humidity conditions and mechanisms of uniform dispersion in the system via the nutrient solution[23]. Historically these contaminations have been managed by methods such as ultra violet radiation which acts as an effective disruptor for biological molecules[24]. The disadvantage of such treatment methods is that they not only eliminate pathogenic microbes, but also beneficial microorganisms. The use of preventative measures is a second method for managing contamination. This can be accomplished by stimulating the “suppressiveness” of the system or by the application of biological control agents[25]. A suppressive system is a system in which a certain disease is suppressed due to the presence of microorganisms in the system that are antagonistic to the pathogen, this definition is adapted from the definition of a suppressive soil[26]. Vallance *et al*[22] provides a good review of pathogenic microorganisms as well as biological control agents used in soilless systems.

In addition to disease resistance, the addition of beneficial microorganisms can have several benefits in soilless systems, discussed below. Two classes of microorganisms, which are commonly added to soilless systems, are plant growth promoting bacteria (PGPB) as well as arbuscular mycorrhizal fungi (AMF).

PGPB are a group of bacteria which partake in key ecosystem processes in the rhizosphere, the narrow region of soil/media around the plants root where chemistry and biology is influenced by the plants growth, through a variety of processes. Many of these processes have been studied and include nitrogen fixation, nutrient extraction, competition with pathogens, production of hormones as well as promotion of plant growth[27]. Gravel *et al*[28] tested five bacterial strains and three fungi to determine whether they were plant growth promoting for tomatoes in hydroponic systems, they found that *P. putida* and *T. atroviride* were growth promoting in both rockwool and an organic growing media. A further study of PGPB in hydroponically grown tomatoes showed that *Bacillus .spp* increased yield in both a Spring and Autumn harvest[29].

AMF is a type of mycorrhiza in which the fungus penetrates the outermost layer of the root of a plant, and this is the most common type of mycorrhiza[30]. This allows for a mutually beneficial symbiotic relationship between the plant and the fungus, whereby the fungus helps the plant absorb mineral nutrients and in return the plant supplies the fungus with sugars. AMF have successfully been colonized in several soilless (hydroponic) growing systems and have shown beneficial growth for several systems and vegetables. AMF have improved the yield of basil[31], increased the shoot mass of pepper plants[32] and have increased the yield in tomato plants in solution recycling and open systems[33]. Another study however found no improvements to fruit yield in tomatoes in a soilless setup[34]. This study suggested that the growing media may not have been appropriate for AMF colonisation or that high ambient temperatures may have influenced the effectiveness of the AMF.

The above studies highlight the importance of the biological health of a soilless growing media, and the importance of considering these characteristics when designing a soilless growing media.

1.2.2. Popular Soilless Growing Media

There are currently a wide range of substrates which are available for hydroponic farmers, and these can broadly be separated into organic and inorganic substrates.

1.2.2.1. Organic Substrates

Organic substrates are normally used when they are available locally, and are often considered the waste of another industry. The best example of this is coco coir, which is the fibrous husk of the coconut and due to the size of the coconut industry, is one of the more popular growing media.

Other organic substrates include tree bark, rice hulls, peat moss, sawdust or a range of other suitable products available locally. Some of the more exotic organic substrates which have been reported for use as growing media include almond shells, animal manure and brewery waste[35].

One of the major advantages of organic substrates is their local availability, and the use of waste streams, meaning that the substrates are environmentally friendly, however this is not universal. The overexploitation of peat, an organic growing media highlights the use of an unsustainable growing media[36]. A further advantage of organic growing media is that due to the organic and compostable nature of these media they are generally compostable and do not cause any disposal issues further downstream. Coco coir has a further benefit, unlike many of the organic and inorganic substrates; it can be compressed to one fifth of its size, reducing transport costs.

The disadvantages of organic substrates include the fact that they degrade over time, meaning that the substrates properties change, and this can affect plant growth[16]. A further drawback, is that many organic substrates are inconsistent as they are not specifically made for use as a growing media[11]. Some organic media may need to be prewashed before use as they contain salts. Without the rinsing of this media, young plants may be burnt (physical damage caused by over fertilisation) by the high salt concentration.

1.2.2.2. Inorganic Substrates

Inorganic substrates are very popular for use in hydroponic growing techniques. The majority of these are rock based, although there are some substrates which are synthetically synthesised.

The most popular of the inorganic substrates is rockwool, made by melting basaltic rocks at high temperature and then extruding them into threads, similar to the process used to make fibre glass. Other popular substrates include perlite (expanded volcanic rock), vermiculite (expanded by converting trapped water into steam) and LECA (lightweight expanded clay aggregate). In some simple hydroponic systems, sand or gravel can be used although these media need to be thoroughly washed and must not react with the nutrient solution.

These inorganic substrates are particularly popular in hydroponics as the majority of these materials are chemically inert and do not interact with the nutrient solution[37]. Whilst this is a benefit when nutrients are circulated in a closed system, any open system would value some chemical interaction, to stop nutrients from leaching through the medium. Furthermore, hydroponic systems are often run with excess nutrient solutions, a reduction in fertiliser use may be possible if nutrients are buffered in the media and available to the plant.

Rockwool and perlite are often reused for 2-3 growing seasons, as their physical properties do not vary greatly with time; after which they need to be disposed of. Some rockwool is recycled, as is often the case in the Netherlands and the United Kingdom, however a large portion of agricultural rockwool ends its life in landfill[38]. Due to the low bulk density of these substrates, they take up a large volume of landfill space and do not decompose with time. A further disadvantage of these inorganic substrates is that they require temperatures of up to 2000 °C, to be melted/ expanded in their production, which is highly energy intensive.

1.2.3. Polyurethanes as soilless growing media

Polyurethane foams have long been thought to be suitable as growing media, with patents being issued as far back as 1976[39]. Their suitability stems from the diversity of the properties of polyurethane foams, which can be manipulated by varying the formulation as well as reaction conditions. These foams can be made to suit the horticultural industry by ensuring open cell foams, with high porosity and high water holding capacity.

Many of the early foams were not specifically made for use as horticultural media and due to this some problems arose, often due to low water holding capacity and some phytotoxic effects have been observed on the plants (it was hypothesised that free amine catalyst in the foam was causing tissue damage to the plants)[40]. Research has shown that PUF can be reused for several growing years, with foam being steam cleaned between uses, and foams of up to 10 years old have successfully been used to grow crops. These horticultural foams (Aggrofoam) were made using offcuts from the polyurethane industry, ground to 1.5 cm pieces and rebonded together. These substrates were further recycled at end of life[41]. Virgin Aggrofoam, Aggrofoam that had been used for one season as well as second foam (Richgrow) were compared against rockwool for growing cucumbers hydroponically. The virgin Aggrofoam performed as well as rockwool and the used Aggrofoam outperformed rockwool and new Aggrofoam in terms of cucumber yield. This was attributed to increased water holding due the addition of organic plant roots in the media from the first growing season. In a second test the Richgrow foam performed as well as rockwool, however unused Aggrofoam had lower yield than rockwool or Richgrow. This was attributed to hot weather which caused this foam to dry out faster than the other media[42].

A recyclable urethane based plant growth substrate (UBS), developed specifically for hydroponic culture was tested against rockwool for growing cucumbers under two watering treatments. The seedlings in UBS lagged behind the rockwool seedlings by one leaf, however this affect was only seen early on and total yield was the same for the rockwool and the UBS substrate under both watering regimes[43]. This UBS substrate was subsequently improved on into a system called SRI Enviro-Grow System (EGS). This substrate consisted of a recyclable urethane material, with two microporous membrane tubes running along the top of the substrate for continuous nutrient delivery. This trial showed no differences in yield in peppers between the rockwool and urethane based substrates[44].

Although there has been little work done on life cycle analysis of fPUF for use as a synthetic growing media, EUROPUR has calculated the greenhouse gas equivalent cost of MDI based fPUF as 2.95 kg CO_2 per kg of foam. This equates to 132 kg of CO_2 produced per cubic meter of foam at a density of 45 kg.m^{-3} and is a 20 %

improvement over rockwool which releases 167 kg of CO_2 into the environment per cubic meter produced[38,45]. A further advantage of PUF as a substrate is that it is easier to recycle or dispose of when compared to non-degradable inorganic substrates.

Polyurethanes can be disposed of using three types of technology. Landfill, incineration and recycling. Landfill is a waste of space and materials for disposal of polyurethane foams and is not considered a viable end of life option due to the low density and lack of biodegradability of fPUF. Incineration is more preferable, where burning waste fPUF can recover heat and reduce waste volume by 99%. However if incompletely combusted polyurethanes can produce toxic gasses and incineration should only be done when there are no viable recycling options. The final and most preferable disposal method is recycling. This can be done physically (by grinding old fPUF and reintroducing it into a virgin fPUF) or chemically (by breaking the fPUF back into its raw ingredients). Yang *et al* provides a review on disposal techniques of polyurethanes[46].

You would expect that the above-mentioned research would have led to several commercial polyurethane foam substrates available for growers, however few have taken hold with rockwool dominating the market. Personal communication with one of the authors of the above research indicated that polyurethane manufacturers were unable to supply adequate support to growers in terms of ideal watering and fertilising regimes for their media. Many of the above studies also revealed that polyurethane based media had much lower water holding when compared to rockwool. This would require different watering and nutrient regimes, something growers may be resistant to change. Although there have been few commercially successful polyurethane based growing media, there are still some currently available. These include the BVB Sublime ® growslabs (a direct competitor to rockwool), WaterGrip ™ (a substrate made for green roofs, made from organic materials and bound with PUF) and Huntsman Vydro ® (a low weight PUF substrate for green roofs with high water holding). This thesis concerns itself with developing a framework for rapid development of polyurethane foams with varying physical and chemical properties, with the goal of determining the optimum properties at specific watering and fertilisation regimes. This would also lead to a deeper understanding of plants

behaviour in this type of media, overcoming some of the shortcomings of previous polyurethane based media research.

The bulk of the work in this thesis concerns the formulation of a novel polyurethane foam based soilless growing media. It is therefore important to develop a deeper understanding of the foaming processes, chemical reactions and chemical components in a polyurethane foam formulation. This remainder of this chapter covers polyurethanes and processes required for formulating a flexible polyurethane foam.

1.3. An Introduction to Polyurethanes

Polyurethanes (PU) are an important class of polymers that are highly versatile due to the diverse chemistry used in their synthesis. Some applications include: furniture, bedding, automotive parts, adhesives and sealants[47]. Polyurethanes account for 6 % of the global consumption of plastics worldwide and 7.4 % of European consumption, only polyolefins, poly(vinyl chloride) (PVC), poly(ethylene terephthalate) (PET) and styrenics hold a larger market share. Polyurethane also accounts for 13 % of all plastic publications in the years 2003-2013, and has seen an annual increase in the number of publications during this period[48,49]. Furthermore, the PU market is predicted to expand at a rate of 7.5 % annually between 2014 and 2020[50]. Plastics in this sense are defined as the main commodity plastics, a group of low cost polymers consisting of: polyethylene, polypropylene, poly(vinyl chloride), styrenics, polyurethanes and poly(ethylene terephthalate). Although PU's are important in the modern day, their discovery is not a new one.

Polyurethanes were first discovered in 1937 by Otto Bayer and his co-workers whilst trying to find alternatives for rubber[51]. The first patent for a polyurethane foam was given to Zaunbrecher and Barth in 1942[52]. However, these polymer foams were not easily to commercialise. It was the mass production of polyisocyanates in the 1950's that made the commercialisation of polyurethanes viable. A further breakthrough for polyurethane foam came when trace amounts of water was accidentally present in one of the reagents, this caused a blowing reaction which released CO_2 and formed voids in the polymer[53]. Polyurethane foam secured its place in the market in 1954

when the first commercial PU foam plant was commissioned[54]. From these roots, PU foams have found use in a range of applications due to their versatility in their production processes and final properties.

Polyurethanes are a class of polymers that are usually formed by the reaction of an isocyanate and a polyol. The reaction of these components forms a urethane group and the repeat pattern of these urethane groups forms part of the backbone of the polymer. An example of a polyurethane is shown in Figure 1.1. The urethane functional group contains a carbonyl group that has a single bond to a nitrogen as well as an oxygen atom. The oxygen and nitrogen atom are singly bonded to a carbon atom. The foaming of polyurethane occurs when a second reaction takes place. This reaction is normally between an isocyanate and another reagent, typically water, and one of the products of this reaction is a gas (often CO_2) that gets trapped within the polymer.

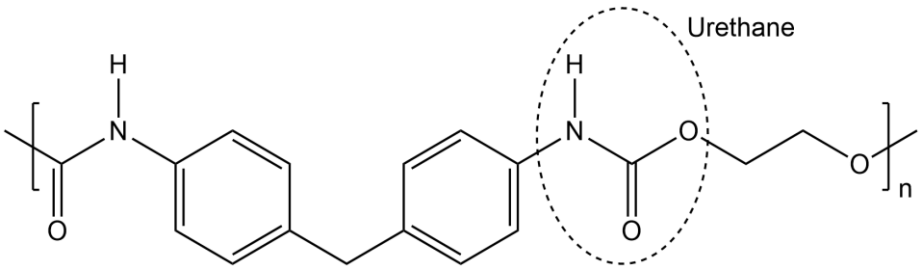

Figure 1.1: Example of a polyurethane polymer and the urethane functional group.

Due to the diverse nature of polyurethanes and the nature of this project, the remainder of this introduction will focus on flexible polyurethane foams (fPUF) and the reactions surrounding their synthesis. More specifically, we will be focusing on the synthesis of fPUF using isocyanates and polyols

1.3.1. Basic Polyurethane Foaming Process

fPUF foaming takes place in several stages. The reagents required as well as the chemical reactions that take place will be covered in detail in the following sections. This section serves to provide a basic understanding of the rheological and morphological stages that occur during the production of a fPUF. The foaming can be

broken up into six stages and this is shown in Figure 1.2 which is adapted from Bicerano *et al*[54] and Artavia and Macosko[55].

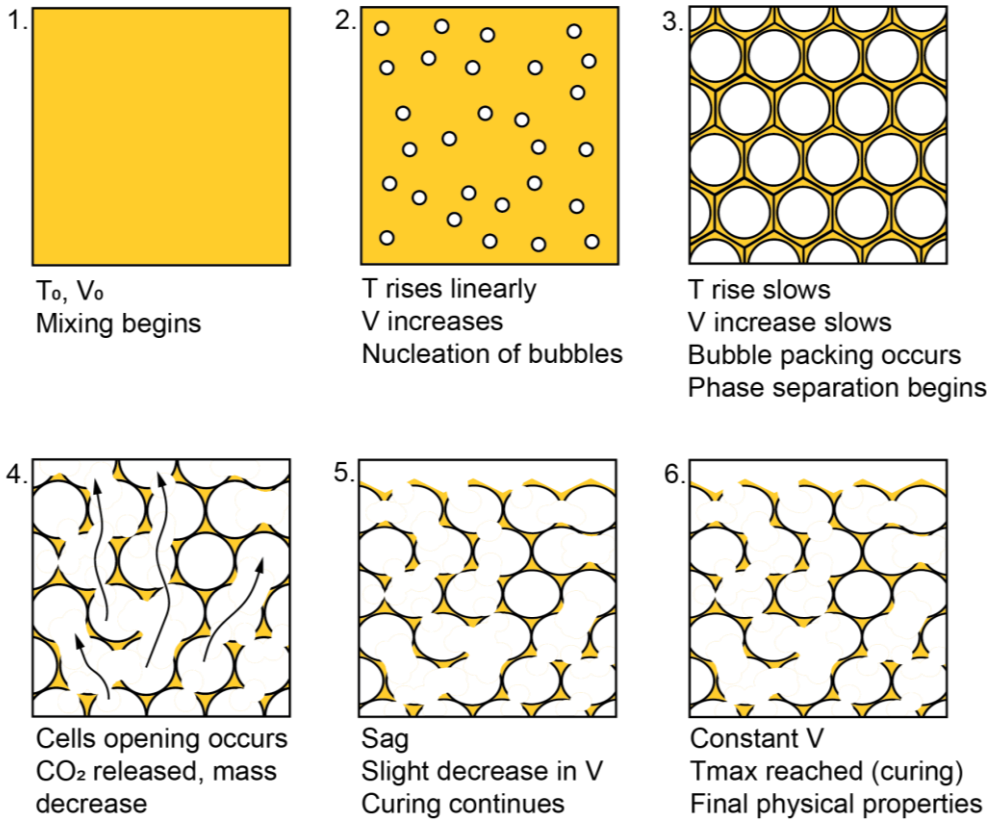

Figure 1.2: Stages of fPUF foam development (1) mixing of isocyanate, polyol and other components. (2) Mixing and dissolved gasses allow for bubble nucleation simultaneous to CO_2 generation due to blowing reaction, bubbles start forming and volume increases. (3) The gelling and blowing reactions continue and the mixtures temperature increases as does volume, bubbles start packing (4) cell opening occurs allowing for trapped CO_2 to escape, slight mass decrease due to lost CO_2. (5) Curing continues, volume decreases slightly due to sag and (6) foam reaches its final volume[54,55]*.*

Components are mixed in stage one, generally consisting of a two part mixture, with part A consisting of an isocyanate and part B consisting of polyols and all other required components. Mixing not only homogenises the components, but also introduces air into the mixture that acts as nucleating sites for bubble formation. At this point the mixture is at its initial volume (V_0) and temperature (T_0).

During stage two the two chemical reactions begin, the gelling (or urethane forming reaction) and the blowing (or gas forming) reaction. As carbon dioxide is formed by the blowing reaction, bubbles nucleate, start forming and the volume of the mixture increases, during this stage CO_2 bubbles are spherical. There is also a rapid increase in temperature as both the gelling and blowing reactions are exothermic.

As bubble volume increases and free space decreases the bubbles start to pack adjacent to one another and take on a dodecahedron shape instead of a spherical one with a thin polymer film separating two adjacent bubbles (cell window) or three/more bubbles (cell strut). As the blowing reaction slows, the volume of the foam starts to plateau and the temperature rise slows. This is shown in stage 3.

The gelling reaction continues and the fPUF continues to develop its mechanical properties. Pressure from trapped CO_2 inside the bubbles then causes the polymer from cell windows to drain and can cause the thin cell wall film to rupture, breaking cell walls and allowing CO_2 to escape. As CO_2 is released, a slight decrease in mass may occur. This is known as cell opening and is shown in stage 4.

If the foam is not sufficiently gelled at the point of cell opening sagging may occur. This causes a slight decrease in volume of the foam. This is shown in stage 5. Throughout stages two to five the gelling reaction continues.

When the temperature reaches a plateau we have reached stage six. The foam gelling reaction has completed and the foam reaches its final volume and density.

1.3.2. fPUF Components

The backbone of PU foams is made up of polyols and isocyanates, however several other compounds are needed to acquire the necessary properties of a foam. These include chain extenders, blowing agents, catalysts, surfactants and any required fillers.

Each of these components are important in PU foam formulations and will be discussed in more detail.

1.3.2.1. Polyols

Polyols, defined as an organic compound that contains several hydroxyl functional groups (diol – two hydroxyl groups, triol – three hydroxyl groups, etc), are the major component in fPUF formulation. All components in a fPUF formulation are measured as a percentage mass of the amount of polyol, or parts per hundred polyol (PPHP). The polyols used for fPUF can generally be broken into three categories. These are polyether polyols, hydroxyl terminated polyesters and hydroxyl bearing oils.

Polyether Polyols

Polyether polyols or polyetherols are the preferred polyols for the synthesis of PU foams, this is mainly due to them having a cost advantage over hydroxyl terminated polyesters.

Commercial polyetherols are synthesised by the reaction between an organic oxide (often propylene or ethylene oxide) with an initiator which contains several active hydrogen atoms. The reaction is done in the presence of a basic catalyst (often potassium hydroxide KOH) and the reaction takes place until the required molecular mass (M_n) is reached. The number of active hydrogens in the initiator directly relates to the number of alcohol groups in the resulting polyetherol. An example of a reaction between ethylene glycol and propylene oxide is shown in Figure 1.3, which leads to the formation of a diol. Similarly a triol could be synthesised by reacting glycerol with propylene oxide.

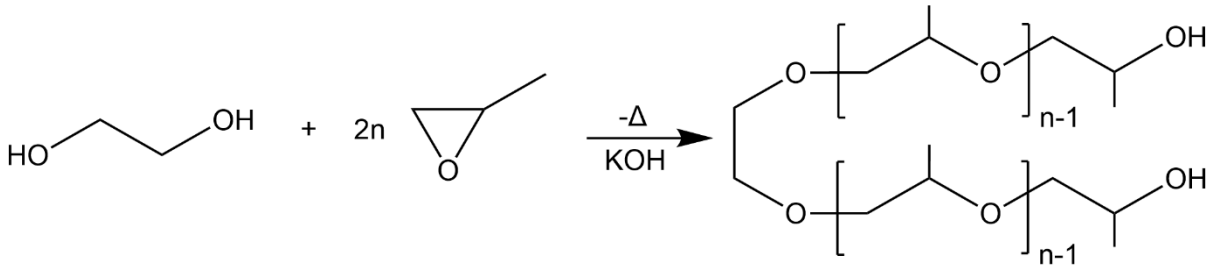

Figure 1.3: Formation of a diol from ethylene glycol and propylene oxide

A reaction of only propylene oxide leads to a polyol with secondary hydroxyls, which are less reactive than primary hydroxyls. This decrease in reactivity is mainly due to steric hindrance caused by groups attached to the carbon atom connected to the hydroxyl group. To increase the reactivity, these polymerisations are started with propylene oxide, and ethylene oxide is added near the end of reaction, increasing the number of primary hydroxyl groups. This addition of ethylene oxide also increases the water solubility of the polyol[56]. Due to this reactivity and rate of the reaction, polyether polyols need to be liquids at reaction conditions[57].

Hydroxyl Terminated Polyesters

The hydroxyl terminated polyesters are versatile in their synthesis as they are formed by the reaction between polybasic acids and polyhydric alcohols. This versatility is one of the major advantages of the polyesters over the polyetherols. A specific application of PU foams which require the use of polyesters is in the manufacture of flame retardant foams [47]. The cost advantage of the polyetherols over the polyesters is due to the polyetherols' monomers being cheaper. A further disadvantage of the polyesters is that they are more susceptible to hydrolysis[58]. An example of the formation of polyethylene adipate via the polycondensation reaction of adipic acid and ethylene glycol is shown in Figure 1.4.

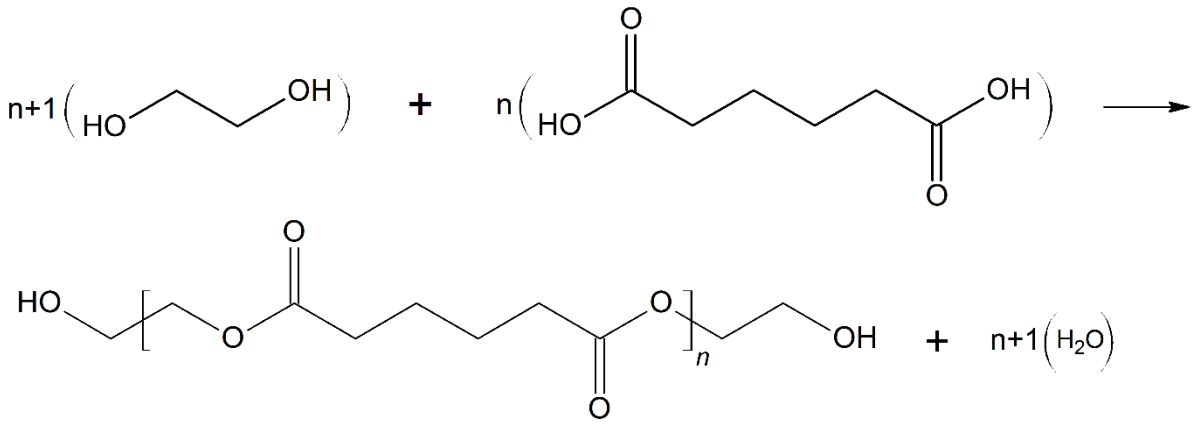

Figure 1.4: Polycondensation of adipic acid and ethylene glycol to form polyethylene adipate.

The fact that aliphatic polyesters are susceptible to hydrolysis can also be seen as an advantage in certain scenarios. The most important of these is the fact that this

susceptibility makes aliphatic polyesters one of the most biodegradable classes of polymers[59].

Hydroxyl bearing oils

A third important group of polyols are the hydroxyl bearing oils. These are of importance polyols for synthesising polyurethanes from renewable feedstock. These include vegetable oils, fatty acids, fatty acids methyl esters, wood, crude glycerol (glycerine) and protein based feedstocks[60]. The most commercially viable of these presently are the bio-based polyols synthesised from vegetables oils.

The majority of the vegetable oils are not suitable to be used directly as polyols as they do not have a hydroxyl group in their fatty acid chain. Generally polyols are synthesised by exploiting the unsaturation of fatty acids. This can be done by several chemical pathways and has been extensively written about by Li, Luo and Hu[60]. The exception to this is castor oil, which is made up of 90 % ricinoleic acid which contains one hydroxyl group on the twelfth carbon and a double bond between the ninth and the tenth[61]. The use of castor oil directly as a polyol has been limited, as the secondary hydroxyl group in ricinoleic acid is less reactive than primary hydroxyl groups found in conventional petroleum based polyols[62]. Lesquerella Oil is a further exception, containing a hydroxyl group in its fatty acid, however any work into using this as a polyol is still in its infancy[63].

1.3.2.2. Isocyanates

Isocyanates are another important component in the synthesis of PU foams, as they play a major part in both reactions governing the formation of foams. The two most popular isocyanates that are used in PU foams are toluene diisocyanate (TDI) and methylene diphenyl diisocyanate (MDI) which are shown in Figure 1.5. TDI and MDI and their isomers are generally used in foaming reactions as they are both aromatic isocyanates which react with -OH groups much faster than aliphatic polyisocyanates. This is important as foaming reactions require high reactivitiy[52]. The aromatic isocyanates are more reactive as they are able to delocalise the negative charge of

the -NCO, increasing the positive charge on the C atom, making it more susceptible to nucleophilic attack from an alcohol.

TDI is usually used as a 80:20 mixture of 2,4-TDI and 2,6-TDI and MDI is used as 4,4'-MDI. TDI and MDI are the most used isocyanates and make up 90 % of the total isocyanate production[64].

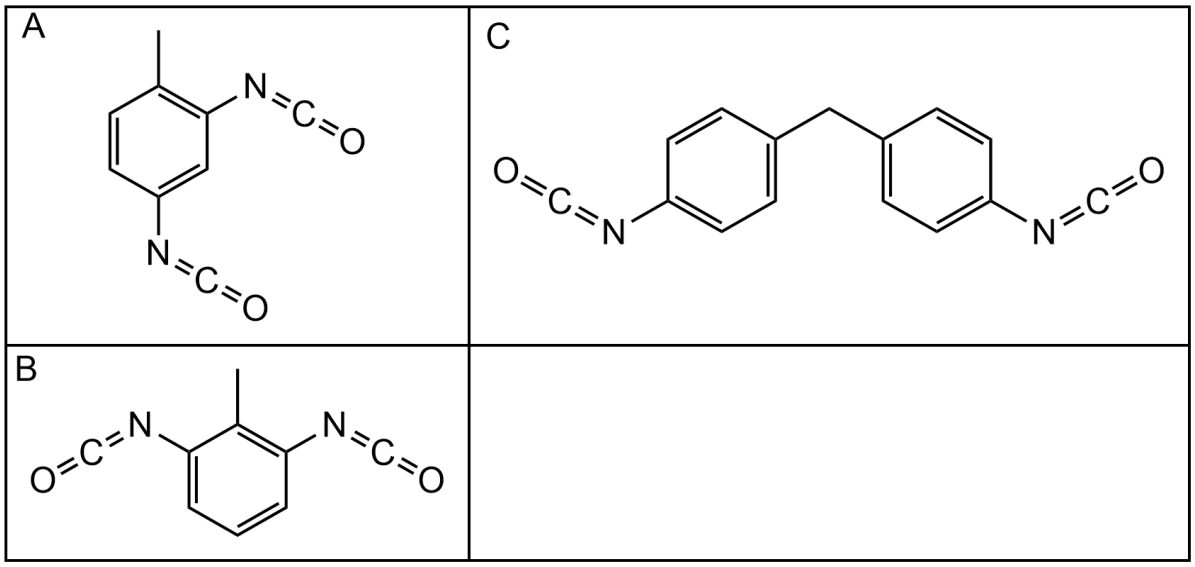

Figure 1.5: Chemical structures of (A) 2,4 - toluene diisocyanate (TDI), (B) 2,6 - toluene diisocyanate (TDI) and (C) 4,4' - methylene diphenyl diisocyanate (MDI).

The aliphatic isocyanates do, however still find use in the synthesis of speciality PU foams. The most popular of these isocyanates are hexamethyl diisocyanate (HDI) and isophorone diisocyanate (IPDI). Their chemical structure is shown in Figure 1.6. Aliphatic isocyanates are generally used when UV stability is important. Aromatic isocyanates have a tendency to yellow in the presence of UV radiation[65].

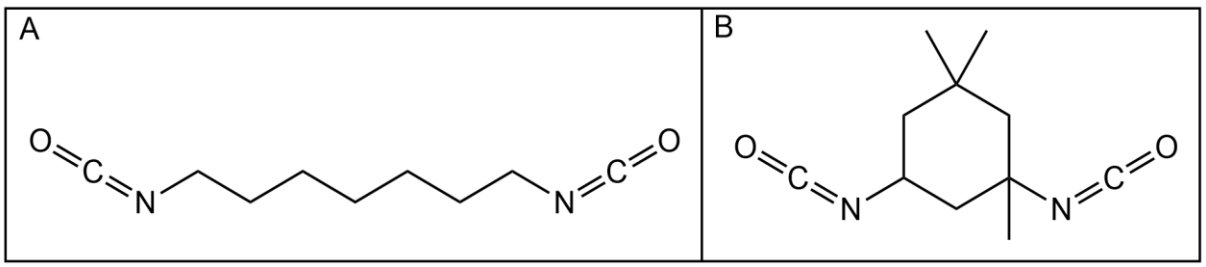

Figure 1.6: Chemical structures of (A) hexamethyl diisocyanate (HDI) and (B) isophorone diisocyanate (IPDI).

1.3.2.3. Catalysts

The two major reactions that occur during the formation of PU foams are known as the gelling reaction and the blowing reaction. The gelling reaction is the formation of urethane links when an isocyanate reacts with a polyol. The blowing reaction is the reaction which forms a gas allowing for the void space in the PU foam. These reactions are further explained in Chapter 1.3.3.

Both the gelling and blowing reaction are catalysed reactions, and their rates need to be balanced to ensure a foam with acceptable mechanical and physical properties.

The types of catalysts used for these two reactions are relatively standard for flexible PU foams in industry. The blowing reaction uses a tertiary amine, typically triethylene diamine and the gelling reaction uses a metal catalyst, normally Tin(II) 2-ethylhexanoate (stannous octoate). Their function and mechanism is further explained in Chapter 1.3.3.4.

Metal salts raise environmental problems, due to leaching from the foam into the environment, and tin salts can be detrimental to polyurethane aging. Amine catalysts are volatile and exhibit an undesired odour[66]. In applications where either of these situations lead to problems autocatalytic polyols offer a solution. A tertiary amine is incorporated into the polyol backbone and this reduces the amount of catalyst required and increases the reactivity of the polyol[67]. The chemical structure of an example autocatalytic polyol is shown in Figure 1.7[68].

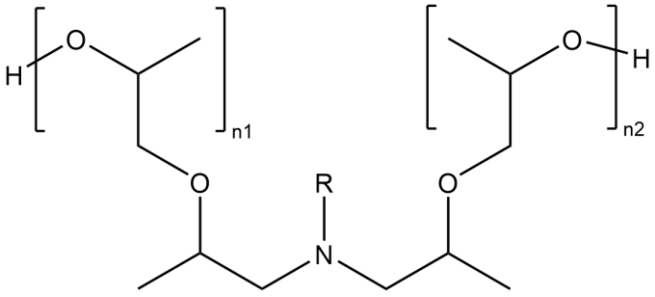

Figure 1.7: Chemical structure of an example autocatalytic polyol[68].

1.3.2.4. Chain Extenders

Chain extenders are low molecular weight polyols, that are used to improve the foam properties by aiding in the phase separation process[69]. These extend the isocyanate based hard segment of the polymer chain, which gives a foam its mechanical strength.

1.3.2.5. Surfactants

PU foams rely greatly on the effectiveness of surfactants, which are normally non-ionic, silicone based surfactants. The major share of silicone surfactants produced are used in PU foams and the growth in production of these surfactants follows the growth trends for PU foam[70].

Surfactants have several important roles in the PU foaming process. The functions of silicone surfactants include: reducing surface tension, emulsifying incompatible ingredients, promoting bubble nucleation during mixing, stabilisation of the cell walls during foam expansion and reducing the defoaming effect of any solids added[71].

Arguably, the most important of these functions is the stabilisation of the cell walls. If a surfactant is omitted, or is below a critical loading in a PU foam formulation, the serious risks of imperfections such as splitting, densification or complete collapse are highly likely. Higher concentrations of surfactant than required can also have negative impacts, over-stabilising the foam. This over-stabilisation causes the formation of closed cells, which reduce airflow through the foam and can cause foam shrinkage[72].

1.3.2.6. Blowing Agents

Blowing agents are used to create the gas that forms the void space in PU foams. Water is generally used as the blowing agent, as it reacts with isocyanates to form CO_2 gas. However, if further gas is required a low boiling point liquid, such as fluorocarbon 11, which absorbs heat from the PU foam reaction and vaporises, can be used. Due to worries about CFC release these types of blowing agents are rarely used[73].

1.3.2.7. Fillers and other Additives

Fillers are generally low cost inert compounds that are added to the formulation to reduce cost. They can however also have an additional benefit to the final product, in this case they are known as functional fillers. Common functional fillers improve the mechanical properties or the flame retardancy of PU foams[47].

Several other additives can be used to suit particular PU foam requirements. These can include: Flame retardants, pigments (colour), plasticisers, bacteriostats (stops bacterial growth), anti-static agents and UV stabilisers, but they will not be part of the work presented in this thesis and are mentioned only for completeness.

There are two main reactions that take place during the formation of polyurethane foams, the first of these reactions is the reaction between the isocyanate and the polyol, known as the urethane reaction. The second reaction is that between the isocyanate and water as a blowing agent. This reaction causes the formation of CO_2 gas which produce the void space in foams.

1.3.3. Polyurethane Reactions

There are two main reactions that take place during the formation of polyurethane foams, the first of these reactions is the reaction between the isocyanate and the polyol, known as the urethane reaction. The second reaction is that between the isocyanate and water as a blowing agent. This reaction causes the formation of CO_2 gas which produce the void space in foams.

1.3.3.1. Urethane Reaction

The urethane reaction is a chemical reaction which gives PU its backbone and name. The reaction takes place between an isocyanate and a polyol, and results in the formation of a urethane link in the polymer as shown in Figure 1.8. This can also lead to the formation of crosslinking points when polyols with functionality >2 are used, and the formation of urethane is often referred to as the “gelling reaction”.

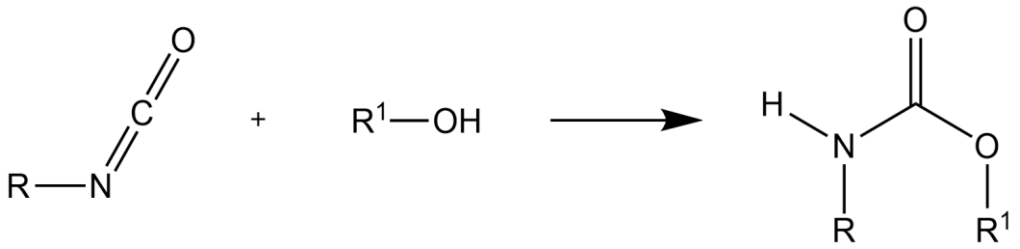

Figure 1.8: The reaction between an isocyanate and an alcohol to form a urethane.

There are a number of secondary reactions that can occur concurrently with the urethane reaction, such as the reaction between a urethane and an isocyanate to form an allophanate as shown in Figure 1.9. This reaction allows for crosslinking of the polymer, however in the synthesis of PU foams, it is generally not observed.

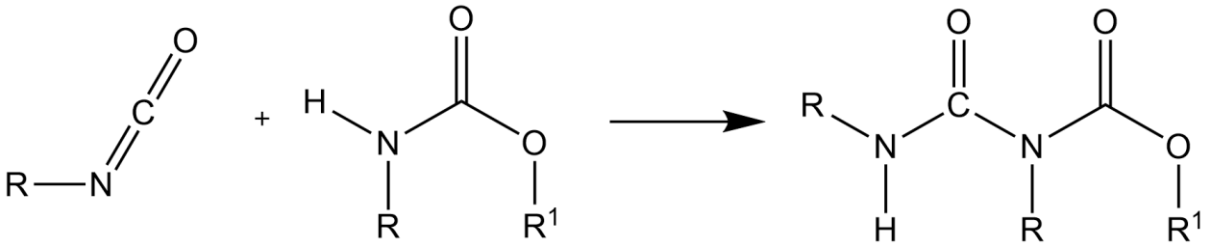

Figure 1.9: The reaction of an isocyanate and a urethane to form an allophanate.

The urethane forming reaction is normally catalysed with an organotin catalyst and the basic mechanism for this is generally accepted to be a Lewis-acid based mechanism for common organotin catalysts[74], tertiary amines can also be used to catalyse the urethane reaction.

1.3.3.2. Blowing Reaction

The blowing reaction that occurs during the synthesis of a PU foam is between the isocyanate group and the blowing reagent, normally water. This reaction ultimately produces an amine and CO_2, the gas which produces the void in a PU foam. The reaction first forms an unstable carbonic acid intermediate, which quickly decomposes into an amine and carbon dioxide as shown in Figure 1.10. The amine that is produced by this reaction can react further with another isocyanate group to produce a urea linkage and form a disubstituted urea as shown in Figure 1.11.

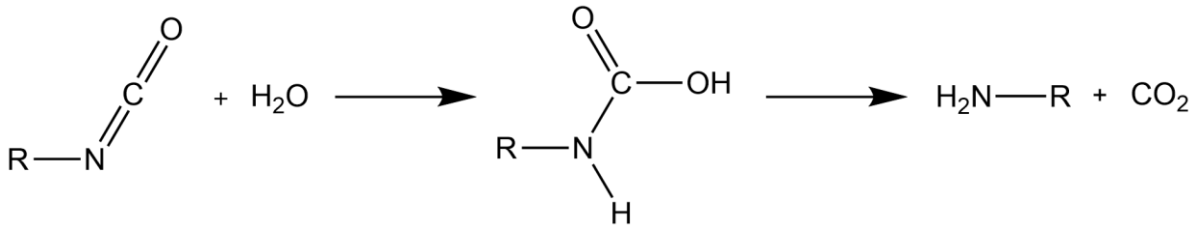

Figure 1.10: The reaction between an isocyanate and water to from an amine and carbon dioxide.

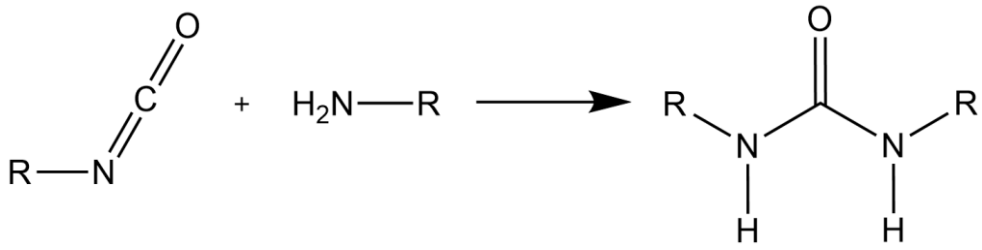

Figure 1.11: The reaction of an isocyanate with an amine to form a disubstituted urea.

The formation of the disubstituted urea acts as a chain extender for the polymer. There is also a further secondary reaction that can occur, which also leads to cross linking points, this occurs when a disubstituted urea reacts with an isocyanate to form a biuret and is shown in Figure 1.12.

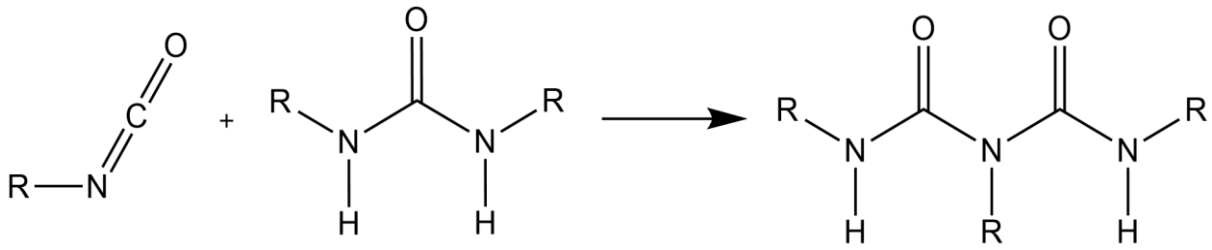

Figure 1.12: The reaction of a disubstituted urea and an isocyanate to form a buiret.

The blowing reaction between an isocyanate and water is also a catalysed reaction, often with a tertiary amine. This reaction consumes two isocyanates groups to form each disubstituted urea.

It has been found that tertiary amines act not only as catalysts for the blowing reaction but also for the urethane reaction, they also have a synergistic catalytic effect with the tin based catalysts[74].

1.3.3.3. Heats of Reaction

Both the reactions, the urethane reaction as well as the blowing reaction are exothermic. Knowing the heats of reaction are important for understanding the kinetics and are required to calculate the extent of isocyanate conversion of isocyanate by measuring the reaction exotherm.

The literature varies on the exact values of these heats of reaction. Artavia and Macosko summarise the literature and values[55]. They also found that they had good agreement between predicted and measured temperature values using a heat of reaction of -93.9 kJ mol^{-1} for the urethane reaction and -125.5 kJ mol^{-1} for the urea forming blowing reaction. These values are used for adiabatic temperature rise calculations presented in this work.

1.3.3.4. Catalysis

The most simple models for both metal based catalysts and amine catalysts, have the catalyst polarising the hydroxyl or the isocyanate group via polar interactions. These models are shown in Figure 1.13[48].

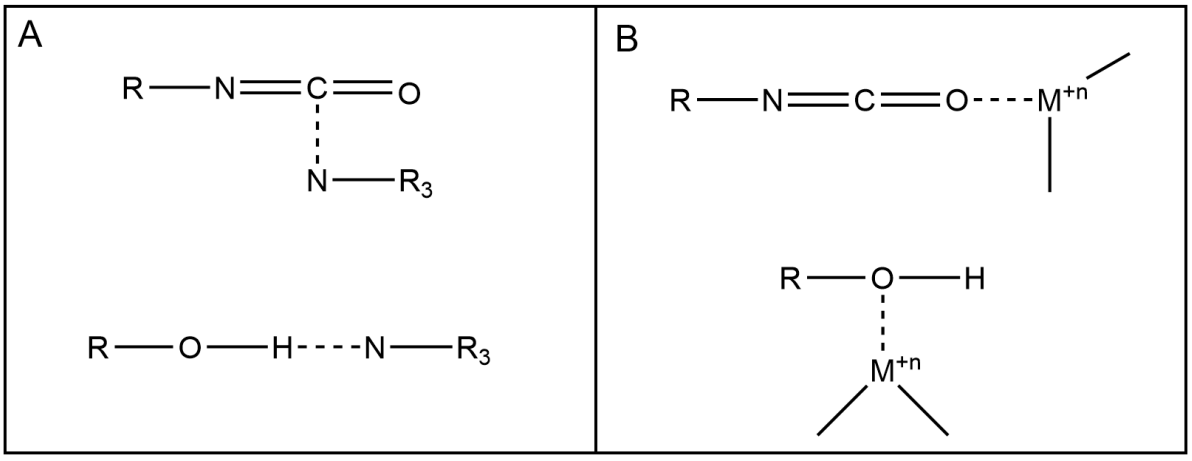

Figure 1.13: Examples of (A) amine catalysts and (B) metal catalysts polarising bonds.

Tin Catalysts

Metal catalysts generally act as Lewis acids, and coordinate to the oxygen atom of the -NCO group. A universal mechanism for all metal salts has not been agreed, and with difficulties in taking controlled measurements, and difficulties in quantifying effects of all intermediate reactants and products it seems unlikely that a unifying mechanism will be found. An example mechanism for the use of metal salt catalysts shown in Figure 1.14.

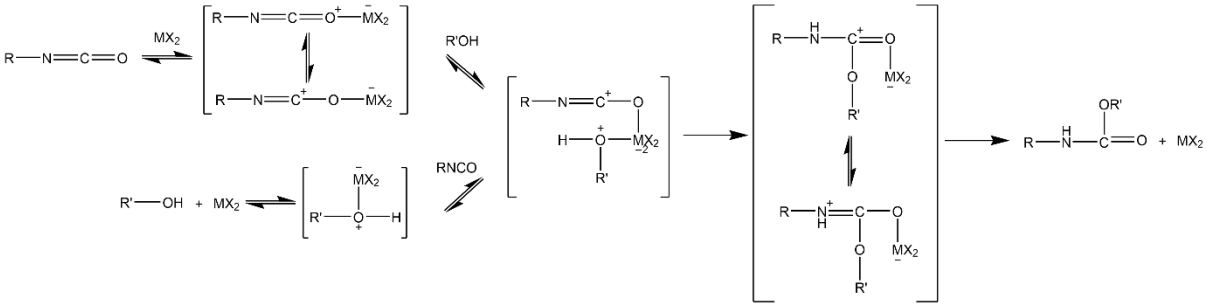

Figure 1.14: Lewis acid mechanism for the use of metal salt catalysts[74,75]*.*

Amine Catalysts

Amine catalysts will coordinate to either the carbon atom of the -NCO group or the hydrogen group of the hydroxyl group. This is shown in Figure 1.15.

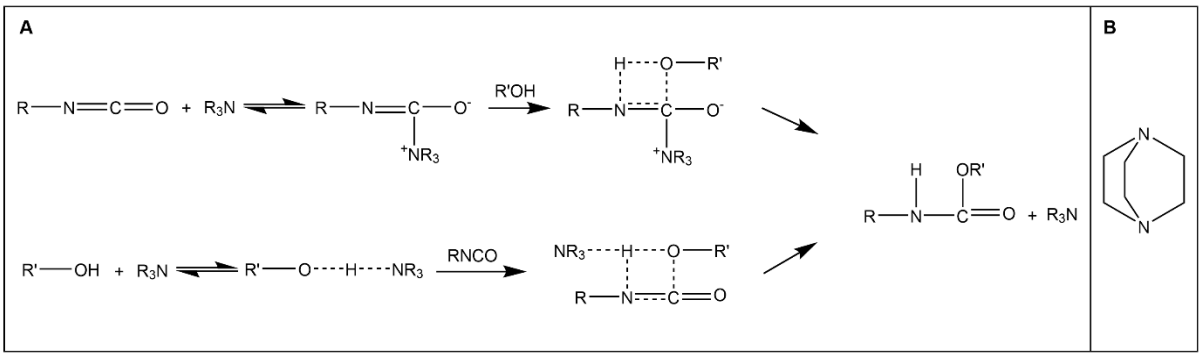

Figure 1.15: (A) Mechanism for the use of amine catalysts[74,75] *and (B) the structure of the most prevalent tertiary amine catalyst 1-4 diazabicyclo[2.2.2]octane.*

Maris *et al*[76] tested the catalytic activity of several common amino catalysts and found several interesting results. Catalytic activity of amines increases with the number of

tertiary amino groups within the catalyst. With regards to cyclic amino catalysts, they all showed relatively low catalytic activity, the exception being 1,4-diazabicyclo[2.2.2]octane or TEDA (the active amino catalyst in Dabco 33LV) which has high catalytic activity. This suggests that TEDA has very low steric hindrance. They also found that the addition of a hydroxyl group in the catalyst reduced the catalytic activity, as the catalyst is quenched by reacting with a free isocyanate.

1.3.4. fPUF Morphology Development

The physical properties of a fPUF depend on the macroscopic cell structure of the foam as well as the nanoscopic morphology of the polymer material within the struts of the foam[55]. Both the macroscopic cell structure and the morphology of the polymer material are highly dependent on the formulation of the foam, with the amount of water playing a crucial role. This is due to the formation of urea in the water isocyanate reaction. These urea segments (hard segment) often phase separate from the polyether-urethane segment (soft segment) due to thermodynamic incompatibility of the hard segment with the soft continuous phase and the ability of these urea segments to form strong hydrogen bonds. If the concentration of water ever exceeds the solubility limit in the polyol mixture, droplets of water can form in the mixture. If this is the case, these droplets lead to high urea concentrations and once these regions reach a certain molecular mass these regions can form a third phase of agglomerated polyurea balls. This third phase is rarely seen in conventional fPUF formulations. The insert in Figure 1.16 shows these three different possible phases in a fPUF.

This hard segment-soft segment phase separation in fPUF has been studied by in situ FTIR, SAXS and rheology and four main rheological regions were identified[77]. Onset of this phase separation was observed to occur at around 50-60 % isocyanate conversion and the increase of water or catalyst reduced the time until phase separation occurred[78]. Phase separation plays an important role in cell opening, with cells opening occurring a few seconds after phase separation takes place. It has been suggested that urea phase separation triggers cell opening, however for this to be the sole mechanism of cell opening, cells walls would all be torn, and this is not the case. SEM has shown some cell walls disappear without debris, indicating that the cell window material is able to flow at the early stage of cell opening, behaving like a

Bingham plastic[79]. The phases of morphology are shown in Figure 1.16 which is adapted from work by Artavia and Macosko[55] and Bicerano *et al*[54] .

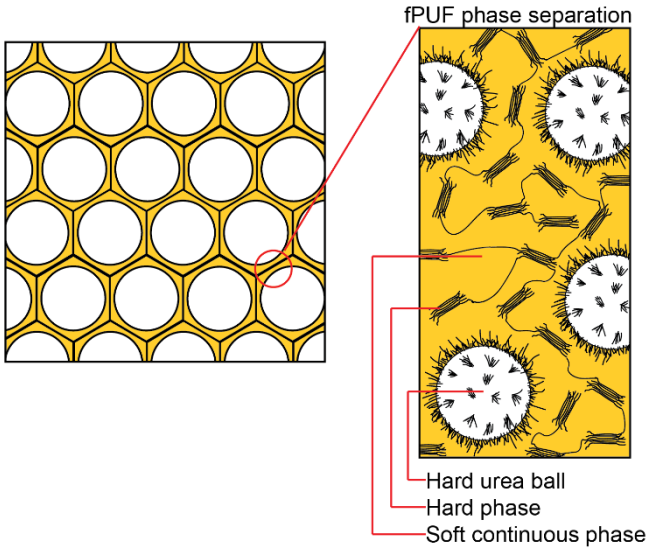

Figure 1.16: The different morphological phases of a phase separated fPUF[54,55].

1.4. Project Aims

The expanding use of controlled environment agriculture (CEA) and urbanisation of food production[80] means there will be an estimated 42 million $m^3.yr^{-1}$ gap in the market for novel growing media[81]. This gap in the market is compounded by pressure to move towards more environmentally friendly growing media in CEA agriculture and has led to the development and use of novel growing media such as polyurethane foams. Although some research has been done into the use of these foams in hydroponic greenhouses, there is little literature[41–44] reported on the development and optimisation of a polyurethane foam for use in horticulture.

The central aim of this study is to optimise a flexible polyurethane foam (fPUF) for use as a hydroponic growing media in controlled environment agriculture. A design of experiments (DoE) approach is taken to achieve this aim. A brief description of this process and objectives is given below.

- The identification of appropriate physical and chemical properties of fPUF foam expected of affecting plant growth in a hydroponic system.

- The development of techniques appropriate for characterising these physical and chemical foam properties.
- Screening and adaptation of a fPUF formulation towards a fPUF with properties more suitable for the horticultural application.
- The use of DoE techniques to develop physical property models, with physical properties as response variables and the catalyst and surfactant package as the factors influencing these responses.
- The development of plant growth and health models using hydroponic growing techniques and a selection of fPUFs with a range of physical properties.
- Optimisation of a fPUF growing media using the plant growth and health models in conjunction with the physical property models.

Chapter 2:
Foam and Plant Characterisation – Methods and Method Development

2.1. PUF Reaction Kinetics

2.1.1. **Adiabatic Temperature Rise (ATR)**

Temperature rise has been used extensively as a method to determine the reaction kinetics of polyurethane foams. This method takes advantage of the highly exothermic reactions that occur during the formation of polyurethane foams as well as the low thermal conductivity of the foams. Initially Adiabatic temperature rise was shown to be an effective method for monitoring kinetics for fast cure polyurethane reactions[82], however it has since been shown that by using a heat loss correction, ATR can be used for polyurethanes with longer reaction times as well[83]. Isocyanate conversion calculated from ATR data has been closely correlated to isocyanate conversion from infrared spectroscopy data, verifying the use of this approach for determining isocyanate conversion[77]. ATR has also been used to model the blowing and gelling reactions for water blown polyurethane foams. Models fitting first order kinetics to the blowing reaction were in good agreement with the experimental data up to a temperature of 140 °C[84]. Further modelling work using temperature rise has successfully modelled rigid polyurethane foams temperature rise, including the estimation of important kinetic properties such as pre-exponential factors, Arrhenius activation energy and heat of reactions[85]. ATR has also proved useful in comparing and understanding reaction rates of soy bean based polyols against conventional polyols[86]. These studies support the use of ATR for monitoring polyurethane foam kinetics and isocyanate conversion.

The ATR curve for a reacting PUF is generated by monitoring the increasing core temperature of a reacting foam housed in an insulated reaction vessel. Although insulating the reaction vessel reduces heat loss, a correction still needs to made to account for any heat loss[83]. The energy equation governing the polyurethane reaction is shown in *Equation 2.1*,

$$\rho c_p \frac{dT_{exp}}{dt} = (-\Delta H)k_1 - U(T_{exp} - T_{amb}) \qquad 2.1$$

where ρ is the density ($kg.m^{-3}$), c_p is the heat capacity ($J.g^{-1}.K^{-1}$), T_{exp} is the reaction temperature (K), t is the time (s), ΔH is the heat of formation of products ($J.mol^{-1}$), k_1 is the rate of formation of products ($mol.m^{-3}.s^{-1}$), U is the global heat transfer coefficient ($J.K^{-1}.m^{-3}.s^{-1}$) and T_{amb} is the ambient temperature (K). When no reaction occurs, *Equation 2.1* can be simplified to

$$\frac{dT_{exp}}{dt} = \frac{U}{\rho c_p}(T_{exp} - T_{amb}) \qquad 2.2$$

and *Equation 2.2* is integrated into *Equation 2.3* between the limits of t_0 and t.

$$\ln(T_{exp} - T_{amb}) = \ln(T_o - T_{amb}) - U'(t - t_o) \qquad 2.3$$

Equation 2.3 can then be plotted, and the slope of this plot will give us the overall heat transfer coefficient U' ($U/\rho c_p$). The data used for the fitting was taken from the cooling portion of the ATR data, long after the maximum temperature had been reached when no reaction occurred. This plot is shown in Figure 2.1 (A) with the data used for fitting shown in grey.

The temperature can then be adjusted for heat loss by combining the *Equation 2.4* with *Equation 2.1* and then integrating such that *Equation 2.5* results,

$$\rho c_p \frac{dT_{ad}}{dt} = (-\Delta H) r_1 \qquad 2.4$$

$$T_{ad} = T_{exp} + U' \int_0^t (T_{exp} - T_o)\, dt \qquad 2.5$$

Where T_{ad} is the adiabatic temperature, corrected for heat loss.

An example of the uncorrected and the corrected temperature profiles are shown in Figure 2.1 (B).

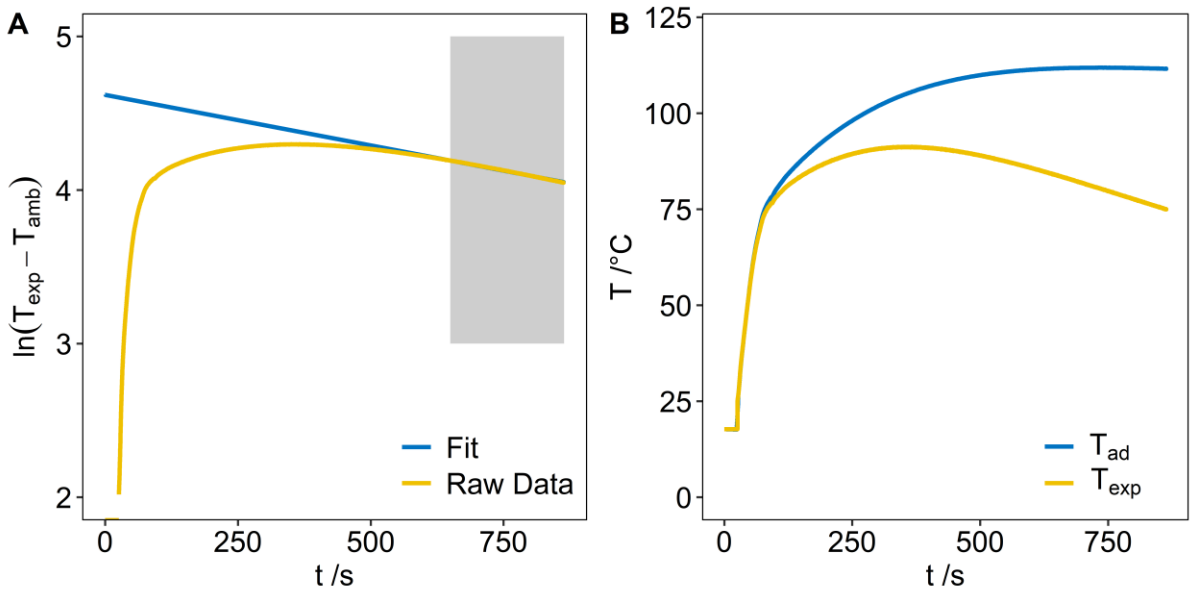

Figure 2.1: (A) Plot showing the data used to calculate the heat transfer coefficient, the grey region shows the region used for curve fitting and (B) shows the corrected (T_{ad}) and uncorrected (T_{exp}) temperature profile.

Using the corrected temperature profile, the isocyanate conversion can be estimated using *Equation 2.6*[87].

$$P_{NCO} = \frac{r(T_{ad} - T_{amb})}{T_{maxcalc}} \qquad 2.6$$

Where P_{NCO} is the isocyanate conversion, r is the isocyanate index defined as the ratio of isocyanate used, compared to the calculated stoichiometric amount required and $T_{maxcalc}$ is the maximum theoretical temperature of reaction if all the isocyanate is consumed and is given by *Equation 2.7*.

$$T_{maxcalc} = \frac{\Delta H}{m_t c_p} \qquad 2.7$$

ΔH is the total enthalpy of formation for both the reactions (J. mol^{-1}), the isocyanate-water reaction as well as the isocyanate-polyol reaction, and can be calculated using the enthalpies from Chapter 1.3.3.3. m_t (g) is the total mass of foam reacted, and c_p is the heat capacity (J. g^{-1}. K^{-1}) of the final foam.

The use of these equations relies on a few important assumptions:

1. The c_p of the foams remains constant over the entire temperature range.
2. There are no external sources of heat.
3. The isocyanate only reacts with water and hydroxyls and forms only urea, urethane groups and CO_2.
4. The solution is well mixed and homogenous.

Measuring the reaction temperature is the most important variable as it gives insight into the isocyanate conversion and it would be necessary to monitor this during PUF reactions.

2.1.2. **Height Rise**

The production of CO_2 during the blowing reaction, causes an increase in volume of PUF and has often been used to monitor the progress of the blowing reaction. Van Thuyne and Zimmer[88] studied flexible PUF reactions and tracked the change in height of a foam using a light sensor which followed the foam height. They found this method well suited for flexible foam, with a large advantage being that the instrumentation did not contact the foam, allowing free foam rise. Baser et al[84] recorded the change in foam height using clear cylindrical reaction vessels and a video camera. They were able to model water blown polyurethane foams as a first order kinetics with regard to water concentration. It would therefore be beneficial to measure foam rise height, and an additional requirement would be doing so without disturbing the foam surface.

2.1.3. **Mass Loss**

Knowledge of the mass of the reactants is important for ensuring reproducible experiments. Shen *et al*[89] modelled PUF box foam density using height and mass loss data, for a low boiling point blowing agent and water. The mass loss during mixing and degassing explained the inefficiencies in the low boiling point blowing agent. It would therefore be beneficial and complementary to the temperature and height data to record mass loss data. More importantly here, mass loss may also be used to give

insight into cell opening time, because as trapped CO_2 escapes a mass loss would be observable.

2.1.4. **FoamPi - An inexpensive open source device for monitoring PUF reactions**

2.1.4.1. *Hardware*

A Raspberry Pi (RPi) was identified as the ideal device for building an inexpensive open source device for monitoring PUF reactions. Several breakout boards were identified for monitoring temperature change, height change and mass change. The Max 31856 breakout board was used in conjunction with a k type thermocouple for monitoring temperature rise. Three thermocouples and breakout boards were installed so temperature could be monitored in various positions within the foam. An Adafruit VL53L0X time of flight (TOF) sensor was used to determine height change; this uses a laser source and matched sensor. These detect the time taken for the laser source to bounce back to the sensor and the distance can be determined from this. It handles a range of 50 mm to 1200 mm. Mass was monitored using a HX711 load cell amplifier and a 1 kg load cell.

An official Raspberry Pi 7” touch screen LCD was connected to make real time data visualisation easier and an external keyboard was attached. These were beneficial however not necessary as any device (pc or smartphone) could connect and run the FoamPi remotely using VNC.

2.1.4.2. *Data Capturing Software*

All code was written in Python 3[90]. Python libraries were available for all the breakout boards and need to be installed as a prerequisite for the FoamPi.py software to work. Table 2.1 shows the libraries used for the boards as well as their Github locations. The HX711 force bar as well as the VL53L0X TOF sensor zero their values before the device begins logging data. The FoamPi is able to take and save all raw data to a .csv file at a rate of approximately six data points per second.

Table 2.1: Python Libraries used for FoamPi.

Board	Github Location
Max31856	https://github.com/johnrbnsn/Adafruit_Python_MAX31856
VLX53L0X	https://github.com/pimoroni/VL53L0X-python
HX711	https://github.com/tatobari/hx711py

2.1.4.3. *Raw Data Processing*

Raw data needed minor processing to remove erroneous readings and reduce data noise.

The mass change HX711 board occasionally recorded erroneous negative values and these were replaced using the value from the previous time step according to *Equation 2.8*. These threshold limits remove any sudden spikes in mass change data that are unexpected for PUF reactions.

$$m_{raw,k} = \begin{cases} m_{raw,k-1} & m_{raw,k} < 0.8 \times m_{raw,k-1} \\ m_{raw,k-1} & m_{raw,k} > 2 \times m_{raw,k-1} \\ m_{raw,k-1} & m_{raw,k} < 0.5 \times m_{max} \end{cases} \qquad 2.8$$

Where $m_{raw,k}$ is the current mass reading, $m_{raw,k-1}$ is the preceding value and m_{max} is the maximum mass (initial reactant mass).

Temperature data was corrected using the equations described in Chapter 2.1.1 to transform raw temperature data into adiabatic temperature rise data.

A 21-point moving average was used to smooth the temperature, height and mass data. Figure 2.2 shows the raw and the corrected FoamPi data.

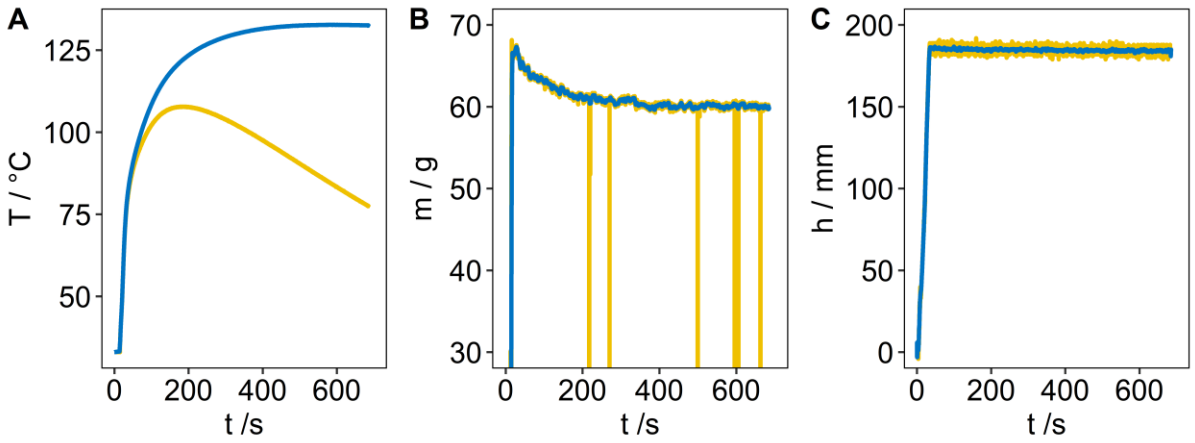

Figure 2.2: Shows the raw (yellow) and corrected (blue) data captured using the FoamPi for (A) Temperature, (B) mass and (C) height.

This corrected data was then used to extract important information from these graphs. Table 2.2 shows and gives a brief explanation for each of these points. Figure 2.3 shows a FOAMAT, a commercial device for monitoring PUF reaction kinetics, which costs approximately £10000 as well as the FoamPI which cost £200.

Table 2.2: Important information extracted from FoamPi data.

Variable (unit)	Description
T_{max} (°C)	Maximum temperature to determine isocyanate conversion.
t_{Tmax} (s)	Time of maximum temperature, important for analysing catalyst activity.
h_{max} (mm)	Maximum foam height, important for analysis catalyst blowing efficiency.
h_f (mm)	Final foam height, important for calculating foam sag.
t_{hmax} (s)	Time of maximum foam height.
Sag (%)	Foam sag, important for understanding open/closed cell ratio.
m_{max} (g)	Initial mass of reactants.
m_f (g)	Final foam mass, important for understanding mass loss.
H_f/m_f ($mm.g^{-1}$)	Normalised maximum height.
sag/m_f ($\%.g^{-1}$)	Normalised foam sag.

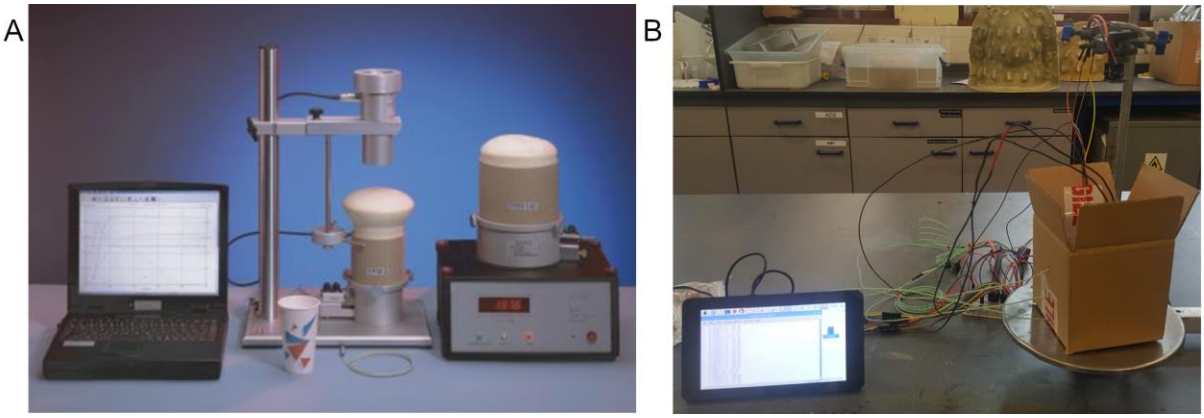

Figure 2.3: (A) The FOAMAT a £10000 system for monitoring PUF reactions and the (B) FoamPi a £200 open source device for monitoring PUF reactions.

2.1.4.4. *Testing*

To determine the precision a set of triplicate experiments was done with a single foam formulation. The temperature mass and height were all monitored. Figure 2.4 shows the corrected temperature, mass and height data as well as the normalised (h/m) data for the replicates. The temperature rise curve is almost identical for the three replicates, showing good reproducibility. The mass curves differ, which is expected as different amounts of reagents may be poured from the mixing vessel to the reaction vessel. The mass values appear to drift, with occasional increases in mass data, which seems unlikely to be true. This could be an effect of airflow in the fume hood or drift from the actual equipment. For this reason mass data was not used for kinetic calculations, and only the final mass was used to normalise the height data. The non-normalised height curves differ significantly; however, when the difference in mass is taken into account the reproducibility increases significantly.

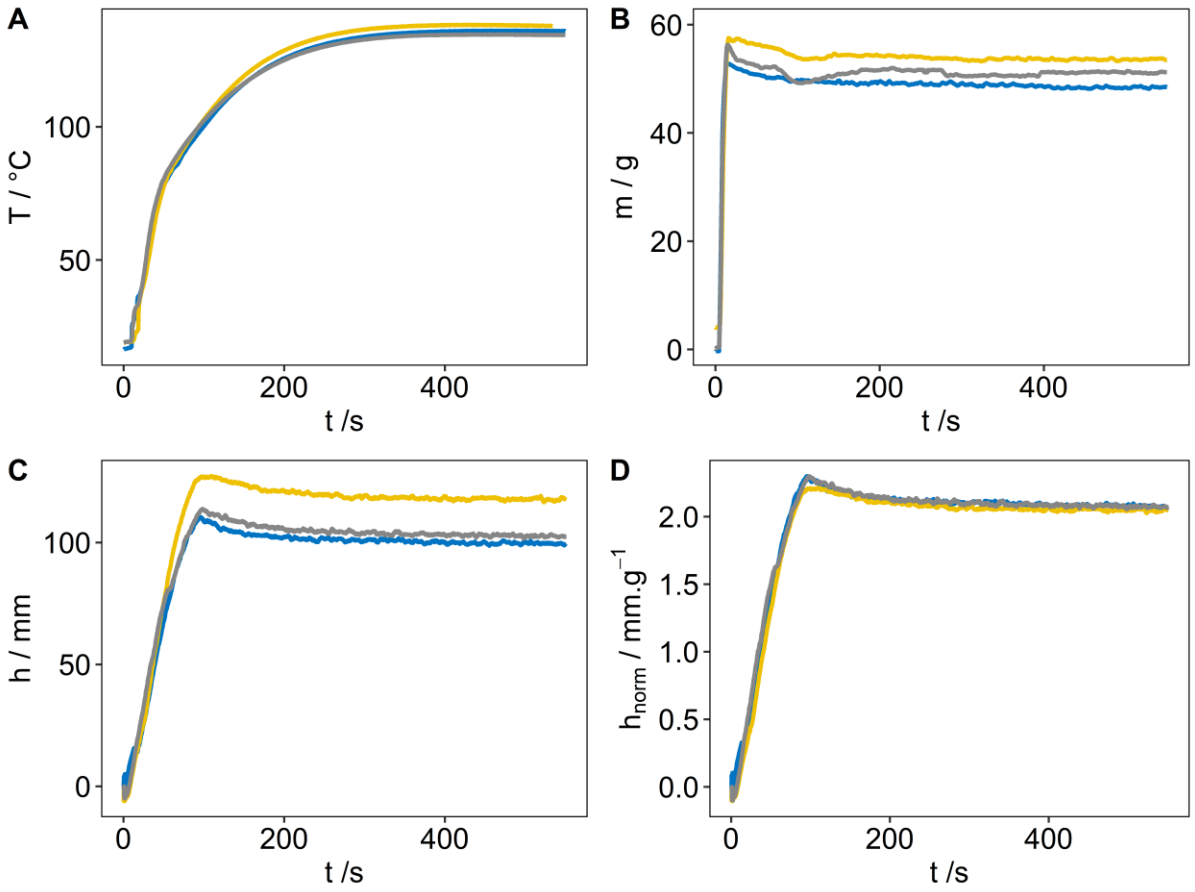

Figure 2.4: Replicate data for a single foam formulation. (A) Corrected temperature, (B) corrected mass, (C) corrected height and (D) height which has been normalised using the mass of reagent in the reaction vessel.

2.1.4.5. *Summary*

Adiabatic temperature rise is a proven method for measuring conversion of isocyanate in PUF reactions. Height and mass change data can be used in conjunction with temperature data to understand relative rates of the blowing and gelling reaction, and gain insight into cell opening. An inexpensive raspberry pi based system (FoamPi) was developed to record these properties. The FoamPi is able to record temperature and change in height accurately; however, due to drift the mass data was not usable. Further work into understanding the root cause of the mass drift may add useful insight into the cell opening time and should be investigated.

2.2. PUF Physical Properties

2.2.1. **Foam Preparation**

Post reaction all fPUF were left to cure for 1 week at room temperature in a fume hood before foams were cut. Cut foam was sampled as is with no further preparation. This post reaction curing allows for the fPUF to develop their ultimate physical properties[91].

2.2.2. **Density**

Density of the PU foams was measured according to ASTM D3574-11 Test A[92], whereby a block of dimensions 50 mm x 50 mm x 25 mm was cut from the core of the specimen. The block was free from external defects or voids. A digital Vernier calliper was used to accurately measure the dimensions of the cut foams. The sample was weighed and the density (ρ) was calculated in kg. m^{-3} using *Equation 2.9*.

$$\rho = \frac{m}{V} \times 10^6 \qquad 2.9$$

Where m is the mass of the sample (g) and V is the volume of the sample (mm^3).

2.2.3. **Cell Size**

Optical microscopy was performed on a Leica M125 C optical microscope. Foam samples were cut in the free rise direction of the foam and cut with a single edge razor blade to ensure a straight edge. This edge was then uniformly coated with a marker pen, without breaking additional cell walls. This was done to contrast cells in the plane against cells deeper in the sample. Magnification for all samples was done at 8x magnification. An example of a sample with and without marking is shown in Figure 2.5. The steps followed are in accordance with ASTM D3576-15[93].

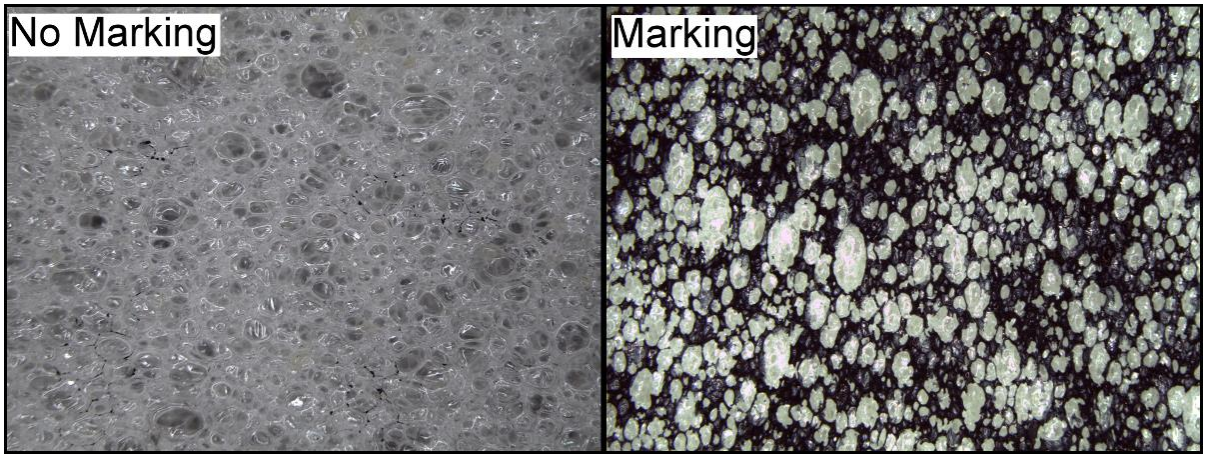

Figure 2.5: Optical microscopy images showing the importance of marking a fPUF sample to provide a single planar view of cells.

These images were then analysed in open source software ImageJ. The colour threshold algorithm was used on the images to reduce them to two colours. A watershed algorithm was then run on the image to complete incomplete cells. The average cell area was then calculated and assuming spherical cells an average diameter of the cell was calculated. At least 200 cells were counted for each sample. A raw image and an image after processing and cell counting is shown in Figure 2.6.

The area and apparent cell diameter were calculated from this data. These were then corrected according to *Equation 2.10*. This correction is necessary to account for the fact that the cells are randomly truncated with respect to their depth in the plane of the foam. The derivation of this equation is available in ASTM D3576-15[93].

$$d = (1.623)d' \qquad 2.10$$

Where d is the actual cell diameter (mm) and d′ is the apparent cell size (mm)

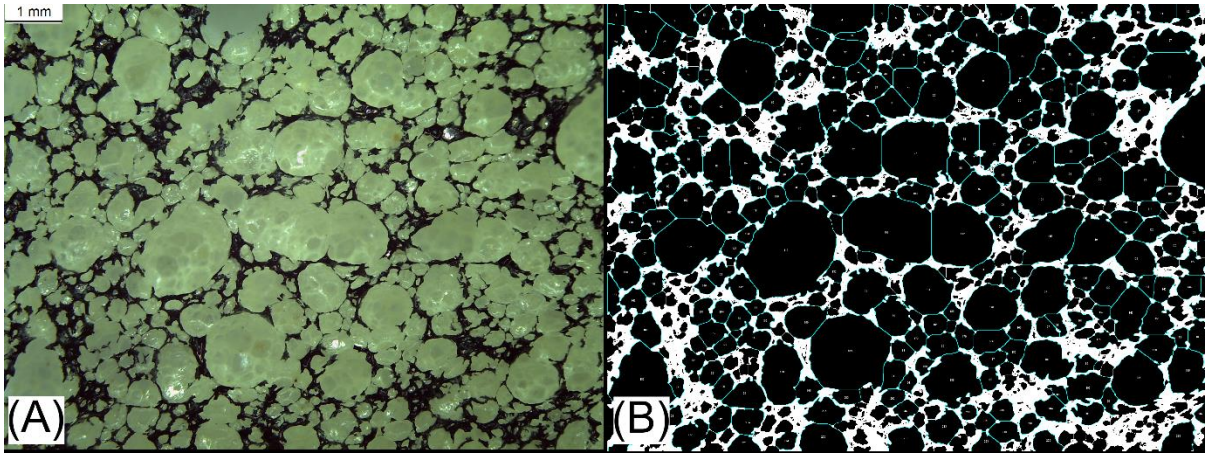

Figure 2.6: Optical microscopy image of a fPUF sample (A) as captured and (B) after thresholding and watershedding with a custom written ImageJ macro.

2.2.4. **Compression Force Deflection (CFD)**

CFD was determined using 50 mm x 50 mm x 25 mm blocks from the core of the foam. CFD was measured according to ASTM D3574-11 Test C[92] using a Zwick/ Roell Z0.5 with a 500 N load cell. The sample was preflexed twice to 75 % of its original thickness at a rate of 250 mm. min^{-1}. The sample was then left to rest for 6 ± 1 min. The compression foot was then brought in contact with the sample and a force of 140 Pa applied. The thickness of the sample was measured. The sample was then compressed to 50 % of this thickness at 50 ± 5 $mm.min^{-1}$, the final force was determined after 60 ± 3s and the CFD_{50} was calculated using *Equation 2.11* in kPa.

$$CFD_{50} = 1000 \times \frac{F}{A} \qquad 2.11$$

Where F is the force observed after 60 s (N) and A is the cross sectional area of the sample (mm^2).

2.2.5. **Water Holding Capacity (WHC)**

Cut samples used for density measurement were also used for water holding tests. Samples were fully submerged in water for 24 hours. After this time, samples were removed from the water and allowed to drain for 15 minutes on a porous metal rack. Samples were then weighed and a wet mass was obtained. The mass of water

retained was then reported as a function of 1 litre of substrate as is the norm in soil sciences. This was calculated using *Equation 2.12*.

$$WHC = \rho \frac{(m_{wet} - m_{dry})}{m_{dry}} \qquad 2.12$$

Where WHC is the water holding capacity ($g_{water}.l_{substrate}^{-1}$), m_{wet} is the foam wet mass (g), m_{dry} is the foam dry mass (g) and ρ is the density of the foam ($kg.m^{-3}$).

2.2.6. **Water Drop Penetration Time (WDPT)**

The WDPT is a test used in soil sciences to determine the hydrophobicity of soils. This involves placing a droplet of water on the soil surface and recording the amount of time taken for the droplet to penetrate the soil completely. For foam samples five drops of 1 % bromophenol blue (to increase optical contrast) were placed individually on the surface of the dry foam samples and the time was recorded for the drop to penetrate the foam surface completely. The foam could then be categorised according to the seven categories defined by Doerr[94] and shown in Table 2.3.

Table 2.3: Soil hydrophobicity categories defined by Doerr[94].

Descriptive Label	WDPT /s
Extremely hydrophobic	> 18000
Very strongly hydrophobic	3600 – 18000
Strongly hydrophobic	600 - 3600
Moderately hydrophobic	180 - 600
Slightly hydrophobic	60 - 180
Hydrophilic	5 - 60
Very hydrophilic	<5

2.2.7. **Air Filled Porosity**

Air filled porosity was calculated by subtracting the water porosity (calculated from the WHC) from the total porosity (calculated from skeletal density).

2.2.8. **PUF Airflow**

ASTM D3574-11 Test G[92] outlines a method for measuring the airflow through a PUF foam. Airflow measurement through the core of slabstock or moulded foam can be used as an indirect measurement of some cell structure features. Yasunaga *et al*[79] determined the effective number of open cells in a fPUF by scanning electron microscopy (SEM) and this correlated well with airflow measurements. This was true above a certain critical effective open cell fraction, approximately 0.08, below which airflow was effectively zero. They determined this threshold was close to the theoretical threshold calculated from percolation theory.

The standard test for measuring airflow through a fPUF involves mounting a 50 mm x 50 mm x 25 mm on top of a vacuum chamber, where a vacuum should be applied using blowers. A differential pressure of 125 Pa should be applied to the sample and the airflow rate should be measured (ASTM D3574-11 Test G[92]).

A simple digital airflow meter was designed and the majority of the parts were 3D printed at The University of Sheffield. All 3D printed parts were covered in a layer of silicone sealant as the 3D print was porous and allowed airflow through the plastic. An Adafruit MPRLS sensor was used to determine the pressure change in the vacuum chamber. A Sensirion SFM 3000 flow meter was used to determine airflow. These were connected to an Arduino Uno and a simple program was written using Arduino IDE to output pressure and airflow values. A 12 V variable power supply was used to vary the blower speed and therefore pressure in the vacuum chamber. Figure 2.7 shows the component and airflow meter.

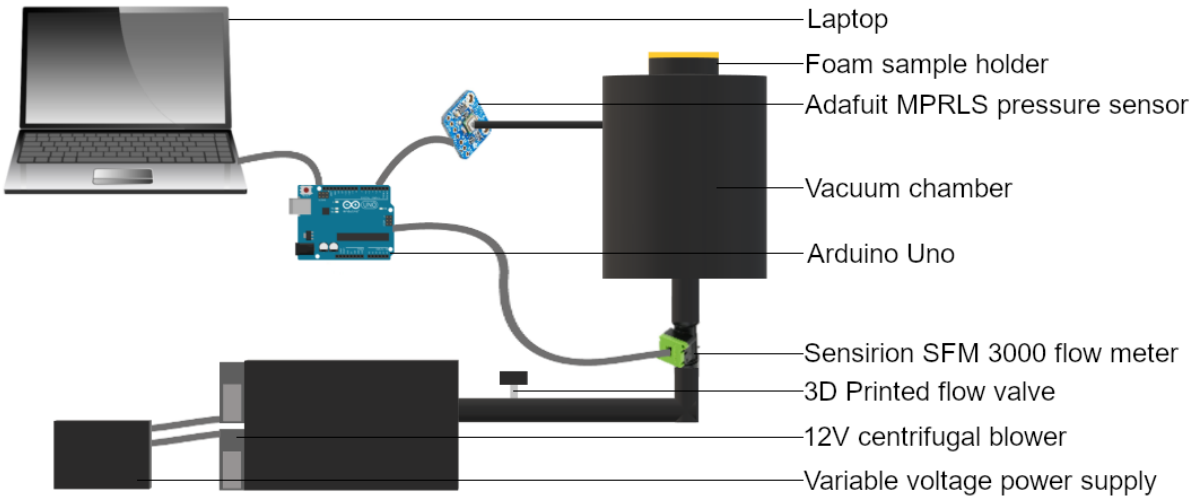

Figure 2.7: A schematic diagram of the 3D printed Arduino controlled airflow meter, using a Sensirion SFM3000 flow meter and Adafruit MPRLS pressure sensor for measuring air flow and pressure respectively.

The airflow meter and the relation between airflow and fPUF open cell fraction was validated by viewing the foams using scanning electron microscopy and determining the effective fraction of open cells. Cells were classified into four different stages, fully open, partially open, pinhole and closed as shown in Figure 2.8 and the effective number of open cells was calculated using Equation *2.13*. This is the same method used by Yasunaga *et al*[79] in their study of cell opening.

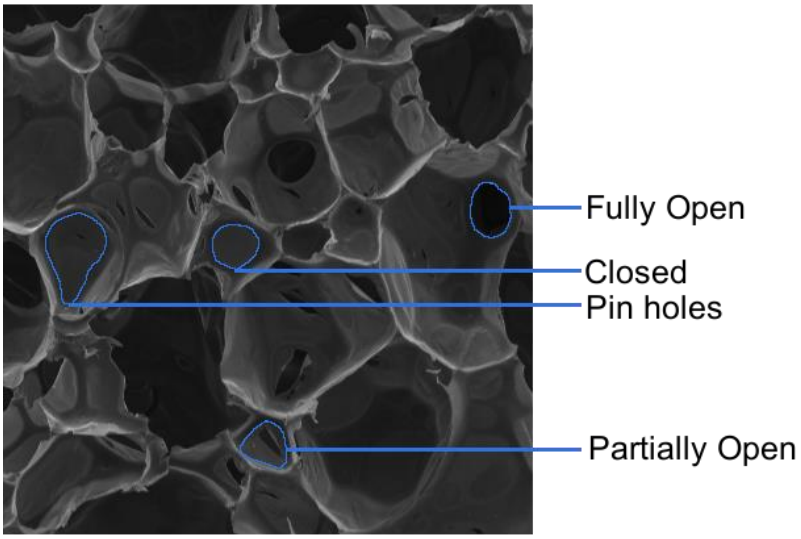

Figure 2.8: Classification of fPUF cell windows from SEM image for determining the effective fraction of open cells. Windows with approximately 50% of the area open or less were classified as partially open.

$$P_{eff} = \frac{N_{open} + 0.5N_{part}}{N_{open} + N_{part} + N_{pin} + N_{closed}} \qquad 2.13$$

Figure 2.9 (A) shows that airflow through the fPUF from the 3D printed Arduino controlled airflow meter correlates well to the effective fraction of open cells with a linear fit having an $r^2 = 0.92$. There is also a threshold minimum fraction of open cells required for there to be any airflow through the foam and this is 0.10. This result is in agreement with Yasunaga *et al*[79] who had a threshold fraction of open cells of 0.08 before any airflow registered. They also calculated the minimum fraction of open cells required for airflow from percolation theory as 0.091 (assuming pentagonal dodecahedron shape cell and that cell windows break randomly). Our observed value is close to this calculated minimum.

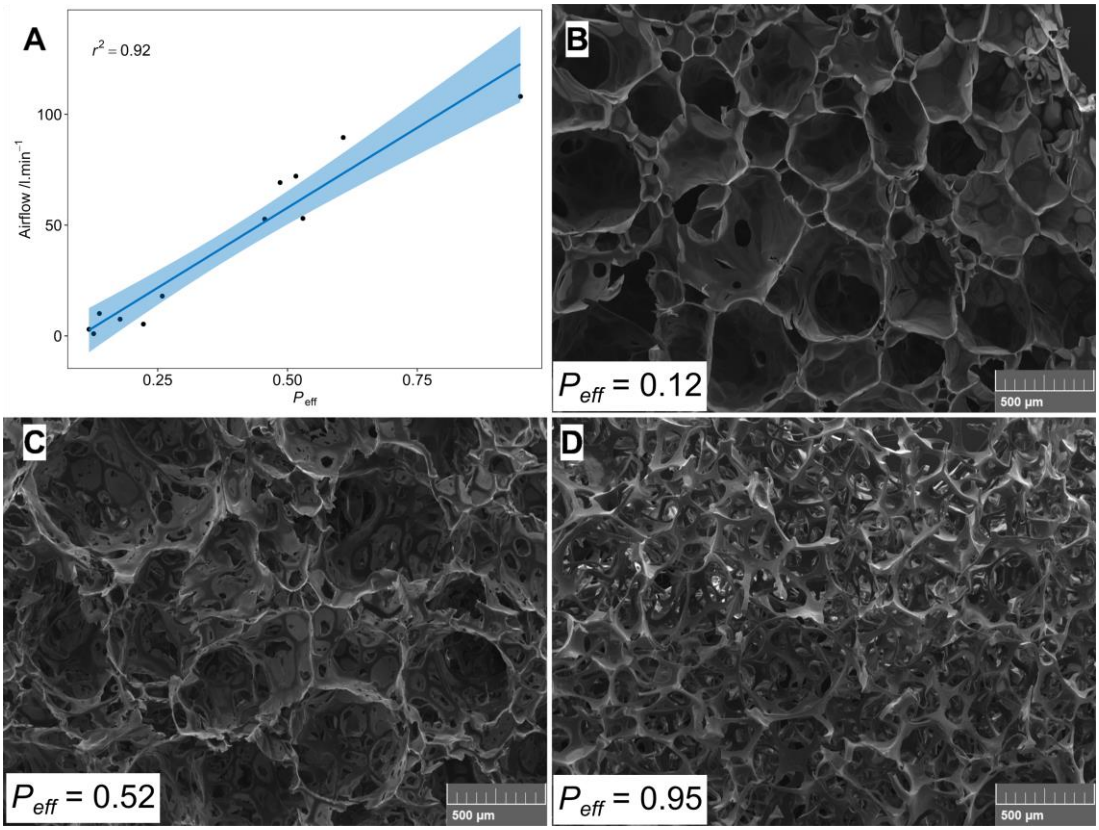

Figure 2.9: (A) Airflow measurements from the 3D printed airflow meter as a function of the effective fraction of open cells (P_{eff}), airflow increases with the fraction of open cells, however below $P_{eff} = 0.10$ there is no airflow. (B) An example fPUF SEM micrograph with majority closed cells ($P_{eff} = 0.12$). (C) An example fPUF SEM micrograph with many partially open cells ($P_{eff} = 0.52$). (D) An example fPUF SEM micrograph with mostly open cells ($P_{eff} = 0.95$).

2.2.9. **Statistical Analysis**

All statistical analysis and graph plotting was done in Rstats[95]. Where appropriate significance between treatments were analysed using 1-way ANOVA, followed by Tukey multiple comparison test.

2.3. PUF Chemical Properties

2.3.1. **Cation Exchange Capacity (CEC)**

CEC is an important indicator for the capacity for soils to buffer nutrients in the media matrix. The CEC for foams was determined using the spectrophotometric method described by Amman *et al*[96]. In this method a large chelated copper complex, $[Cu(Trien)]^{2+}$ is used to replace all interlayer ions in a clay. The remaining $[Cu(Trien)]^{2+}$ ions in the exchange solution can then be determined by UV vis spectrophotometry and the CEC of the foam can be calculated.

A 0.01 mol solution of $CuSO_4$ was made up, by dissolving 2.50 g of $CuSO_4.4H_2O$ in 1000 ml of deionised water. 1.46 g of triethylenetetramine was added to this solution and allowed to react for 1 hour even though the reaction was visible instantly (solution changing to a dark blue colour). The 0.01 mol solution of the $[Cu(Trien)]^{2+}$ solution was used for exchange experiments.

100 mg (more if CEC was expected to be low) of foam was added to a 10 ml sample vial. 8 ml of the $[Cu(Trien)]^{2+}$ was added to this sample. Vials were placed on a shaker for 30 minutes and then either centrifuged at 4000 RPM for 10 minutes or filtered and the supernatant/ filtrate were kept for analysis. 3 ml of supernatant/ filtrate were transferred to an appropriate cuvette. Absorption was measured at 577 nm on a Varian Cary 50 Probe UV vis spectrophotometer[97].

The CEC was then calculated in $cmol_c.kg^{-1}$ using *Equation 2.14*.

$$CEC = 2 \times 100 \times \frac{(C_0 - C_s)V}{m_s} \qquad 2.14$$

Where C_0 is the initial $[Cu(Trien)]^{2+}$ concentration ($mol.l^{-1}$), C_s is the $[Cu(Trien)]^{2+}$ concentration determined by UV vis ($mol.l^{-1}$), V is the volume of solution reacted (l) and m_s is the mass of foam/clay sample (kg). We multiply by two as $[Cu(Trien)]^{2+}$ has a charge of 2 and multiply by 100 to get to the standard unit of $cmol_c.kg^{-1}$. All samples were done in triplicate and the mean CEC as well as standard error are reported.

2.3.2. **Statistical Analysis**

All statistical analysis and graph plotting was done in Rstats[95]. Where appropriate significance between treatments were analysed using 1-way ANOVA, followed by Tukey multiple comparison test.

2.4. Plant Growth Properties

2.4.1. **Survivability**

Plant deaths were noted during the growth trial and plotted using a Kaplan-Meier survivability curve[98]. This is defined as the probability of the plant surviving in a given amount of time, while considering several small time intervals. Separate treatments were compared pairwise using the log rank test, which tests the null hypothesis that there is no difference between the two populations' survivability curves.

2.4.2. **Plant Height**

Plant height was measured twice a week as well as at the end of the trial. The area under the height curves (AUC) was determined by fitting exponential growth curves to the height data for individual plants and integrating the area underneath each of these fitted curves.

2.4.3. **Plant Shoot Mass**

The above ground plant mass (shoots) was harvested and weighed to determine the shoot wet mass. Shoots were dried at 70 °C for five days before being weighed and analysed as shoot dry mass. Although root mass was also of interest the nature of fPUF growing media does not allow for collection of roots. The foams are a single polymer network where plant roots grow into the porous cellular region of the foam, this connectivity of the roots and substrate make it impossible to retrieve the roots without damaging them. Wet shoot mass, dry shoot mass as well as the percentage water is reported.

2.4.4. **Plant Greenness**

Chlorophyll, the green plant pigment, is the essential element of photosynthesis, the process of converting light and CO_2 into usable sugars. The entire process of photosynthesis is based on chlorophyll levels within the plant cells, and therefore by monitoring its levels we can determine plant productivity[99]. Changes in chlorophyll levels are also one of the most obvious signs of plant stress[100] and chlorophyll content can change due to many biotic and abiotic factors. Some examples of this in tomatoes include a decrease in chlorophyll content due to salt stress[101], due to the combination of heat and drought stress[102] as well as due to nutrient deficiency[103]. It was of interest to determine whether growth media physical and chemical properties influenced plant health and whether this changed over time. A non-destructive test monitoring chlorophyll content was therefore required.

2.4.4.1. *Measuring plant greenness*

The easiest method for measuring chlorophyll in a non-destructive manner is the use of a Soil Plant Analysis Development (SPAD) chlorophyll meter. The SPAD meter measures a difference in light absorbance between 650 nm and 940 nm and generates a SPAD value. The absorbance is measured in the red region (650 nm) as this is where strong chlorophyll absorption takes place and the near infrared region (940 nm) is measured to determine differences in leaf structure. Several studies have shown good correlation between SPAD values and plant health indicators such as N nutrition

index, plant N concentration and chlorophyll levels[104–106]. Reproducibility and usability of SPAD readings are however affected by many factors including plant growth stage, leaf thickness, leaf position and measurement point on the leaf[107]. It was therefore decided that a method that analysed the entire plant would be more appropriate.

A substantial amount of work has been reported in the literature correlating plant chlorophyll levels to RGB values obtained using optical photography or scanning. This has been done on a variety of plant species, including potato[108], wheat[109], amaranth and quinoa[110].

A standard method has been developed for estimating chlorophyll content in *Arabidopsis* seedlings from RGB data[111] and this will be used as a framework for estimating chlorophyll content of crops of interest. The methodology involves photographing the plant material, using a colour checker chart to normalise between different cameras and lighting conditions and then uses a model to fit RGB colour data to chlorophyll extraction data.

Photos were taken with a Nikon D60 camera, with a F-stop of f/3.5, an iso speed of ISO-100 and the exposure time was varied to keep the lighting conditions as similar as possible throughout experiments. All photos were shot in sRGB colour space. A Datacolor SpyderCHECKR 24 colour card was included in each photo for colour calibration and correction. Photos were taken once a week during plant growth trials.

Due to the number of samples and photographs an automated method was required for colour correction and plant thresholding. This required automatic recognition of the Datacolor SpyderCHECKR 24 colour card, automatic correction of the image and automatic thresholding of the image, selecting only for plant shoot matter in the image. Python 3.6[90] was used for image analysis. The RGB values of the corrected, threshold image were then used to fit a model to chlorophyll data, as discussed below.

Identification

Colour checker identification was handled using an existing python package (colour_checker_detection)[112]. This worked well on images where the colour checker

was positioned in the same orientation as the photo, however it struggled to identify all of the swatches within the colour checker. Figure 2.10 (A) shows the automatic identification of the colour checker and swatches and shows some unidentified swatches. This example also shows a swatch being identified twice. Identification of the missing swatches was based on the fact that the colour corrector chart was identified correctly every time and the fact that the colour corrector chart was always in the same orientation (six swatches high and four swatches wide). A mask was generated for the known area of the colour checker as well as the identified swatches. The missing swatches were then identified by splitting the colour checker into 35 blocks and determining whether there was an identified swatch at the centre of each block. If no swatch was identified it was assumed that colour_checker_detection missed it and a new swatch was added to the mask, 15 pixels by 15 pixels in size. Figure 2.10 (B) shows the colour checker split into 35 blocks for identification of missing swatches and (C) shows the final mask used for obtaining RGB values.

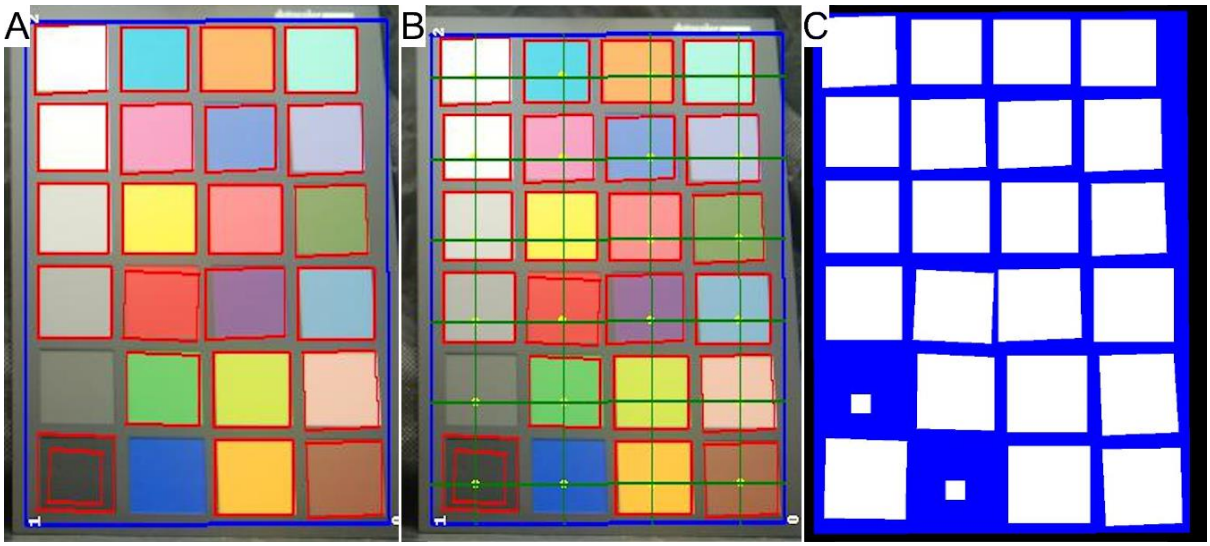

Figure 2.10: Automatic identification of the colour checker and swatches.(A) colour checker (blue) and swatches (red) identified by colour_checker_detection (B) colour checker split into 35 blocks for identification of missing swatches and (C) final mask with all swatches identified, used for RGB correction.

Correction (error reduction)

An average RGB value was taken over the area of each swatch to minimise error. A matrix of equations in the form of *Equation 2.15* were used to minimise the error

between swatch reference colour and photographed colour. Linear regression minimised the average error over all 24 swatches by varying the 18 (6 for each colour channel) correction constants. The error was calculated for each swatch as well as the average error per swatch using *Equation 2.16* and *2.17*[113]. These correction constants were used to correct the image on a pixel by pixel base, using *Equation 2.15*.

$$CC_{Corr} = \beta_{1,CC}R_i + \beta_{2,CC}G_i + \beta_{3,CC}B_i + \beta_{4,CC}R_i^2 + \beta_{5,CC}G_i^2 + \beta_{6,CC}B_i^2 \qquad 2.15$$

Where CC_{corr} is the corrected colour channel (R, G or B) value, β is the correction constants for each channel, and R_i, G_i and B_i are the observed red, blue and green values for each colour swatch.

$$\Delta RGB_i = \sqrt{(R_{ref,i} - R_i)^2 + (G_{ref,i} - G_i)^2 + (B_{ref,i} - B_i)^2} \qquad 2.16$$

$$\varepsilon = \sum_{i=1}^{N} \frac{\Delta RGB_i}{N} \qquad 2.17$$

Where ΔRGB_i is the error between the reference swatch and the photographed swatch, ε is the average error per swatch and N is the total number of swatches.

The average error ε was decreased from a value of 69.6 ± 0.400 to 16.2 ± 0.0546 using this method. This reduction of error was deemed sufficient for chlorophyll extraction and more complex correction models were not tested. Figure 2.11 visualises this reduction in error, showing the distance in RGB space between swatches in the (A) raw image (no correction) and the reference swatches and (B) shows the distances between the corrected swatches and the reference swatches. Figure 2.12 shows an example of (A) a raw colour chart, (B) the corrected colour chart as well as the (C) reference colour chart used for developing the colour correction constants.

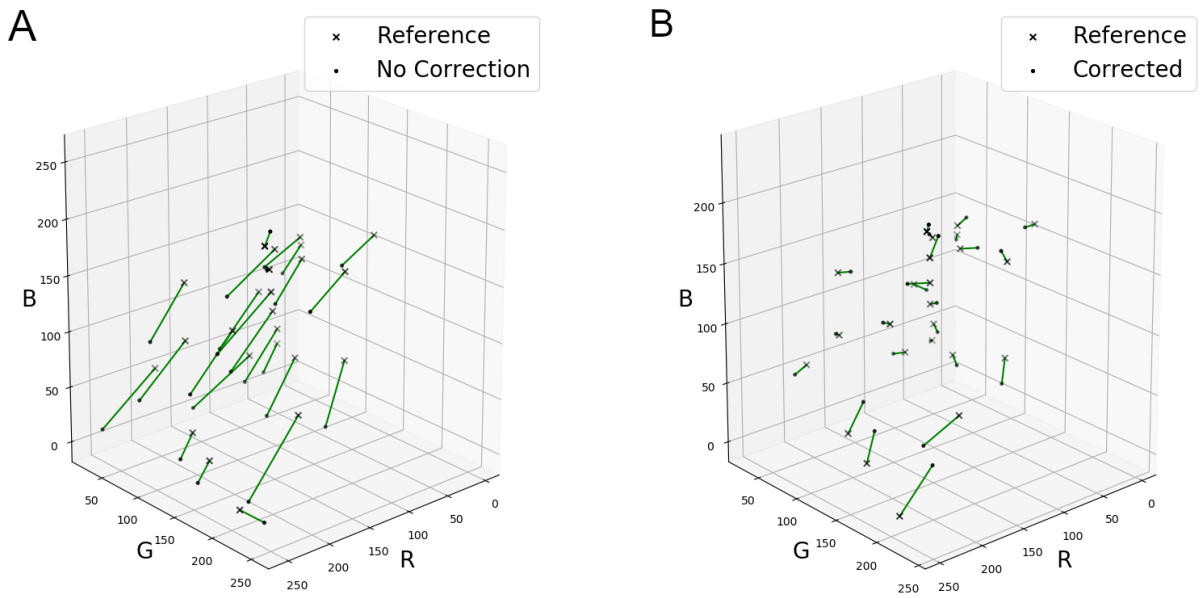

Figure 2.11: (A) The difference between the 24 reference swatches and the raw swatches in RGB colour space and (B) the difference between the 24 reference swatches and the corrected swatches in RGB colour space.

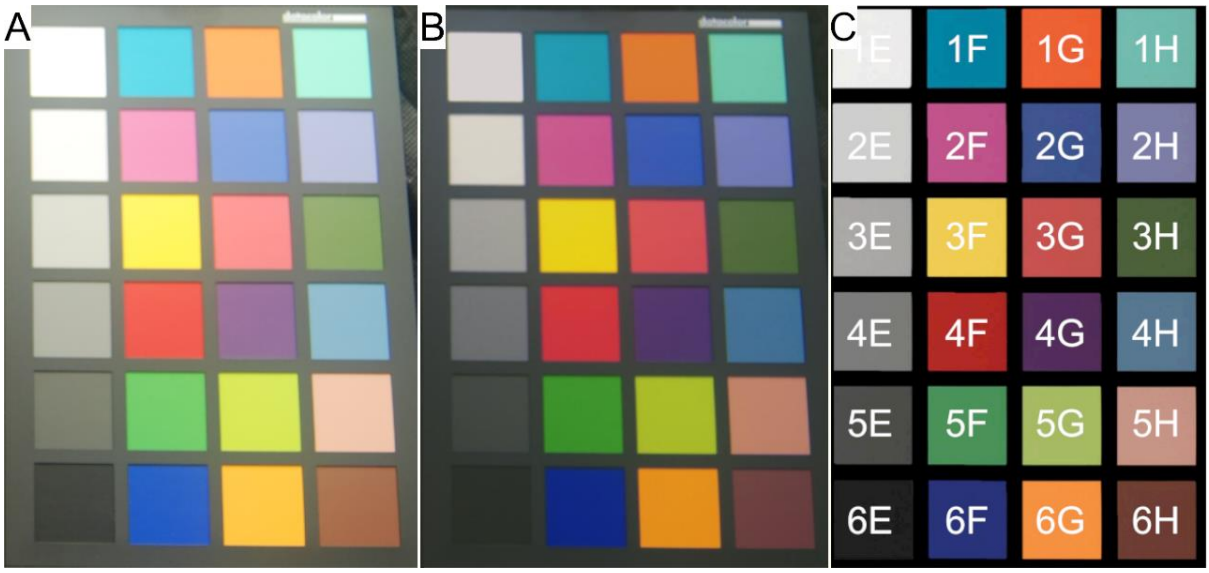

Figure 2.12: (A) An uncorrected colour checker, (B) corrected colour checker and (C) reference colour checker.

The colour correction chart was blacked out for image thresholding. Figure 2.13 shows a raw image for chlorophyll approximation (A) and Figure 2.13 (B) the corrected image, with the colour corrector blacked out.

Thresholding

Woebbecke *et al*[114] tested 5 different colour vegetative indices to distinguish living plant material from background material and soil. Excess greenness (ExG) proved to provide near binary images, between living plant matter and background. ExG is calculated using *Equation 2.18* and normalised chromatic coordinates determined using *Equation 2.19*.

$$ExG = 2g - r - b \qquad 2.18$$

Where r, g and b are the normalised chromatic coordinates calculated as follows

$$r = \frac{R}{R + G + B}, g = \frac{G}{R + G + B} \text{ and } b = \frac{B}{R + G + B} \qquad 2.19$$

and R, G and B are colour coordinates in the raw image.

A further index, excess redness (ExR) was defined by Meyer and Neto[115] and was used with ExG to further improve on this thresholding technique. ExR is calculated according to *Equation 2.20*. Excess greenness minus excess redness (ExG – ExR) performed the best of their thresholding indexes. This index worked exceptionally well for naturally lit single plants with different soil backgrounds.

$$ExR = 1.4r - g \qquad 2.20$$

Following this methodology led to excellent results with spring onion trials, producing near binary images separating plant matter. A threshold index value (ExG - ExR) of 0.3 was used to threshold the image. Figure 2.13 (C) shows a result from application of this thresholding technique.

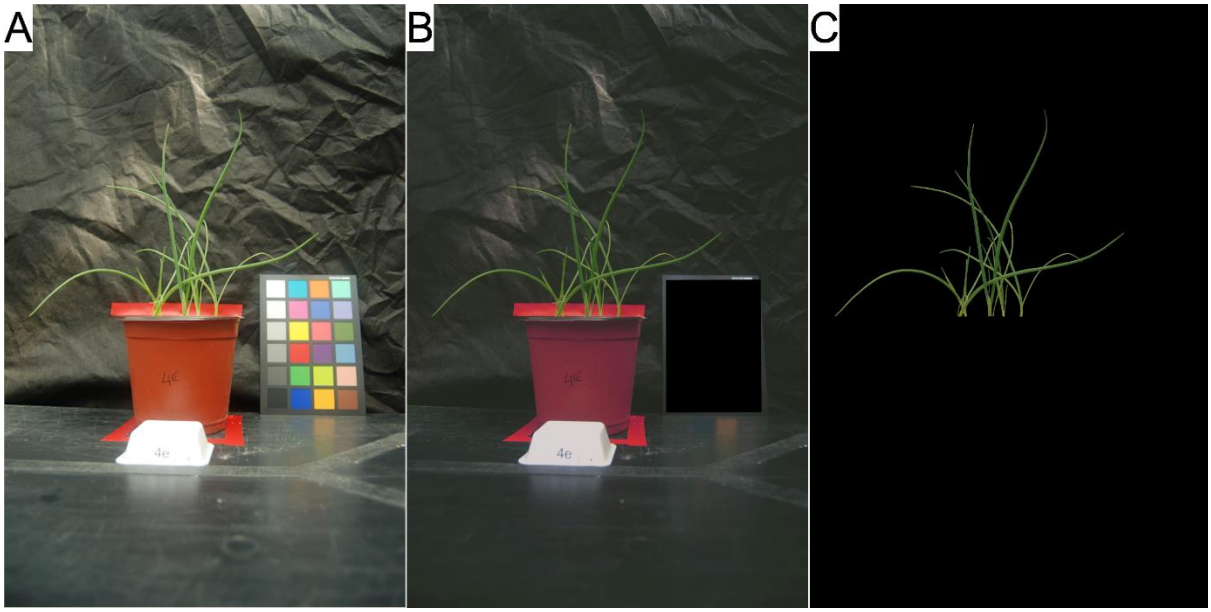

Figure 2.13: (A) Raw image for chlorophyll approximation, (B) colour corrected image, (C) threshold image showing the leaf matter used to extract RGB data.

2.4.4.2. *Chlorophyll Extraction*

Chlorophyll was extracted from the youngest leaves and chlorophyll content was determined using UV-Vis spectrophotometry. 70 -100 mg of fresh leaf matter was ground to a paste with a pestle, with 3 ml of 80 % acetone solution. This turbid paste was transferred to a centrifuge tube. A further 1.5 ml of 80 % acetone was used to rinse the mortar and pestle and the final solution was brought up to 5 ml with 80 % acetone[116]. Chlorophyll extraction was allowed to take place in the dark overnight. Vials were then centrifuged at 4000 RPM for 10 minutes and absorption of the supernatant was taken. Absorption was measured at 646 nm and 663 nm and the chlorophyll content was calculated according to *Equation 2.21*, *Equation 2.22* and *Equation 2.23*[117].

$$C_a = 12.21A_{663} - 2.81A_{646} \qquad 2.21$$

$$C_b = 20.13A_{646} - 5.03A_{663} \qquad 2.22$$

$$C_t = C_a + C_b \qquad 2.23$$

Where C_a is the amount of chlorophyll *a*, C_b is the amount of chlorophyll *b* and C_t is the amount of total chlorophyll (all in $\mu g.ml^{-1}$). A_{663} and A_{646} is the absorption at specific wavelengths.

2.4.4.3. *RGB - Chlorophyll model selection*

Riccardi *et al*[110] found that that the exponential function, *Equation 2.24,* led to the best correlation between total chlorophyll to the RGB colour bands in quinoa and amaranth leaves. This equation has also been used to correlate RGB colour bands to total chlorophyll in Arabidopsis plants with good results[111].

$$C_t = e^{(\beta_1 R + \beta_2 G + \beta_3 B + \beta_4)} \qquad 2.24$$

Photographs were taken of spring onion samples, and the same samples had chlorophyll content determined spectrophotometrically. The corrected RGB colour bands were fitted to *Equation 2.24*. Figure 2.14 shows the predicted and actual chlorophyll content. The fit has a $r^2 = 0.75$ which is close to the $r^2 = 0.81$ value found in the arabidopsis study[111]. The slightly lower value may be due to the spring onion samples being done on a mass basis instead of an area basis. The variable thickness of spring onion leaves, sampled from different parts of the plant may have reduced the model's accuracy.

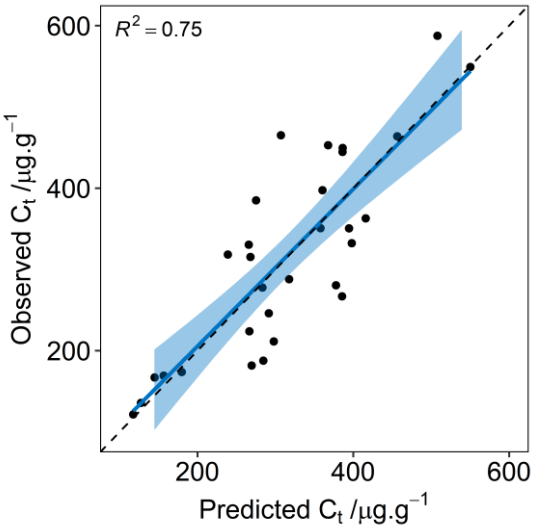

Figure 2.14: Predicted and observed chlorophyll content of spring onions using RGB colour bands, the dashed line shows the y = x line.

2.4.5. **Plant Chemical Composition**

For chemical composition plant tissues were dried at 70 °C and homogenised in a mortar and pestle to a size of < 1 mm. The homogenised samples were dried further at 70 °C until a constant mass was recorded and were stored in a desiccator until required.

2.4.5.1. *Phosphorous Content*

Phosphorous content in plant tissues can be determined spectrophotometrically by acid digesting samples and reacting the digested sample with an acidic molybdate solution in the presence of ascorbic acid, which forms and reduces a phosphomolybdic acid[118].

50 mg of dried tissue samples were digested in 1 ml of concentrated sulphuric acid at 350 °C for 15 minutes. 500 µl of hydrogen peroxide was added and the samples were reheated at 350 °C until the H_2O_2 had fully decomposed into water and O_2[119]. Samples were removed from the heat and left to cool in the fumehood overnight. 9 ml of deionised water was added taking the volume up to 10 ml.

The developer solution consisted of a 0.0078 mol solution of ammonium molybdate made up by dissolving 4.8g of $(NH_4)6Mo_7O_{24}.4H_2O$ in 200 ml of 2 M sulphuric acid solution and a 0.00062 mol solution of antimony potassium tartrate made up by dissolving 0.1 g of $C_6H_4O_7SbK$ in 100 ml of 2 M sulphuric acid solution. These solutions were added together and brought to a final volume of 500 ml using deionised water. A 0.1 mol solution of L-ascorbic acid was made by dissolving 0.88 g of $C_6H_8O_6$, in 50 ml deionised water[120].

0.05 ml of acid digest sample was added to a polystyrene cuvette, and the digested sample was neutralised using 0.05 ml of a 3.44 M sodium hydroxide solution. 0.5 ml of the developer solution and 0.2 ml of the ascorbic acid solution were added. This was made up to 3.8 ml using deionised water and allowed to develop for 45 minutes. Absorption was measured at 882 nm on a Cecil 1020 spectrophotometer.

The sample's phosphorus concentration was calculated using a standard calibration curve, constructed using known concentrations of sodium dihydrogen orthophosphate ($NaH_2PO_4.H_2O$) and is reported in mg P per gram dried shoot.

2.4.5.2. *Nitrogen Content*

Nitrogen content was also determined spectrophotometrically using the same sulphuric acid and hydrogen peroxide digestion procedure as that used for phosphorus determination. Organic nitrogen is reduced to ammonia during this digestion, as is the majority of nitrate, with some loss of nitrate. However the amount of nitrate in plant leaves when compared to the amount of organic nitrogen is low, meaning this loss is negligible[121]. Samples were neutralised and diluted by adding 0.5 ml of 3.44 M sodium hydroxide and 9 ml of deionised water to 0.5 ml of the digested sample.

Nitrogen determination required the use of two solutions, A and B. The A part solution consisted of 20 g of trisodium citrate, 17 g of salicylic acid, 5 g of sodium hydroxide and 0.2 g of sodium nitroprusside, dissolved in 500 ml of deionised water. The B part solution consisted of 0.4 g of sodium dichloroisocyanurate and 5 g of sodium hydroxide dissolved in 500 ml of deionised water[122].

0.05 ml of diluted acid digest sample was added to a polystyrene cuvette. 1 ml of solution A and 0.25 ml of solution B were added to the cuvette. This was made up to 3.8 ml using deionised water and allowed to develop for 30 minutes. Absorption was measured at 650 nm on a Cecil 1020 spectrophotometer.

The sample's nitrogen concentration was calculated using a standard calibration curve, constructed using known concentrations of ammonium chloride (NH_4Cl) and is reported in mg N per gram dried shoot.

2.4.6. **Statistical Analysis**

All statistical analysis and graph plotting was done in Rstats[95]. Plant survivability analysis used the survival and survminer R packages to determine, plot and analyse the Kaplan-Meier survivability curve. Differences between treatment means of plant height and greenness were analysed by repeated measures analysis of variance (ANOVA) and differences between treatment means (AUC, aboveground biomass, as well as chemical composition) were analysed by 1-way ANOVA, followed by Tukey multiple comparison test.

Chapter 3:
Raw Material Characterisation
and
PUF formulation

3.1. Characterisation of Isocyanate

One isocyanate was used for this study. SpecFlex NE 112, a polymeric MDI with low functionality used in the production of flexible slabstock and moulded foam. The DOW Chemical Company supplied this product.

3.1.1. **End Group Analysis**

The equivalent weight of the isocyanate used, SpecFlex NE 112, was determined according to ASTM D2572-19. Isocyanate is reacted with an excess of secondary amine, which converts the isocyanate to urea, and the remaining amine can be back titrated with an acid. For this a solution of dibutylamine in butan-2-one (3 % v/v) was added to a 250 cm^3 conical flask containing the isocyanate. Triplicate blank samples were also prepared. After 30 minutes, 25 cm^3 of isopropanol was added and a few drops of bromocresol green indicator were added. The mixture was titrated to a straw yellow end point with a 0.1 M solution of hydrochloric acid. The isocyanate equivalent weight was calculated using *Equation 3.1*. The average blank titre was 43.5 cm^3.

$$E_n = \frac{1000 \times g\ sample}{M \times (B - A)} \qquad 3.1$$

Where B is the average ml of HCl solution consumed in the blank flasks, A is the HCl solution consumed by the sample in ml and M is molarity of the HCl solution.

Table 3.1 shows the calculated equivalent weight of the Specflex NE 112, this correlates closely with the published value of 130 $g.mol^{-1}$. This calculated value was used for all further foam formulation.

Table 3.1: Equivalent weight of Specflex NE 112 from end group analysis

Sample Mass /g	Titre /cm^3	E_n /$g.mol^{-1}$
0.305	20.4	132.2
0.319	19.1	130.7
0.329	18.2	129.8
0.339	18.0	132.7
0.337	18.6	135.2
Mean ± SE		**132.1 ± 0.93**

3.2. Characterisation of Polyols

Three polyols were used for this study. Voranol 3322, a high propylene oxide content polyether polyol. It is a general purpose, nominal 3400 molecular weight triol used in the production of slabstock fPUF. Voranol 1447, a high ethylene oxide content polyether triol, designed for the production of soft and hypersoft flexible slabstock foams. It is also a highly efficient cell opener. Specflex Activ 2306 is a novel autocatalytic polyol formed by an alkoxide polymer initiated from an amine resulting in a tertiary amine centered polyether polyol. It is designed for the reduction or complete removal of amine catalysts in fPUF formulations. This is important for applications, which require low volatile organic compound (VOC) emissions. All three polyol products were supplied by The DOW Chemical Company.

3.2.1. **End Group Analysis**

The hydroxyl number and equivalent weight of the polyols was determined according to ASTM D4274-16 test method E[123]. The hydroxyl is reacted with an excess of acid anhydride, to form an ester, the excess anhydride is then hydrolysed to acid and can be back titrated with an with a base. Duplicate samples of polyol were weighed (between 8 g and 15 g, depending on estimated equivalent weight) into 250 cm^3 round bottom stoppered flasks. Two blank samples were also prepared. 40 ml of pyromellitic dianhydride (PMDA) reagent (51 g PMDA dissolved in dry dimethyldiamide, DMF, to a volume of 1000 ml) was added to each of the flasks, and then 10 ml of imidazole (IMDA) reagent (105 g PMDA dissolved in dry DMF to a volume of 1000 ml) was added. The flasks were stoppered and the solutions mixed by swirling. 2 drops of DMF were added to the flasks and they were heated in a water bath for 15 minutes at

75 °C. 75 ml of water were added to each of the flasks, which were swirled to mix and 10 ml of thymolphthalein indicator solution (10 g thymolphthalein dissolved in distilled water to a volume of 1000 ml) was added and the flasks were titrated with a 0.5 N solution of sodium hydroxide to a pale blue end point. The hydroxyl number of the polyols were calculated using *Equation 3.2*. The average blank titre was 71.6 cm^3.

$$\text{Hydoxyl Number (OH)} = \frac{(B - A) \times N \times 56.1}{\text{g sample}} \qquad 3.2$$

Where B is the average ml of NaOH solution consumed in the blank flasks, A is the amount of NaOH solution consumed by the sample in ml, N is the normality of the NaOH solution and 56.1 is the equivalent weight of KOH, $mg.meq^{-1}$.

Table 3.2 shows the calculated OH numbers as well as the equivalent weight (molar mass per mole of functional group), calculated by dividing the equivalent weight of KOH by the OH number of the polyol. The OH numbers for the two common polyols, Voranol 1447 and Voranol 3322, correlate closely to the published values, which are 36 $mg_{KOH}.g^{-1}$ and 48 $mg_{KOH}.g^{-1}$ respectively. The equivalent weights calculated for the polyols were used for all further formulation calculations.

Table 3.2: Hydroxyl number and equivalent weights of polyols from end group analysis.

Sample	Sample Mass /g	Titre /cm^3	OH Number /$mg_{KOH}.g^{-1}$	E_n /$g.mol^{-1}$
Voranol 1447	11.25	57.4	35.4	1584
	11.24	56.5	37.7	1488
Mean ± SE			**36.5 ± 1.14**	**1537 ± 47.88**
Voranol 3322	8.77	56.6	48.0	1169
	8.79	56.8	47.2	1188
Mean ± SE			**47.6 ± 0.374**	**1179 ± 9.252**
Specflex Activ 2306	14.74	54.1	33.3	1685
	14.74	56.3	29.1	1927
Mean ± SE			**31.2 ± 2.09**	**1805 ± 121.1**

3.2.2. **Ethylene Oxide Content**

Ethylene oxide content of polyols was determined according to ASTM D4875-11 test method A[124]. A few drops of polyol were added to deuterated chloroform to make 1 ml of an approximately 10 % polyol solution. A drop of trifluoroacetic acid was added to this solution, which was mixed well and added to a NMR tube. The ^{1}H NMR spectra (5 to 0 ppm) of this mixture was then taken on a Bruker AV 400 MHz instrument.

Chemical shifts for the propylene oxide (PO) methyl proton resonances range from about 0.6 to 1.6 ppm (area A) and chemical shifts for the ethylene oxide (EO) and propylene oxide methylene and methane protons range from about 2.8 to 4 ppm (area B). The EO content was determined by integrating the area of these two ranges and comparing the ratio of the two using *Equation 3.3*.

$$EO = \frac{33 \times Z}{33 \times Z + 58} \times 100 \qquad 3.3$$

Where Z is (Area B/ Area A) – 1, 33 is the grams of EO per mole after weighting for the number of EO protons vs PO protons and 58 is the grams PO per mole.

Table 3.3 shows the ethylene oxide content for the analysed polyols. Voranol 1447 has the highest EO content, which agrees with the supplier's statement that 1447 is a high EO content polyether triol for production of hypersoft flexible slabstock foams. Voranol 3322 is a general purpose heteropolymer triol used in the manufacture of slabstock foams and has the lowest EO content. The catalytic polyol, Specflex Activ 2306 has an EO content of 21.9 %.

Table 3.3: Ethylene oxide content of polyols from NMR.

Sample	EO content /%
Voranol 1447	73.2
Voranol 3322	13.2
Specflex Activ 2306	21.9

3.3. Polyurethane Foam Formulations

The individual component loadings for all formulations were calculated, as is the standard in polyurethane foams, whereby loadings are expressed as a part per hundred polyol (PPHP), by weight. In this practice, total loading of polyols is designated as 100 and all other components are expressed as a percentage of this. An example fPUF formulation from an industrial guidebook for flexible polyurethane foams[69] is shown in Table 3.4.

Table 3.4: An example fPUF formulation[69].

Component	Loading (PPHP)
Polyol	100
MDI	40 - 80
Water	3 - 4.5
Surfactant	0.3 - 1.2
Amine Catalyst	0.1 - 0.7
Tin Catalyst	0 - 0.3

For all experiments, a stoichiometric ratio (r) of 1.05 was used. This ratio is the ratio of isocyanate used, compared to the amount of isocyanate needed to fully react with all available active hydrogens. This is show in *Equation 3.4.*

$$r = \frac{[NCO]}{[NCO_{eq}]} \qquad 3.4$$

Where [NCO] is the loading of isocyanate used in PPHP and $[NCO_{eq}]$ is the loading of isocyanate required to react with all active hydrogens. $[NCO_{eq}]$ is calculated using *Equation 3.5*.

$$[NCO_{eq}] = \sum \frac{En_i}{L_i} \qquad 3.5$$

where En_i is the equivalent weight of each compound containing reactive hydrogens, and L_i is the loading of that component in PPHP. The calculated equivalent weights of

the three polyols (Chapter 3.2.1), were used. The equivalent weight used for water was nine as it reacts with isocyanate once to make an amine which then reacts with a second isocyanate to form a disubstituted urea as discussed in Chapter 1.3.3.2 The equivalent weight used for the surfactants was 935. The equivalent weight for DMEA used was 89.14. The additive and other catalysts were excluded from these calculations, as they have no reactive hydrogen groups.

Unless otherwise stated all components of the formulation except the isocyanate (part B) were mixed together at 3000 RPM for 90 seconds using an overhead mixer and a turbine stirrer. This stood for 2 minutes to debubble before reacting with the isocyanate. Pre weighed isocyanate was added and the solution was mixed again for 6 seconds at 3000 RPM before being poured to a clean reaction vessel (600 ml polypropylene cup). Foam was left to cure in the fume hood at room temperature for one week after reacting.

The DOW Chemical Company (Michigan, United States) kindly supplied the polyols and isocyanate products. Silicone based surfactants as well as DMEA samples were kindly supplied by Evonik Industries (Essen, Germany). Sodium Bentonite was purchased from Alfa Aesar. BYK Additives and Instruments (Wesel, Germany) kindly supplied Cloisite samples. Deionised water was used for all formulations and all reagents were used as received.

3.4. Formulation Screening

The starting formulation was developed using the guideline shown in Table 3.4. This starting formulation is shown in Table 3.5. Voranol 3322 is a general purpose, nominal 3400 molecular weight triol used in the production of slabstock fPUF. Specflex NE 112 is a polymeric MDI with low functionality used in the production of flexible slabstock and moulded foam. The sole blowing agent used was water. Dabco 33LV is a tertiary amine catalyst composed of 33 % triethylene diamine and 67 % dipropylene glycol. It strongly promotes the gelling reaction when used alone however catalyses both the blowing and gelling reaction when used as a co-catalyst[125]. It is suitable in a variety of flexible and rigid foam formulations. Tin(II) 2-ethylhexanoate (stannous octoate) is the

industry standard gelling catalyst for use in the manufacture of slabstock fPUF or moulded foam applications. Tegostab BF 2470 is a highly active silicone based surfactant based on a polysiloxane polyoxyalkylene block copolymer used in a range of fPUF foams including slabstock and molded foams.

Table 3.5: Starting fPUF formulation.

Component	Loading (PPHP)
Voranol 3322	100
Specflex NE 112	69.4
Water	4
Dabco 33LV	0.3
Stannous Octoate	0
Tegostab BF2470	0.8

3.4.1. **Catalyst Package**

An initial concern in the formulation shown in Table 3.5 was the use of a tin-based gelling catalyst. Tin has been shown to accumulate in plants where water has been contaminated with heavy metals from mine run-off[126]. This introduces a food safety concern, especially when stannous octoate as well as several other PU catalysts including Dabco 33LV have been shown to be cytotoxic, with Dabco 33LV being the least toxic of the catalysts tested[127]. However Wheeler *et al*[128] identified tertiary aromatic amines as a source of plant toxicity in plant plug trials. It would therefore be best to also reduce or remove the tertiary amine Dabco 33LV as well.

A set of experiments was performed to determine whether the addition of stannous octoate was necessary to give sufficient conversion in the specific formulation (this set of experiments are referred to as SnRed for the remainder of this chapter). The stannous octoate loading was varied from 0 to 0.6 PPHP and the rest of the formulation remained the same as Table 3.5. The isocyanate conversion is shown in Figure 3.1.

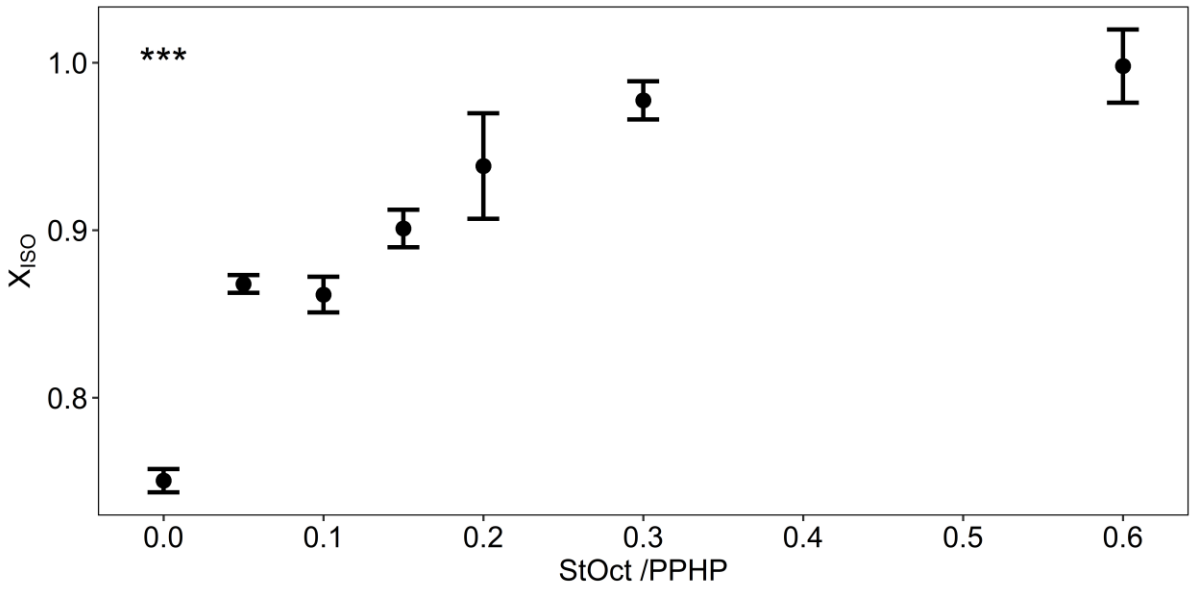

*Figure 3.1: Isocyanate conversion at various loading of a stannous octoate catalyst for the SnRed dataset. Error bars represent ± 1 standard error. Asterisks indicate significance of catalyst loading on conversion, ***p < .001 (ANOVA).*

Figure 3.1 shows an increase in reaction conversion with an increase in catalyst loading, however an increase from 0.3 PPHP stannous octoate to 0.6 PPHP only increased conversion from 97 % to 99 %. An isocyanate conversion of more than 90 % was considered a complete reaction, under the assumption that the remaining isocyanate will react to completion during the week long post reaction curing time. Therefore, a minimum of 0.15 PPHP stannous octoate catalyst was required to reach the necessary conversion. A loading of 0.15 PPHP stannous octoate was considered still to high for the application and worries about food safety meant that it was more appropriate to consider replacing the stannous octoate with alternative gelling catalysts.

Dimethyl ethanol amine (DMEA) is a highly efficient blowing catalyst and is particularly well suited as a co-catalyst. It has the added benefit of being reactive due to the primary alcohol group. This reduces the likelihood of the catalyst being mobile and leaching from the foam. A second catalyst was identified from The DOW Chemical Company range of catalytically active polyols. Specflex Activ 2306 is a novel autocatalytic polyol formed by an alkoxide polymer initiated from an amine resulting in a tertiary amine centered polyether polyol. A second set of catalyst screening tests were done by independently loading DMEA as well as Specflex Activ 2306 to

determine whether a catalyst package consisting of these two catalysts would be suitable for the selected formulation (This set of experiments are referred to as NewCat for the remainder of the chapter).

Figure 3.2 shows the effect of loading of the two new catalysts on isocyanate conversion. A loading of 0.6 PPHP of DMEA was sufficient to get an isocyanate conversion of 90 %. Specflex Activ 2306 required much higher loadings. A loading of 15 PPHP resulted in an 82 % isocyanate conversion. This lower catalytic activity is likely due to the much higher molecular mass per amine unit. Even though the catalytic activity of the Specflex Activ 2306 was much lower per unit mass it was decided that a catalyst package using both these catalysts would be tested in experimental design trials. The combination of catalysts would allow for finer tuning of the balance of gelling and blowing reactions. The fact that both catalysts have reactive hydroxyl groups minimises the chances of these catalysts leaching out of the foam polymer network.

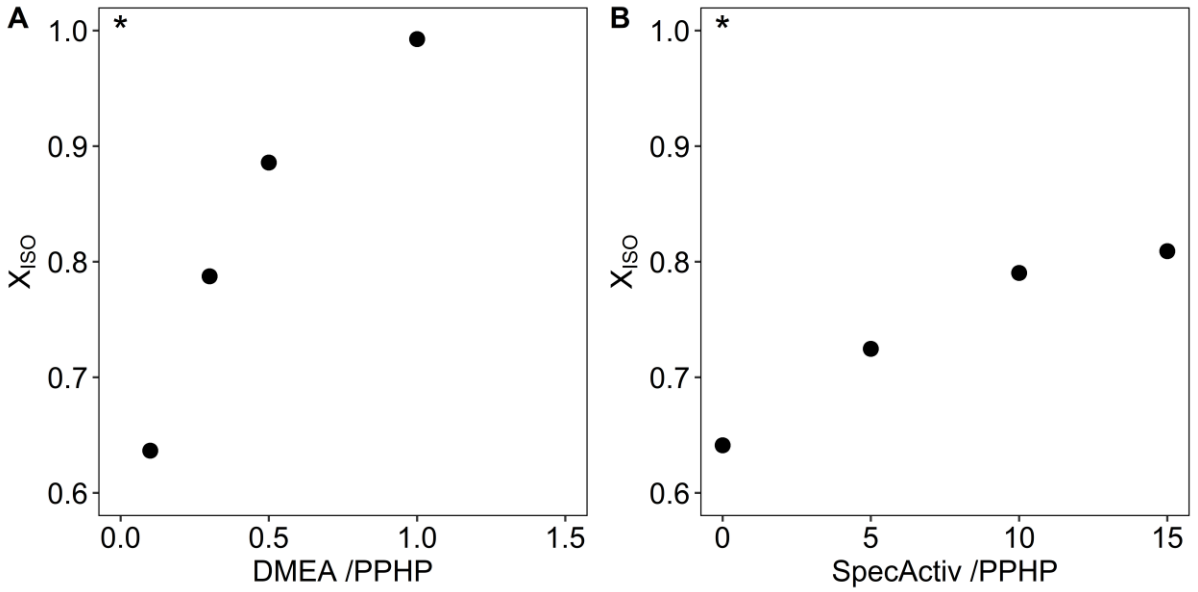

*Figure 3.2: Effect of catalyst loading in the NewCat series on isocyanate conversion (A) DMEA and (B) Specflex Activ 2306. Asterisks indicate significance of catalyst loading on conversion, *p < .05 (ANOVA).*

3.4.2. **Water Holding Capacity**

Water holding capacity was expected to play an important role in the success of fPUF as a plant growth medium. The water holding capacity for several common growing media are shown in Table 3.6.

Table 3.6: Water holding capacity for several common soilless growing media.

Substrate	WHC /$g_{water}.l_{substrate}^{-1}$
Rockwool	503 - 862[129,130]
Coco Coir	201 - 786[131]
Perlite	200 - 689[132,133]
Vermiculite	580 - 834[130]

The large range in water holding of some of the media shown in Table 3.6 is due to variations in experimental methods as well as substrate variation. If we compare the WHC of common substrates to the suggested water holding capacity from Chapter1.2.1.1, it is clear that most of these substrates fall within the suggested range. The watering regime and nutrient application for soilless systems can be optimised around the properties of the substrate. The high WHC of rockwool allows for shorter irrigation cycles than substrates with low WHC. This is especially beneficial in open systems, where excess water drains from the system and is lost to the surroundings, in these systems rockwool is generally fed 20 – 30 % excess solution to leach minerals within the rockwool and reduce salt build-up[17]. A fPUF substrate would need to have a WHC similar to rockwool to ensure similar watering regimes could be used, and waste water could be minimised.

The WHC of SnRed are shown in Figure 3.3. The water holding capacity decreases with an increase in the stannous octoate concentration. A possible explanation for this behaviour is that the increase in stannous octoate favours the gelling reaction over the blowing reaction, increasing the number of closed cells in the foam and reducing the WHC. The WHC values are much lower than the WHC of industry standard growing substrates. It was therefore necessary to identify possible methods for increasing WHC.

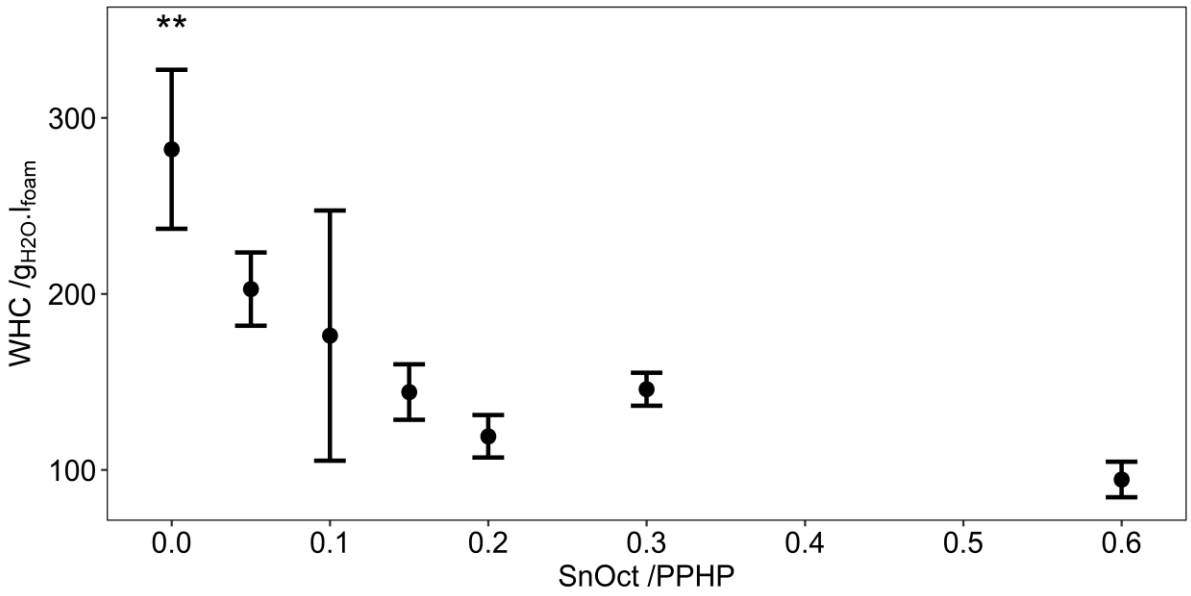

*Figure 3.3: WHC at a range of stannous octoate catalyst loadings from the SnRed dataset. Error bars represent ± 1 standard error. Asterisks indicate significance of catalyst loading on WHC, **p < .005 (ANOVA).*

3.4.2.1. *Sodium Bentonite Trial*

Bentonites are a special group of the smectite group of clays, having lower valence electrons substituted for Si^{4+} and Al^{3+} in the crystal structure. This leaves a negative charge which is balanced by "exchangeable" cations located mostly on the interlayer crystal surfaces. When this "exchangeable" cation is primarily sodium it is known as sodium bentonite[134]. Sodium bentonite also has a high CEC, ranging between 50 – 100 $cmol_c.kg^{-1}$. This property of Sodium bentonite as well as its ability to absorb a large amount of water has led to it being used as a soil additive where both these properties improve the soil quality[135]. Sodium bentonite has also been used as an additive for PUF, in a non-horticultural context, as a cell opener[136] and at low loadings has improved mechanical strength as well as flame retardancy of foams[137]. The cell opening properties of sodium bentonite are of interest as an increase in open cells would further increase the water holding of the system. Sodium bentonite is therefore a good candidate for an additive for fPUF to increase the WHC.

An experiment was designed to determine the effect of sodium bentonite on the physical and chemical properties of a fPUF to be used as a hydroponic growing

substrate. The fPUF formulation used is shown in Table 3.7. Five formulations with varying amount of sodium bentonite (0, 2, 5, 10, 20 PPHP) were tested. The bentonite trial was done simultaneously to the NewCat trial, hence the addition of DMEA, however Specflex Activ 2306 had yet to be tested so Dabco 33LV was used as the sole gelling catalyst.

Table 3.7: fPUF formulation with varying sodium bentonite content.

Component	Description	Part by weight
Polyol	Voranol 3322	100
Water	Distilled	4
Silicone Surfactant	Tegostab BF2470	0.65
Gelling Catalyst	Dabco 33LV	0.3
Blowing Catalyst	DMEA	0.5 *
Isocyanate	Specflex NE 112	70.1
Bentonite	Sodium Form	0 – 20

*DMEA needed to be increased to 1 PPHP for 10 and 20 PPHP loadings of Sodium Bentonite in order to achieve stable PUF.

Foams were synthesised in accordance to the method described in Chapter 3.3 and several physical foam properties (density, CFD, WHC, WDPT and air porosity) were determined according to the methods in Chapter 2.2. In addition to these physical properties the CEC of the bentonite clay as well as the foam were determined.

The CEC of neat sodium bentonite was measured to be 93.6 ± 0.77 $cmolc.kg^{-1}$ via spectrophotometry, this value was confirmed using ICP-OES, where CEC was calculated as 97.2 $cmol_c.kg^{-1}$. Figure 3.4 shows the physical and chemical properties of the resulting foams and Table 3.8 shows the ANOVA table for these properties.

The addition of sodium bentonite had a significant effect on all physical and chemical properties of the foam. Density increased in a linear trend with an increase in sodium bentonite. Mechanical properties (CFD) decreased to a minimum at a loading of 10 PPHP sodium bentonite; further increase of bentonite did not affect the CFD. WHC increased considerably with a 2 PPHP addition of sodium bentonite, any further addition had little effect on the WHC. The addition of sodium bentonite increased the water holding to above 700 $g_{H2O}.dm^{-3}$, which is within the range of rockwool's WHC.

Although the sodium bentonite increased the WHC above the required threshold, a secondary problem arose. The water drop penetration time (WDPT) for all of the bentonite foams were greater than 50 minutes. Even though the addition of bentonite decreased the WDPT, these foams were still categorised as “strongly hydrophobic” or “very strongly hydrophobic” according to Doerr[94]. The CEC increased linearly with an increase in sodium bentonite. However these values were below the expected CEC, likely due to some sodium bentonite particles being encapsulated by PUF and unable to take part in ion exchange. The air filled porosity followed the opposite trend to the WHC, which is expected as the skeletal density of the foam was constant for all tests.

A subset of these foams were selected for preliminary plant growth trials. This study was carried out in a temperature controlled greenhouse at the Arthur Willis Environmental Centre (AWEC) at the University of Sheffield with a day/ night regime of 12 h at 20 °C / 12 h at 15 °C from 2018/03/09 until 2018/04/20 (6 weeks). Supplementary lighting was used to achieve a minimum solar irradiation of 1000 $W.m^{-2}$ (Phillips Mastercolour CDM-T Elite MW 315W/942 1CT). The only variable tested was sodium bentonite loading, which was varied between 0, 2 and 10 PPHP. Pots with a diameter of a 12 cm and a volume of 1 l were used. Seeds of *S. lycopersicum* var. Subarctic plenty (Premier Seeds Direct, Wiltshire, UK) tomatoes were pre-germinated and one seedling planted per pot with 5 replicates at each clay loading. Growing conditions followed the guidelines set by Schwarz et al[138]. Plants were supplied with Long Ashton solution[139] via a dripper feed delivering 2 l. hr^{-1}. The solution was changed every two weeks and the concentration sequentially increased from
20 %, to 40 % and to 60 % strength over the 6 week growth period. pH of the nutrient solution was maintained between 5.5 and 6 and was adjusted using a 10 % phosphoric acid solution.

Plant heights were measured twice a week during the trial and at the end of the trial above ground biomass was harvested, dried for 5 days at 70 °C and weighed.

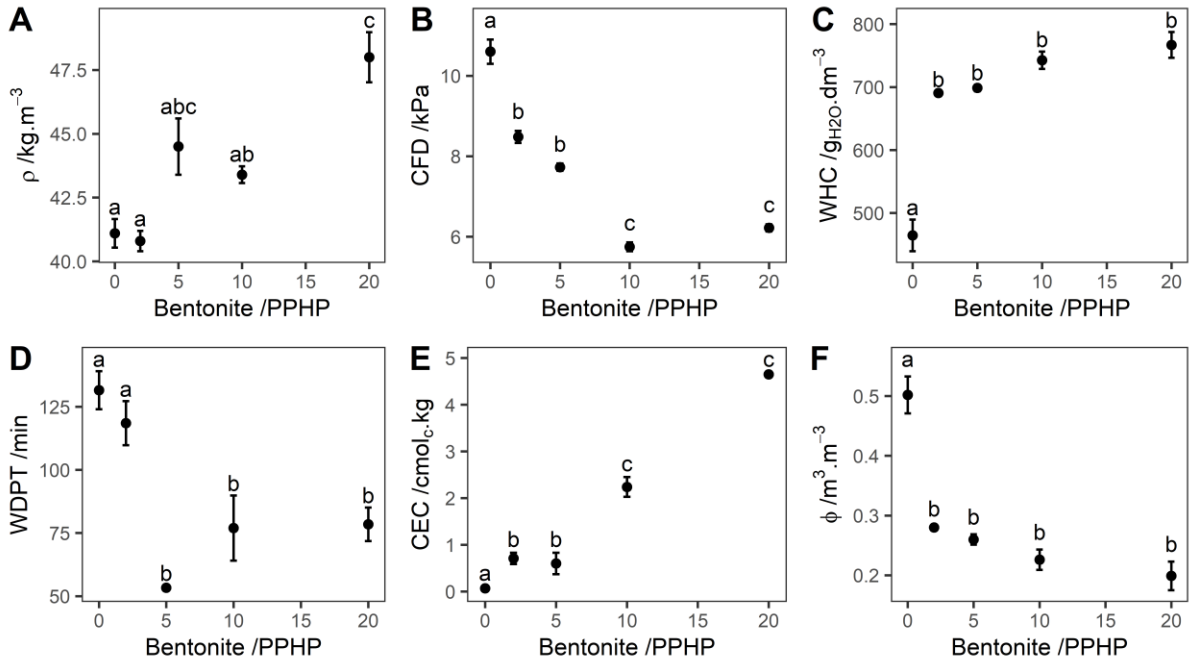

Figure 3.4: Physical properties of PUF with varied sodium bentonite loading. (A) Density (B) compression force deflection, (C) water holding capacity, (D) water drop penetration time, (E) cation exchange capacity, (F) air filled porosity. Error bars represent ± 1 standard error. Points with differing letter codes are significantly different (ANOVA followed by Tukey multiple comparison test at $p < .05$, see Table 3.8).

Table 3.8: ANOVA results for polyurethane foam physical and chemical properties.

Property	d.f.	F	*p*
Density	4,10	9.63	0.002
CFD	4,10	90.66	<0.001
Log_{10}(WHC)*	4,9	28.87	<0.001
WDPT	4,10	11.04	<0.001
CEC	4,10	9.63	<0.001
Air Filled Porosity	4,9	34.68	<0.001

** Data were Log10 transformed due to lack of homogeneity of variance and analysed by ANOVA, untransformed data are presented in Figure 3.4.*

Figure 3.5 shows the height of tomato plants over time (days after planting, DAP) for foams with varying quantities of sodium bentonite. The height of the plant increased over time (ANOVA: d.f. = 15, 170; F = 1912.9; $p < .001$) as expected. The height also increased with an increase in sodium bentonite (ANOVA: d.f. 2, 170; F = 151.04; $p < .001$). This effect was confirmed by integrating under the height curve for each

plant and determining a total AUC (mm.DAP) value. The AUC is only significantly different at sodium bentonite loading of 10 PPHP. This agreed with the dry mass data that also showed that the addition of sodium bentonite only improved plant growth at a loading of 10 PPHP. AUC data and plant dry mass data is shown in Figure 3.6.

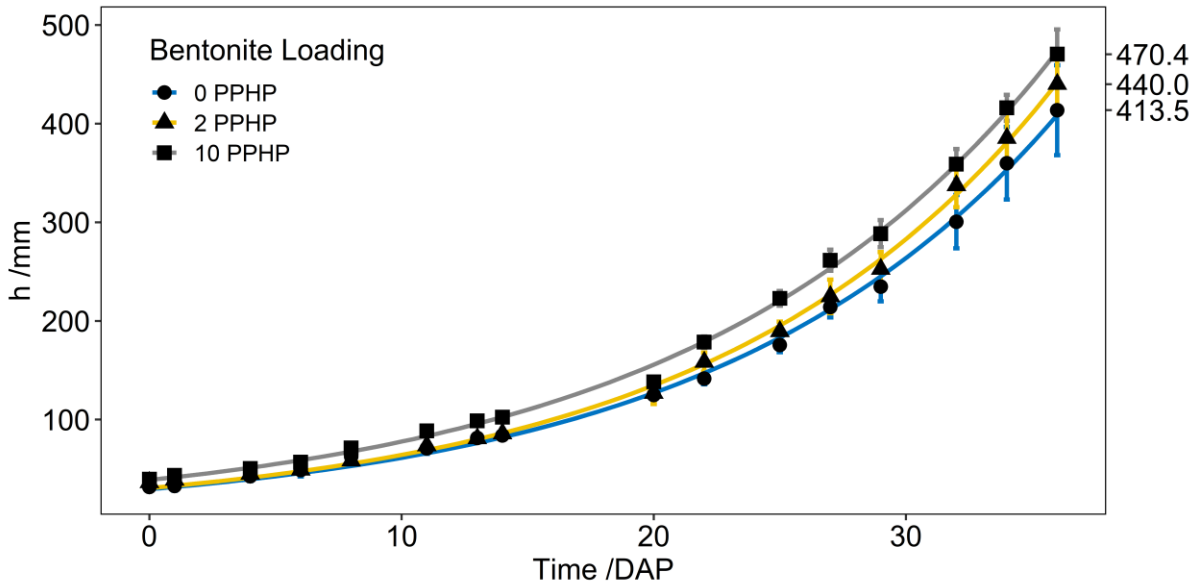

Figure 3.5: Height of plants grown in PUF with varying amounts of sodium bentonite, final plant heights (mean) shown on right. Error bars represent ±1 standard error.

Statistical analysis of physical and chemical properties showed that no one physical or chemical foam property had a significant influence on plant growth. The combination of these changes by the addition of sodium bentonite had a positive effect on tomato vegetative plant growth. The fact that bentonite had a significant influence on all the physical and chemical properties made it impossible to determine which physical properties of fPUF were important for plant growth.

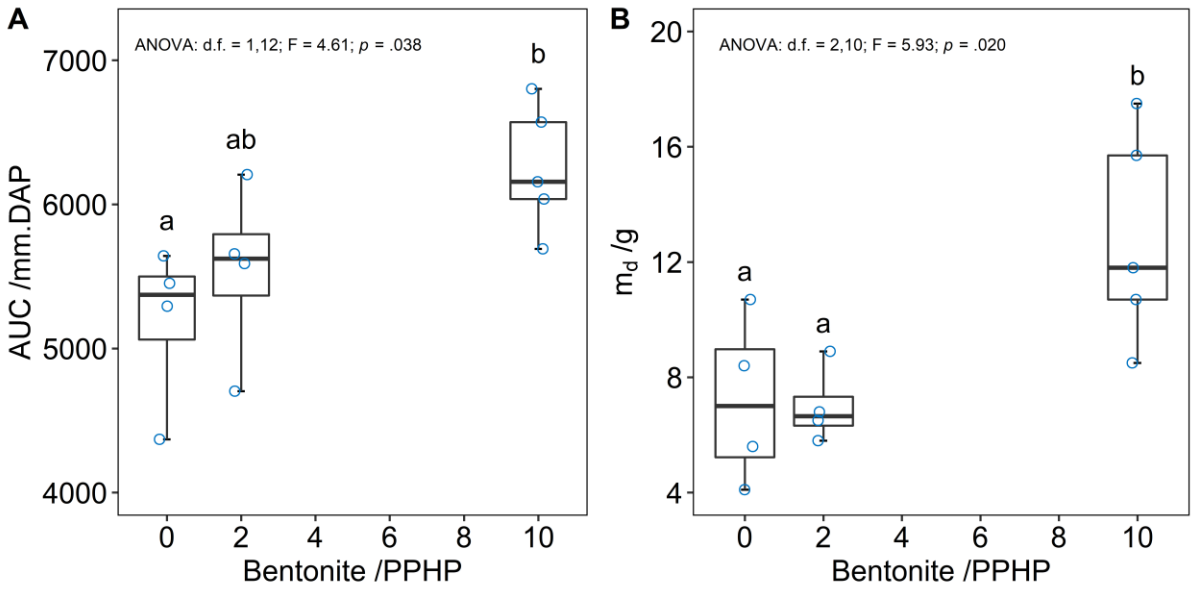

Figure 3.6: (A) The indicated area under curve (AUC) of plant heights with varied sodium bentonite loadings. (B) The dry mass of shoots with varied sodium bentonite loadings. Points with differing letter codes are significantly different (ANOVA followed by Tukey multiple comparison test at p<.05). Box plots show median, 1st and 3rd quartile and whiskers show maximum and minimum points.

The addition of sodium bentonite increased the WHC of foams to a level that was comparative to rockwool. This water took a long time to be absorbed, indicating that the foam was still “strongly hydrophobic”. The addition of sodium bentonite improved vegetative growth however, it was not possible to determine which physical and chemical properties were responsible for this improvement.

3.4.2.2. *Increasing EO content*

Increasing the EO content of the fPUF was identified as a second method for increasing the WHC and hydrophilicity of foam. The structural units in EO are more polar when compared to PO structural units. This increase in polarity increases the hydrophilicity of the soft segment of the fPUF[140]. Kwon et al[141] used polyethylene glycol (PEG) and sodium alginate as a polyol to synthesis hydrophilic PUF. They used varying molecular mass PEG and showed that water absorption went up with molecular mass. A range of PEG with different molecular mass at several loadings with Voranol 3322 were used to determine the effect on foam hydrophilicity. The PEG

molecular masses used were 200, 400, 600, 800, 1000. PEG with molecular mass higher than this have melting points approaching 45 °C, even PEG 1000 has a melting point of 33-40 °C, and needed to be heated for reactions to take place in the liquid phase.

The formulations used for this trial are shown in Table 3.9, for all these experiments the isocyanate index was 1.00. The water holding capacity and the WDPT were the foam properties of most interest.

Table 3.9: fPUF formulations using PEG as a polyol.

Component	Loading (PPHP)
Voranol 3322	42 - 80
PEG	2 - 40
Specflex Activ 2306	18
Water	4
TegoStab BF 2470	10
SpecFlex NE 112	70 - 117

Results showed that increasing the PEG molecular mass and PEG loading increased the WHC of fPUF. The inverse of this was seen in the WDPT, with the WDPT decreasing with both the PEG and molecular mass. Figure 3.7 shows the WHC and WDPT data for this trial.

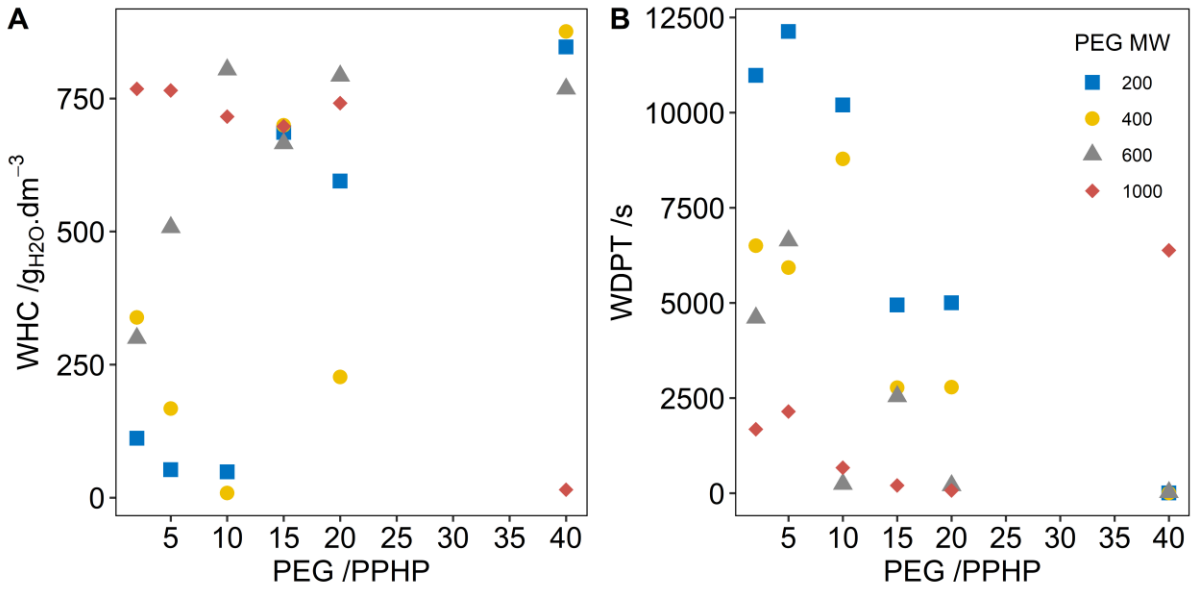

Figure 3.7: (A) Water holding capacity and (B) water drop penetration time of fPUF samples with different loading and different molecular mass PEG.

The relationship between PEG loading, molecular mass and the water absorption properties of the fPUF were confirmed by modelling the responses (WDPT and WHC) as a function of the PEG loading and molecular mass according to *Equation 3.6*.

$$y = \beta_1 x_1 + \beta_2 x_2 + \beta_3 x_1 x_2 + \beta_4 x_1^2 + \beta_5 x_2^2 + \beta_6 \qquad 3.6$$

Where y is the response, x_1 is the molecular mass of the PEG used and x_2 is the loading of the PEG. This model takes into account a linear contribution from each factor, a curvature term from each factor as well as an interaction term between the two factors.

Equation 3.7 and *Equation 3.8* are the fitted models and the ANOVA table for both models is show in Table 3.10. Contour plots for the modelled data are shown in Figure 3.8. The model for WHC indicates that an increase in molecular mass or loading of the PEG increases the WHC and the interaction term signifies that at very high loadings and high MW this behaviour inverts and you get a drop in WHC. The model for the WDPT indicates a similar trend, an increase in either MW or loading the decreases the WDPT and again an interaction term that suggests at very high loadings and high MW you get an increase in WDPT.

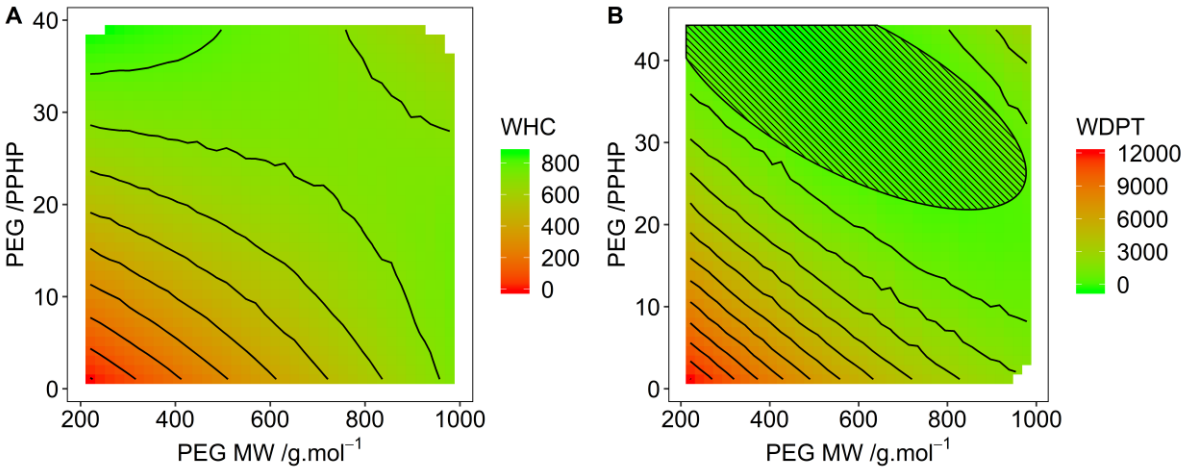

Figure 3.8: Contour plots for the PEG loading and molecular weights models predicting (A) fPUF water holding capacity and (B) fPUF water drop penetration time over the ranges tested. The hatched area in (B) indicates the region of interest where the predicted WDPT is below 60 seconds, foams within this region are predicted to be hydrophilic.

Foams with high WDPT (> 700 $g_{H2O}.dm^{-1}$) as well as low WDPT (< 5 seconds) which would be classed as “very hydrophilic” were made, using PEG 400 at a loading of 40 PPHP.

$$WHC = 0.391x_1 + 12.3x_2 - 0.0535(x_1 - 550)(x_2 - 15.3) - 0.000480(x_1 - 550)^2 + 0.408(x_2 - 15.3)^2 + 210 \quad 3.7$$

$$WDPT = - 8.07x_1 - 205x_2 + 0.535(x_1 - 550)(x_2 - 15.3) + 0.0130(x_1 - 550)^2 + 5.77(x_2 - 15.3)^2 + 951 \quad 3.8$$

Table 3.10: ANOVA table for models predicting WHC and WDPT of fPUF with varying loading and MW PEG.

Property	R^2	d.f.	F	*p*
WHC	0.68	5,17	7.14	<.001
WDPT	0.87	5,17	23.13	<.001

The models can furthermore predict a minimum EO content of a formulation required for the resulting foam to be classed as “hydrophilic”. For a foam to be considered

“hydrophilic”, it needs to have a WDPT of less than 60 seconds. Figure 3.9 (A) shows the required amount of PEG for the different molecular weights to make a hydrophilic foam. Figure 3.9 (B) shows the EO percent required of SS for the formulation to produce a hydrophilic foam. The model could not find a loading for the 1000 MW PEG that would produce a hydrophilic foam. This correlates to the raw data, where WDPT had a minimum at 20 PPHP loading and a WDPT of 71 seconds. There is then a drastic increase at 40 PPHP loading. This may be due to do difficulties in mixing the solid PEG 1000 or changes to foam morphology, requiring a different catalyst or surfactant package.

All of the PEGs used have a lower equivalent weight than the base polyol and therefore require additional isocyanate to maintain stoichiometry. Therefore, the reduction in mass of PEG required to reduce a given WDPT with increasing PEG molecular mass can be explained by the decrease in isocyanate required for reaction and therefore a reduction in the hydrophobic hard segment content. Figure 3.9 (C) shows the amount of EO required in the soft segment to produce a hydrophilic foam as a function of the isocyanate content.

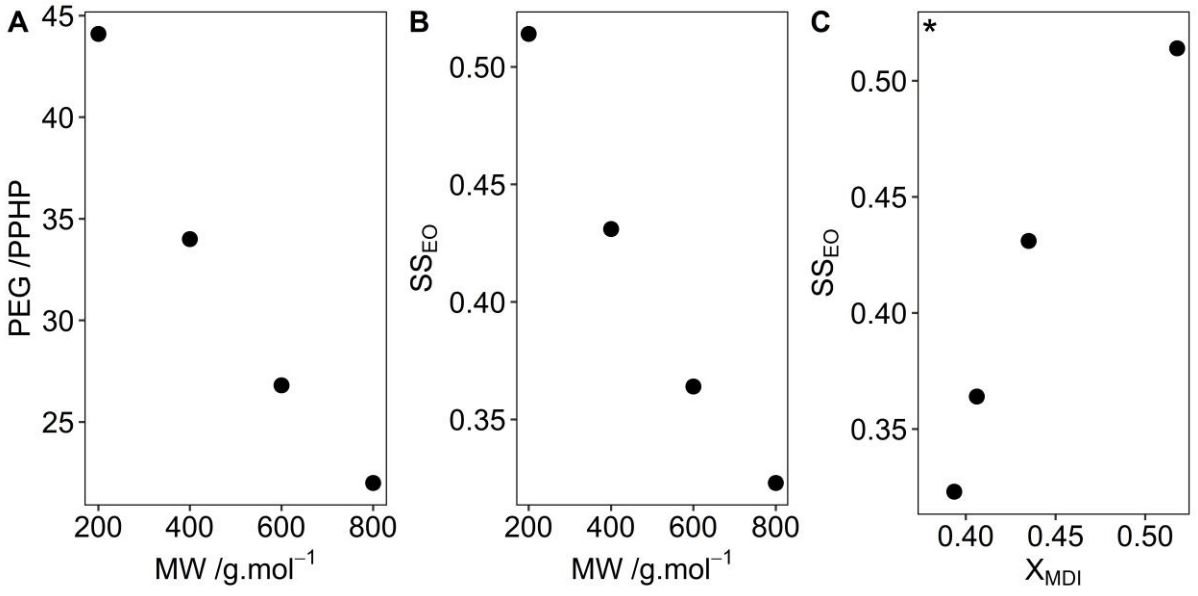

*Figure 3.9: (A) PEG loading required to produce a hydrophilic foam defined as a foam with a WPDT of less than 60 seconds, (B) polyol mass fraction EO required to produce a hydrophilic foam and (C) relation between EO content required to produce a hydrophilic foam and the amount of MDI. Asterisk indicate significance of MDI loading on required SS EO content for hydrophilic foam, *p < .05 (ANOVA).*

fPUF were formulated using PEG of different molecular masses and at different loadings. A general trend was identified with WHC increasing and WDPT decreasing with an increase in either molecular mass or loading. These trends did not hold true when the formulation used high mw PEG at a high loading, likely due to problems with mixing arising from using PEG 1000 which was solid at STP, although it may also be possible that this high mw PEG was affecting the polymer morphology and a different catalyst or surfactant package may be required. PEG with molecular weight of 200, 400, 600 and 800 required a loading that led to a polyol mixture that consisted of 51 %, 43 %, 36 % and 32 % ethylene oxide respectively to produce a “hydrophilic foam”.

3.4.2.3. *Voranol 1447*

The knowledge gained using the PEG experiments made it possible to identify a polyol that could meet all the criteria for producing a hydrophilic foam. Dow Polyurethanes suggested Voranol 1447 as an appropriate polyol for our application. Voranol 1447 is a polyether triol with a high ethylene oxide content (~ 73 %) and is a highly efficient cell opener designed for the production of soft and hypersoft flexible slabstock foams. It has an equivalent molecular mass of 1537 $g.mol^{-1}$ (Chapter 3.2.1) which is much higher than any of the PEG polyols tested, allowing for lower amounts of isocyanate to be used, improving the foam hydrophilicity. Personal communication with A. Birch and P. Cookson (Dow Polyurethanes) indicated that a combination of Voranol 3322 and Voranol 1447 would only work if either component made up more than 75 % of the polyol mixture due to miscibility issues (i.e. a 50:50 mixture of these two polyols is immiscible).

The polyol mixture would need to have a minimum ethylene oxide comparable to the PEG trials. A threshold EO content of 30 % was used to determine what ratio of polyols would be sufficient. A 75 % Voranol 3322 polyol mixture would have an EO content of 28.2 %. A 75 % Voranol 1447 polyol mixture would have an EO content of 58.2 %; it was therefore decided to move forward with this polyol composition.

3.5. Conclusions

End group analysis was done to determine the equivalent weights for polyols and isocyanate. Voranol 1447 had an equivalent mass of 1537 $g.mol^{-1}$, Voranol 3322 had an equivalent mass of 1179 $g.mol^{-1}$, Specactiv 2603 had an equivalent mass of 1805 $g.mol^{-1}$ Specflex NE 112 had an equivalent mass of 132.1 $g.mol^{-1}$. EO content of the polyols was determined by NMR. Voranol 1447 had an EO content of 73.2 %, Voranol 1447 had an EO content of 13.2 % and Specactiv 2306 had an EO content of 21.9 %.These values correlated closely to available supplier values. The determined values are used for all further stoichiometric reaction calculations and for determining EO content of polyol mixtures.

An initial generic fPUF formulation was used to determine how appropriate a stock formulation would be for the application of developing a synthetic growing substrate. The generic formulation had several shortfalls, which were dealt with in order of priority. The first was a catalyst package that could (a) leach tin into the plant and cause food safety concerns or (b) volatise tertiary amine and damage the stems of the plants. SnRed trials showed that a reduction in the tin catalyst concentration caused deleterious reductions in the conversion of isocyanate. This would introduce further problems of the foam having unreacted reagents, so a new catalyst package was required. The NewCat trials demonstrated that a stable foam could be made using DMEA and that isocyanate conversions nearing 100% could be achieved with 1 PPHP DMEA. A reactive amine catalyst, Specflex Activ 2306 could also be incorporated although conversions were much lower than the DMEA test. The incorporation of this catalytically active polyol could still prove important tuning the gelling/ blowing reaction.

The second shortfall of this formulation was very low water holding capacity. Sodium bentonite was added to the formulation to improve the WHC. Sodium bentonite significantly affected all physical properties of the foam, improving both WHC and WDPT. The addition of bentonite also improved the vegetative growth of tomato plants, however, it was not possible to determine which physical and chemical properties of the foam were responsible for this improvement. The WDPT of these

foams was still high and the foams were classed as “strongly hydrophobic” or “very strongly hydrophobic” using the classification proposed by Doerr[94].

To solve the hydrophobicity problem the incorporation of a hydrophilic polymer was tested. The addition of PEG at varying MW and loadings allowed models to be developed predicting the amount of EO required to make hydrophilic foams. These models suggested that PEG with higher MW, required lower loadings to make hydrophilic foams and this was related to the hard segment generated by the additional isocyanate required by the stoichiometry of the system.

Voranol 1447 was identified as a polyol that would meet the criteria for producing a hydrophilic foam, and a 75 % Voranol 1447 : 25 % Voranol 3322 polyol mixture would have a EO content of 58.2 %. This is higher than the threshold EO content required to reach a WDPT of 60s.

Chapter 4:
Experimental Design -
Modelling fPUF Physical Properties

4.1. Introduction

Chapter 3 led to a better understanding of polyurethane foam formulations that were more suitable for application as a soilless growing media. It was established that a polyol composition of 75 % Voranol 1447 and 25% Voranol 3322 would likely lead to hydrophilic foams. The use of DMEA as a catalyst led to high conversion of isocyanate at a sufficiently low loading of 1 PPHP and the use of Specflex Activ 2306 was suggested to help tweak the ratio of blowing and gelling reactions.

The addition of sodium bentonite increased the water holding capacity of foams and improved tomato growth in a hydroponic growth trial. The sodium bentonite changed many of the physical properties and it was not possible to determine which physical properties were affecting plant growth. To help understand which physical properties influenced plant growth it would be necessary to make a set of foams with a large range of physical properties.

The use of the two catalysts would allow for some varying of physical properties, however to increase the range of physical properties between samples, two surfactants were decided on. Tegostab 2470 is a highly active silicone surfactant with wide processing latitude and is designed for flexible open cell formulations. To contrast this Tegosbab 8476 is a non-hydrolysable polyether-polydimethylsiloxane-copolymer typically used in closed cell applications. It leads to foams with very fine cells with a closed cell structure. The use of these two surfactants in multiple ratios and loadings should allow for foams with cell structures ranging from fine to course and fully open to fully closed. To help ensure that the correct ranges of factors are tested and to gain the most insight into results an experimental design approach was taken to formulating fPUFs.

4.2. Experimental Design Process

Nearly all scientific experiments can be broken down into three phases: planning the experiment, carrying out the experiment and the analysis and interpretation of the data. When the planning involves the use of statistical methods, carrying out the

experiments uses randomisation and blocking where necessary and analysis or interpretation uses statistical analysis of the data, then this is known as the experimental design process[142]. The use of statistical methods in the planning phase is known as the design of experiments approach (DoE). Montgomery[143] defines the steps required for a successful approach to design of experiments. This outline has been followed by Fechter *et al*[144] for successfully modelling PVC formulations for mine cables and methodology used here is adapted from this work.

1. *Define problem*
2. *Selection of response variables*
3. *Choice of factors and ranges*
4. *Choice of experimental design*
5. *Performing the experiment*
6. *Statistical analysis of the data*
7. *Conclusions and recommendations*

4.3. fPUF DoE

4.3.1. **Problem Statement**

The problem is that the catalyst and surfactant package in a fPUF formulation play a major role in determining the physical properties of the resulting foams. Greater understanding of the effect of catalysts and surfactants on fPUF physical properties is required.

The aim of this design of experiment is to determine empirical models that describe the relationship between the catalysts/surfactant package and several important fPUF physical properties (density, cell size, WHC, WDPT) suspected of being of importance for the use of fPUF as a synthetic soilless growing media.

4.3.2. **Selection of Response Variables**

Two groups of responses were selected for this DoE. The reaction kinetic response is important to ensure complete reaction of the reagents. The most important of these is the maximum reaction temperature, from which isocyanate conversion is determined. The time until maximum temperature, final foam height and time until maximum height were also selected as response variables.

Foam physical properties were selected as the remaining response variables. The four physical properties analysed and modelled were density, cell size, water holding capacity (WHC) and water drop penetration time (WDPT). Table 4.1 lists the response variables.

Table 4.1: List of the selected kinetic and physical response variables for the DoE trail of a fPUF.

Property	Type	Response
Isocyanate Conversion	Kinetic	y_1
Time to maximum temperature	Kinetic	y_2
Foam Final Height	Kinetic	y_3
Time to maximum height	Kinetic	y_4
Density	Physical	y_5
Cell Size	Physical	y_6
WHC	Physical	y_7
WDPT	Physical	y_8

4.3.3. **Choice of factors and ranges**

The components of interest are the catalyst and surfactant package, composed of two reactive catalysts, DMEA and Specflex Activ 2306 and two surfactants Tegostab BF2470 and Tegostab 8476. These four factors will be used for the DoE.

The ranges used for these factors is a combination of information gathered from Chapter 3 as well as practical limitations to produce stable foams. A fPUF formulation was designed with these ranges and the list of components and loading is shown in

Table 4.2. For modelling purposes, all factors were represented as a mass fraction of PUF instead of PPHP. This was done to account for changes in the sum of components between samples. All other components in the formulation were kept constant, ensuring that the amount of isocyanate and therefore the amount of hard segment and soft segment remained constant.

Table 4.2: Formulation and loadings of components used for DoE trial of a fPUF as well as the four selected factors (two catalysts and two surfactants).

Component	Factor (mass fraction)	Loading (PPHP)
Voranol 3322		15 - 25
Voranol 1447		75
Specflex Activ 2306	x_1	0 - 10
DMEA	x_2	0 - 2
Tegostab BF2470	x_3	0 - 1
Tegostab 8476	x_4	0 - 1
Water		4
Sodium Bentonite		30
SpecFlex NE112		72

4.3.4. **Choice of experimental Design**

4.3.4.1. *Empirical models*

The choice of empirical model will dictate the number of minimum experiments required to fit the model. The minimum number of experiments will influence the choice of experimental design as well. The choice of empirical model should be based on existing knowledge of the system as well. However, if little information is known about the system, a set of screening experiments and a linear response in the form of *Equation 4.1*[142] are used to refine the model.

$$y_i = \sum_{1 \le i \le q} \beta_i x_i + \epsilon \qquad 4.1$$

Where q is the number of factors (x), y is the response, β_i is the fitting parameter and ϵ is the random error term. ϵ is known as the random error term, however this term also accounts for the contribution of all the other components in the fPUF which are kept constant.

In Chapter 3 screening experiments revealed curvature in the temperature rise with an increase in catalyst. This is expected as the loading of catalyst nears saturation; its effect on maximum reaction temperature will decrease. In this situation catalyst saturation is defined as the amount of catalyst required for 100 % isocyanate conversion. Similar curvature would be expected in physical properties such as cell size, an increase in surfactant loading would reduce cell size to a point and then cell size would remain roughly constant[145]. This subject matter knowledge gives us an advantage in model selection and it is obvious that *Equation 4.1* would under fit the true system. A quadratic empirical model such as *Equation 4.2* may be better suited for the fPUF system where pairwise interaction of catalyst and surfactant might be anticipated. Third or higher order models are highly unlikely for industrial processes[146] therefore higher order models were not explored.

$$y_i = \sum_{1\leq i\leq q} \beta_i x_i + \sum_{1\leq i<j\leq q} \beta_{ij} x_i x_j + \sum_{1\leq i\leq q} \beta_{ii} x_i^2 + \in \qquad 4.2$$

Where $x_i x_j$ is an interaction term, accounting for any synergism or antagonism between terms and x_i^2 is a curvature term. The number of terms in *Equation 4.2* when there are four factors is 15, the error term, the four main effects, six interaction effects and four curvature effects. The minimum number of experiments required to fit an empirical model needs to be greater than the number of terms in the fitting model. This means a minimum of 16 experiments is required to fit *Equation 4.2* compared to a minimum of 5 for fitting *Equation 4.1*.

4.3.4.2. *Experimental Design*

The simplest experimental design is a full factorial design of experiments. The simplest of these is a 2^2 design involving two factors with two levels (high and low). This would require four experiments; however, the information gathered by this type of design

would be limited. We would gather no information about curvature. The next type of design would be a 3^2, meaning three levels would be tested. A 3^2 factorial design would require nine experiments and would give insight into the main, interaction and curvature effects. Figure 4.1 shows a 2^2 and 3^2 full factorial design of experiments. The problem with this type of experimental design is that the number of experiments increases rapidly with an increase in levels or factors[147]. A full factorial DoE for the fPUF formulation, with three levels and four factors would require 81 experiments; consequently for a complex formulation a full factorial experiment would not be feasible.

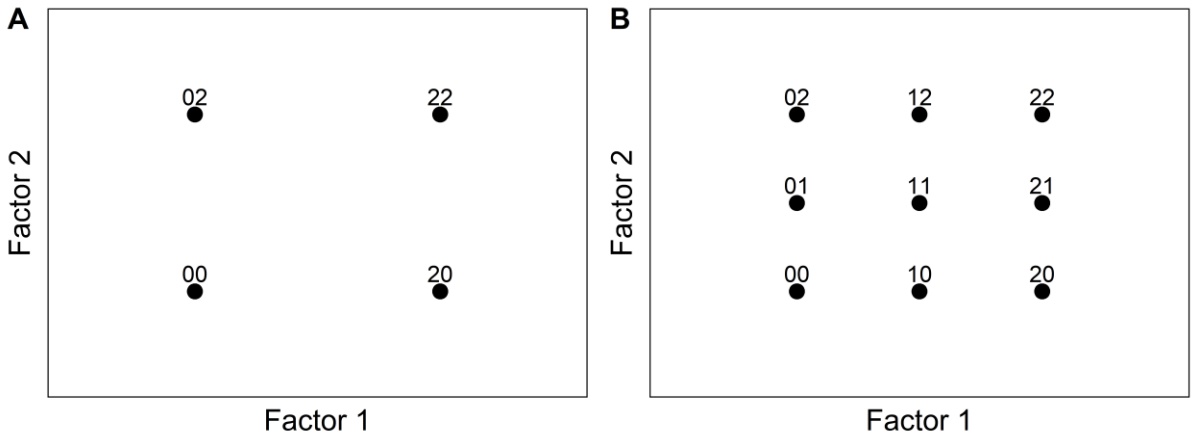

Figure 4.1: Examples of a full factorial experimental design trial full using a (A) 2^2 and (B) 3^2 DoE.

Computer aided DoE can be used to reduce the number of experiments required without decreasing the robustness of the fitted models. One option is the use of a D-optimal design, which if given the general empirical model as well as the number of experiments will optimise the experimental points for the specific empirical model.

A second computer aided DoE technique is known as the space filling technique. This technique is intuitive, when given the number of required experiments; a space filling technique calculates the optimum spacing and places the points equidistant in the experimental space. Figure 4.2 gives an example of a d-optimal and a space filling experimental design of three factors with 10 experiments. In this example the d-optimal design is a 3^2 design with one repeat run in the centre. Although the space

filling design is not as optimised for model fitting, it increases the likelihood of an experimental point being near to a response's global minimum or maximum.

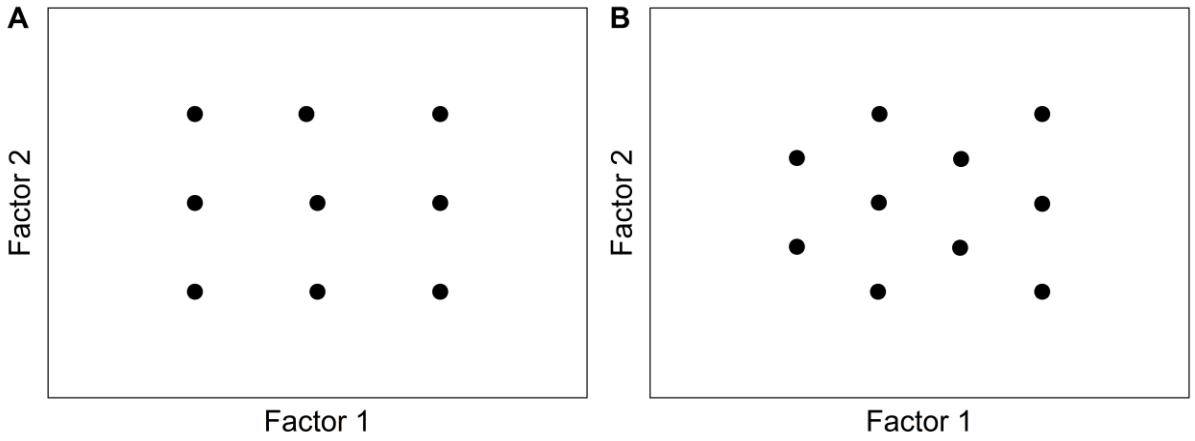

Figure 4.2: Examples of the experimental space and experimental points for a (A) d-optimal and (B) space filling experimental design.

The use of a combination of these two experimental designs would give us the advantage of both design techniques.

Although a minimum of 16 experiments were required, it was decided to do double this minimum. Doubling the number of experiments reduces the error between samples, which was expected to be high, due to experimental errors such as mixing speed and time variations as well as variations in room temperature and humidity during foam reaction and curing. A 16 point d-optimum design, using *Equation 4.2* was done as well as a 16 point space filling design for a total of 32 formulations. Experimental design was done in JMP®, Version 14.3.0. SAS Institute Inc., Cary, NC, 1989-2019.

4.3.4.3. *Model Selection*

fPUFs were synthesised, and physical properties were measured and the general model form, *Equation 4.2*, needed to be optimised and reduced to models appropriate to each response.

This reduction in model complexity is important as several factors may not influence the desired response and are therefore not required in the model. This reduces the

risk of overfitting and simpler models are more likely to accurately represent the true process. One method for doing this is the use of stepwise linear regression. This method fits each possible variation of *Equation 4.2* by adding or removing one variable at a time using the variable's statistical significance[143]. Stepwise regression has several statistical shortcomings, these are described in detail by Harrell[148] and yet this method has been successfully used for over 30 years to reduce the number of terms in empirical models[149].

An improvement to stepwise linear regression is the addition of a penalty to the algorithm. This penalty reduces the variance at the cost of introducing an additional bias[150]. Depending on the type of penalty added this is known as ridge or lasso regression and if a combination of the two is used this is known as elastic net regression. Instead of adding or removing variables by their statistical significance, variables with low contribution to the response have their coefficients reduced towards zero (ridge) or set to zero (lasso)[151]. Elastic net combines these, reducing coefficients towards zero and sets those that are insignificant to zero. Elastic net regression overcomes many of the statistical shortcomings of stepwise linear regression[152].

K-fold cross validation is a technique that maximises the robustness of models in small data sets. The technique randomly divides data into k subsets, using each subset once as a validation set and all remaining data as the training set to fit the model[153]. The model giving the best validation statistic (average r^2 for all subsets) is then selected. This technique can be used in conjunction with elastic net regression giving robust models, with low likelihood of overfitting. A k-fold subset value of 3 was used. All residuals were checked for normality and homogeneity of variance.

Stepwise regression was used for initial model reduction, further reduction was done using Elastic net regression in JMP®, Version 14.3.0 validated using k-fold cross validation.

4.3.5. **Performing of experiments**

All experiments were given a random sample number between 1 – 32 and the order was randomised to reduce error and bias. fPUF reactions were all done according to

Chapter 3.3. The FoamPi was used to monitor the fPUF reaction temperature and height. Reacted foams were left to cure for one week before being cut for analysis. Foam properties (density, cell size, water holding capacity and water drop penetration time) were all determined according to Chapter 2.2. Data was checked for normality and skewed data, and data that had non-normal distributions was transformed as appropriate. All response values were rescaled between -1 and 1 using the transformation in *Equation 4.3*. This range is selected as it accounts for the situation where the response variable has no relation to the selected factors. In this case, the mean of the data would be zero. The model fitting parameters would also all be zero. All models were fitted using these rescaled data.

$$y^* = 2\left(\frac{y - y_{min}}{y_{max} - y_{min}}\right) - 1 \qquad 4.3$$

Where y^* is the transformed response, y_{min} and y_{max} are the minimum and maximum responses respectively.

4.4. Results (Statistical Analysis of data)

4.4.1. **Scatter plot matrix**

Scatter plot matrices are an effective tool for exploratory analysis of multivariate data[154]. A scatter plot matrix is a collection of scatter plots of each combination of the continuous variables within a system. It is useful for determining any obvious bivariate relationships between variables and displays a large amount of data on a single page. Figure 4.3 shows the scatter plot matrix for the fPUF experimental design experiment. All response variables are the normalised and scaled responses, with obvious outliers removed.

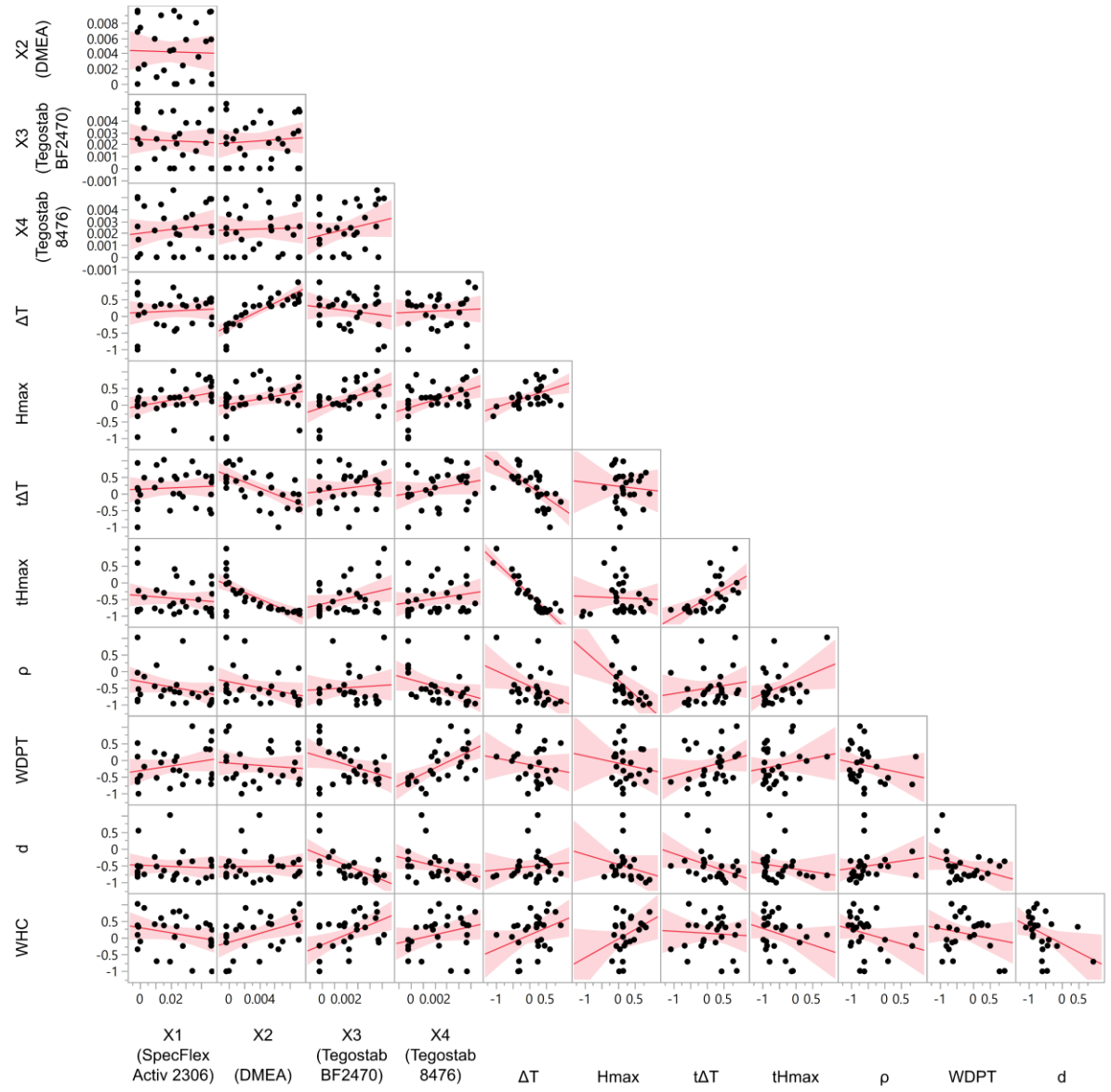

Figure 4.3: Scatter plot matrix for the experimental design of fPUF comparing all pairs of factors and responses for obvious bivariate relationships. x_1 – x_4 are the factors where x_1 is the Specflex Activ 2306 mass fraction, x_2 is the DMEA mass fraction, x_3 is the Tegostab BF2470 mass fraction and x_4 is the Tegostab 8476 loading. The kinetic responses are ΔT (maximum temperature change), H_{max} (maximum foam height), tΔT (time until maximum temperature change) and tH_{max} (time until maximum height). The physical property responses are ρ (density), WDPT (water drop penetration time), d (cell size) and WHC (water holding capacity).

The Pearson's correlation coefficient determines the strength of the linear correlation between any of the sets of data. The absolute value of the Pearson's correlation coefficient varies between zero and one. With zero indicating no correlation and one

indicating a perfect linear relationship. The sign of the coefficient indicates whether this correlation is positive or negative.

The only obvious bivariate relationships that appear to exist on Figure 4.3 are between kinetic responses and between kinetic responses and factors. Figure 4.4 (A) examines the bivariate relationship between the maximum temperature change and the mass fraction DMEA and Figure 4.4 (B) examines the time required for the foam to reach maximum height and the mass fraction of DMEA. In both these cases the mass fraction DMEA is strongly correlated to the response variables, increasing the maximum temperature and decreasing the time for the reaction to reach maximum height. Plotting these two response variables against one another in Figure 4.4 (C) reveals how well correlated these two variables are to each other. It is likely that the underlying principles governing the maximum temperature rise and time to maximum height are correlated in our system. One explanation is the use of DMEA as a blowing catalyst, which is much more active than the Specflex Activ 2306 catalyst as shown in Chapter 3.4.1. Considering the majority of heat generated during fPUF formation is due to the blowing reaction, it would make sense that an increase in the rate of blowing reaction would also increase the maximum reaction temperature whilst reducing the time taken for the foam to expand to its maximum height. Figure 4.4 (D) shows a bivariate relationship between the time required to reach maximum temperature and the maximum temperature (of thermocouple 2). This relationship (r = -0.65) is not as well correlated as the relationship shown in Figure 4.4 (C) (r = -0.92), indicating that there is likely a further factor affecting the time taken to reach maximum temperature, likely the effect of the mass fraction of Specflex Activ 2306.

There appears to be curvature to both Figure 4.4 (A) at low DMEA loading and (B) at low and high DMEA loading. Although there are some identifiable linear relationships between kinetic variables, the lack of fit and appearance of curvature suggests that linear relationships do not fully explain the effects of factors on response variables. This supports the use of the general model *4.2* and the reduction of the model using the methods discussed in Chapter 4.3.4.3.

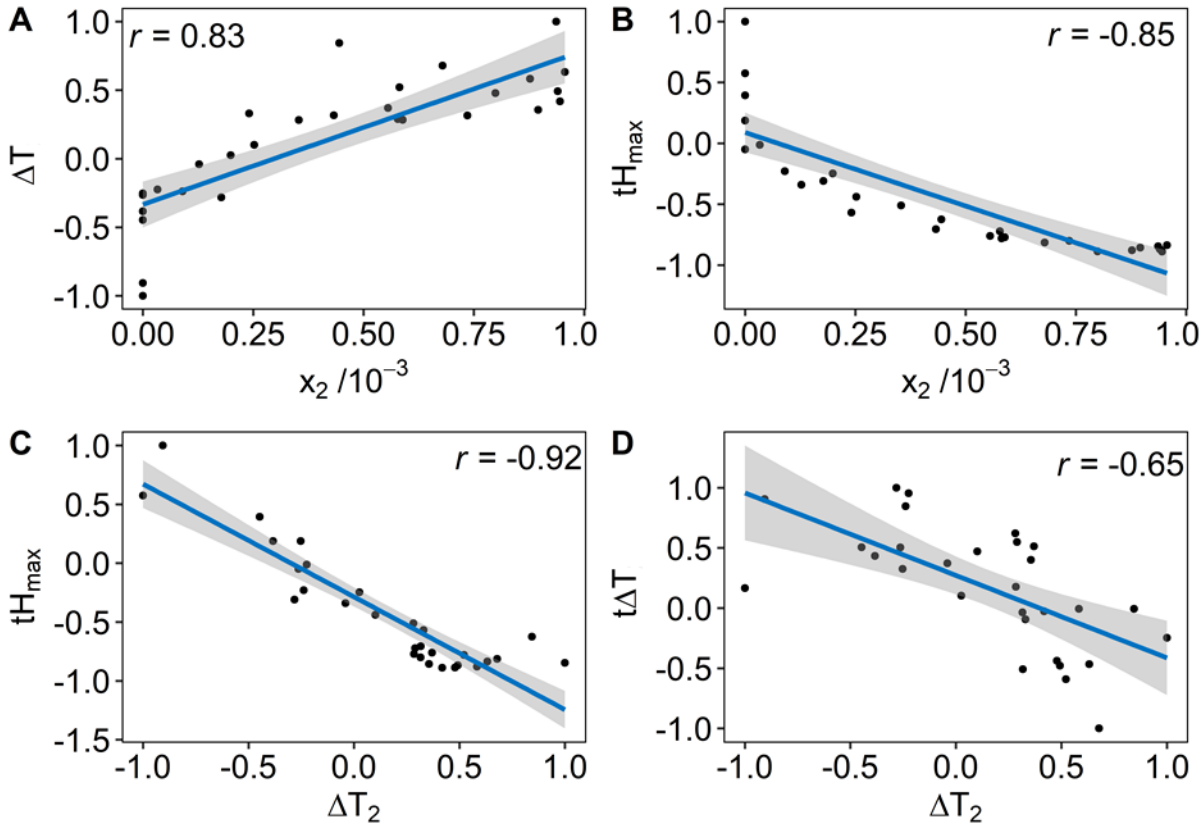

Figure 4.4: Select Bivariate relationships from Figure 4.3 between (A) maximum temperature change and x_2 (mass fraction DMEA) (B) time until maximum height and x_2 (mass fraction DMEA), (C) time until maximum height and maximum temperature change and (D) the time required to reach maximum temperature change and maximum temperature change. r is the Pearsons correlation coefficient for each of the relationships.

4.4.2. **Model Selection**

4.4.2.1. *Reaction Kinetics*

Isocyanate Conversion

Isocyanate conversion is calculated using *Equation 2.6* from the maximum temperature, in the adiabatic temperature rise data.

$$P_{NCO} = \frac{r(T_{ad} - T_{amb})}{T_{maxcalc}} \qquad 2.6$$

Equation 2.13 shows model that best fits the isocyanate conversion and Table 4.3 shows the ANOVA table for all the kinetic models. The table shows the complexity of the model required (number of terms), the r^2 of the model fit, the kfoldr^2, which is the mean r^2 of each fold as well as the ANOVA statistics, the degrees of freedom d.f. of the model, the F statistic and the *p* statistic.

$$y_1 = 6.43x_1 + 138x_2 - 1910(x_1 - 0.0248)(x_2 - 0.00409) - 20800(x_2-0.00409)^2 - 0.128 \quad 4.4$$

The statistical significance of each term can be determined using the t-ratio, the higher the absolute value of the t-ratio the greater significance the term has on the response. The sign of the t-ratio indicates whether the term is positive or negative and a t-ratio of less than two indicates that the term has a p-statistic greater than .05 (which is generally taken as the limit for indicating that the term meets significance). Figure 4.5 (a) shows the predicted isocyanate conversion values against the actual isocyanate conversions, (b) the t- ratio for each of the terms and (c) a contour plot showing the influence of the two catalysts on the conversion of isocyanate.

Table 4.3: ANOVA table for the models fitting the fPUF kinetic data.

Property	complexity	r^2	kfold r^2	d.f.	F	*p*
Isocyanate conversion	5	0.89	0.82	4, 22	45.6	<.0001
Time of max temperature	7	0.78	0.56	6, 20	11.86	<.0001
Final height	8	0.78	0.41	7, 20	10.4	<.0001
Time of max height	3	0.86	0.82	2, 24	77.5	<.0001

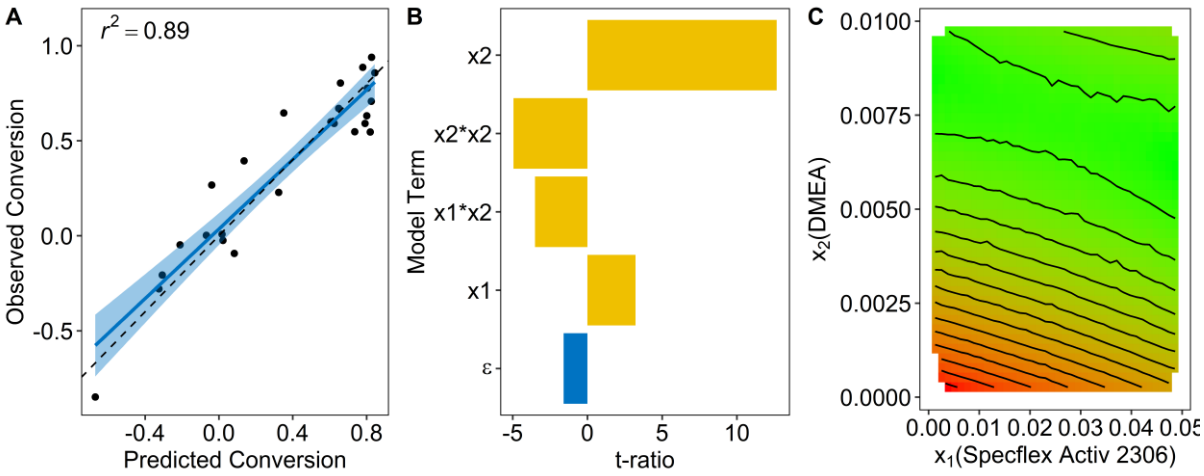

Figure 4.5: (A) predicted and observed isocyanate conversions with the blue line indicating the fit and confidence interval and the dashed line indicating the y = x line, (b) t-ratio for isocyanate conversion terms and (c) contour plot showing the influence of the two catalysts on isocyanate conversion with green indicating high conversion and red indicating low conversion. x_1 is the Specflex Activ 2306 mass fraction and x_2 is the DMEA mass fraction.

The information shown in Figure 4.5 gives important insight into understanding the model for isocyanate conversion. The t-ratio shows that all model terms are significant (yellow) except for the error term (blue), implying that the quantity of the two catalysts explains almost all variation. The fact that the two linear terms are positive indicates that an increase in catalyst loading increases conversion, however x_2 is much more significant. This would make sense for several reasons. The model is based on the mass of the catalyst component not the number concentration of the catalytic sites. DMEA (x_2) has a much lower functional molecular weight (higher mass fraction of amine) than Specflex Activ 2306 (x_1). It is also primarily a blowing catalyst and approximately 85 % of the isocyanate in the formulation is consumed by the blowing reaction, so it is logical that the DMEA loading plays a more significant role in the model. The two negative terms, the interaction term and curvature term, indicate that there is a saturation of catalyst such that any further increase in loading will not increase conversion. At this saturation point the isocyanate conversion also approaches 100 %.

Time to Maximum Temperature

The time until maximum reaction temperature required a more complex model to explain the variations, *Equation 4.5* gives the model for predicting the time until maximum reaction temperature. Table 4.3 gives the ANOVA table for this model. Figure 4.6 (A) shows the predicted values against the actual values and (B) gives the t-ratio test for the model.

$$y_2 = -6.39x_1 - 110x_2 + 112x_3 + 89.4x_4 - 91100(x_3 - 0.00232)(x_4 - 0.00259) + 1010(x_1 - 0.0256)^2 + 0.651 \quad 4.5$$

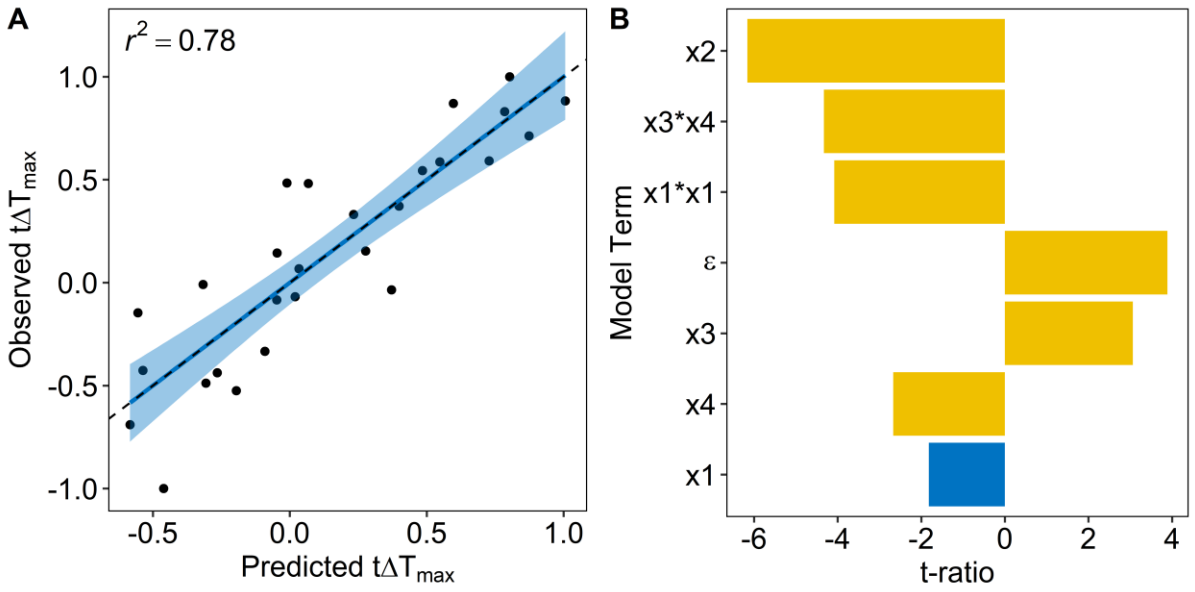

Figure 4.6: (A) Predicted time until maximum temperature and observed time until maximum temperature with the blue line indicating the fit and confidence interval and the dashed line indicating the y = x line and (B) t-ratio for terms in model for predicting time until maximum reaction temperature. x_1 is the Specflex Activ 2306 mass fraction, x_2 is the DMEA mass fraction, x_3 is the Tegostab BF2470 mass fraction and x_4 is the Tegostab 8476 loading.

It is difficult to visualise the influence and interaction between the four factors in this model in a static, 2 dimensional representation, however JMP gives a useful tool, the prediction profiler. This allows for the effect of each factor to be visualised across the entire range of loadings. An example static point from this prediction profiler from JMP

for the time until maximum reaction temperature is shown in Figure 4.7. From Figure 4.6 (B), the DMEA loading (x_2) is again the most significant term in the model, implying that this has the greatest influence on the time for the reaction to reach maximum temperature. This high significance can be explained by the fact that this catalyst is primarily catalysing the blowing reaction, which is the largest contributor to reaction temperature rise. This high significance of the error term as well as the unexpected significance of the surfactant terms indicates that a large portion of the variance is not explained by the selected factors. This may be due to experimental error with samples having slightly different mixing times and speeds.

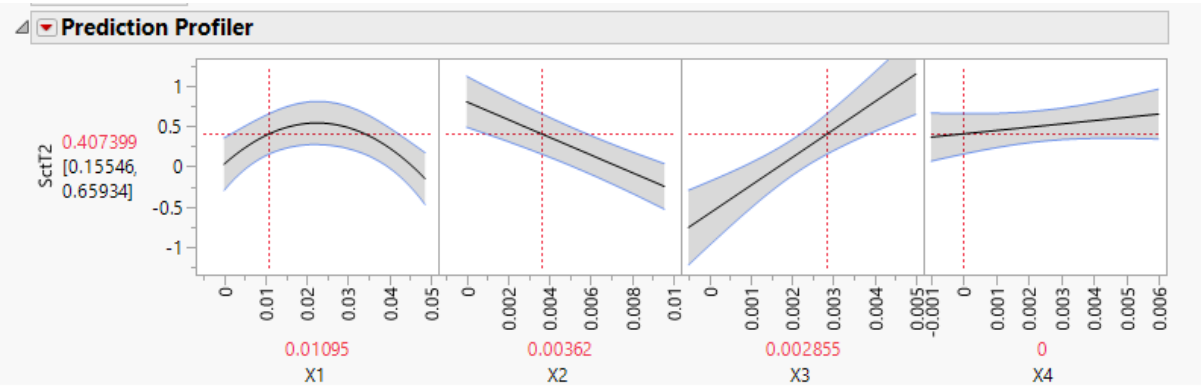

Figure 4.7: Static image from the dynamic prediction profiler in the JMP software showing the rescaled time to maximum temperature response as a function of the factor loadings, where x_1 is the Specflex Activ 2306 mass fraction, x_2 is the DMEA mass fraction, x_3 is the Tegostab BF2470 mass fraction and x_4 is the Tegostab 8476 loading.

Final Height

The equation for the model for the final foam height is shown in *Equation 4.6*. Table 4.3 gives the ANOVA table for this model. Figure 4.8 (A) shows the predicted final height against the actual final height and (B) shows the t-ratio for each of the model terms.

$$y_3 = 8.76x_1 + 46.4x_2 + 42.1x_3 + 64.2x_4 + 3210(x_1 - 0.0247)(x_3 - 0.00244) + 1277(x_2 - 0.00409)(x_3 - 0.00244) + 17080(x_2 - 0.00409)(x_2 - 0.00409) - 0.208 \quad (4.6)$$

The final height is again a function of all four of the factors. However in this case, this is more likely be related to the physical and chemical processes occurring during the fPUF reaction. From Figure 4.8 (B) all four of the linear variables have a positive influence on the height. Considering both catalysts are able to catalyse the blowing reaction (although DMEA is a stronger blowing catalyst) and both surfactants are polyether siloxane based surfactants that stabilise cell walls, the positive influence of all linear variables makes sense. We again see curvature of the DMEA loading (x_2), indicating that there is a saturation point where increasing the catalyst no longer increases the foam height. According to the supplier, Tegostab 8476 (x_4) has a stronger ability to stabilise cell walls when compared to Tegostab BF2470 (x_3) and the model also shows this, with x_4 being more significant than x_3 which on its own does not reach statistical significance.

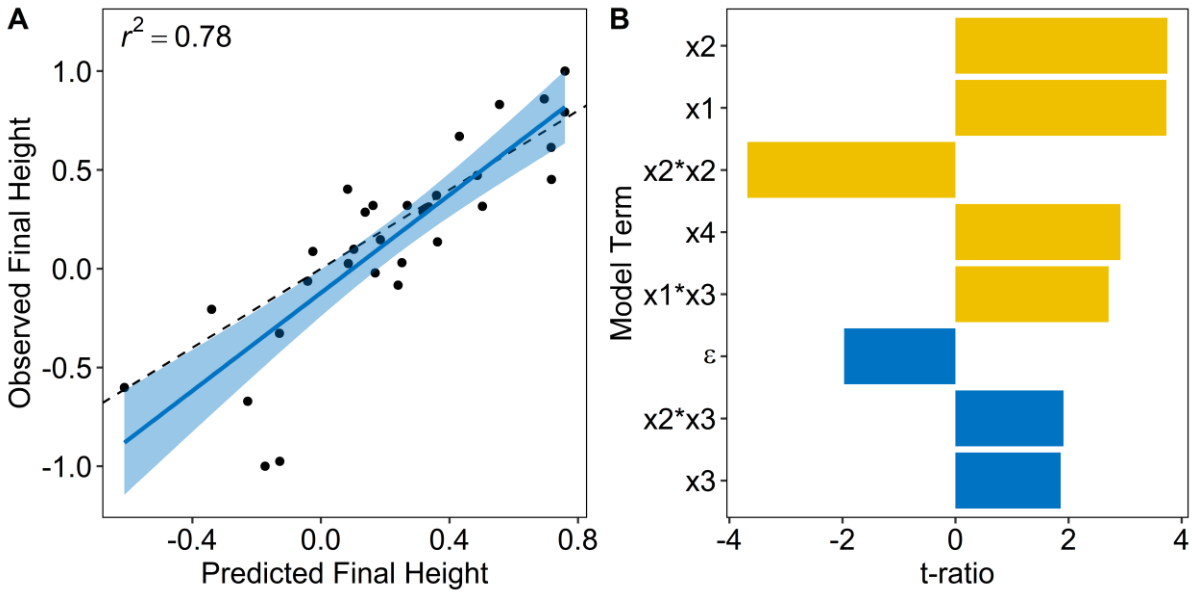

Figure 4.8: (A) Predicted final height and observed final height with the blue line indicating the fit and confidence interval and the dashed line indicating the y = x line and (B) t-ratio for terms in model for predicting final foam height. x_1 is the Specflex Activ 2306 mass fraction, x_2 is the DMEA mass fraction, x_3 is the Tegostab BF2470 mass fraction and x_4 is the Tegostab 8476 loading.

Time to Maximum Height

The time until the maximum height achieved is closely correlated to the maximum temperature data as seen from the bivariate data, so it should follow that it has a model that is similar to that of the isocyanate conversion. This is the case, with the time until maximum height only being a function of the DMEA loading (x_2). The model is shown in *Equation 4.7*. Table 4.3 again shows the ANOVA table and statistics for this model.

Figure 4.9 (A) shows the actual values against the predicted ones, (B) shows the t-ratio for the model and (C) shows the actual model fit to the experimental data.

$$y_4 = -133x_2 + 20500(x_2 - 0.00428)^2 - 0.106 \qquad 4.7$$

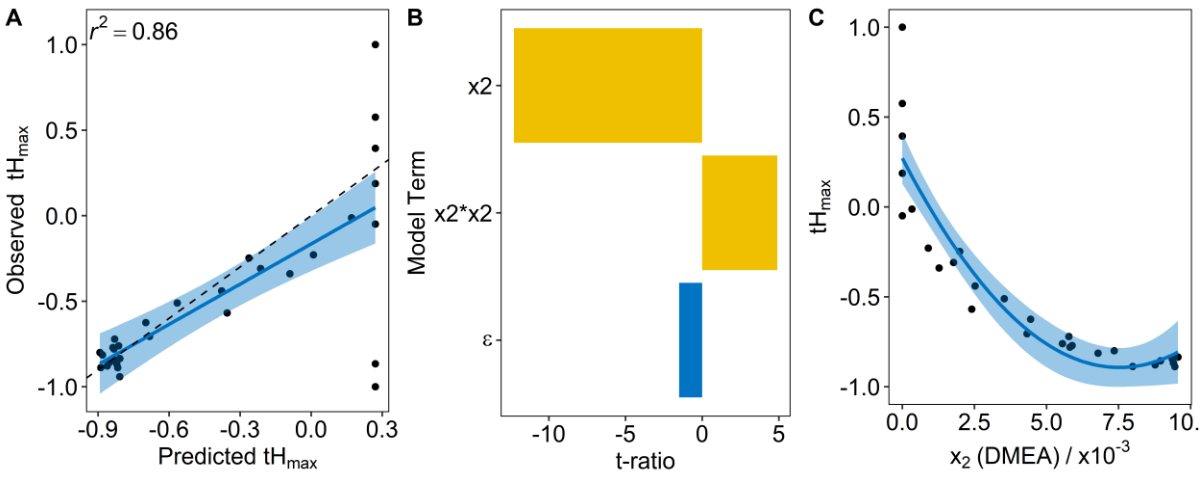

Figure 4.9: (A) predicted and observed time until maximum height with the blue line indicating the fit and confidence interval and the dashed line indicating the y = x line, (B) t-ratio for time until maximum height terms and (C) time until final height as a function of mass fraction DMEA, model fit shown in blue.

DMEA loading (x_2) explains almost all the variation of the time taken to reach maximum height, and if we again consider that this is an amine catalyst that favours the blowing reaction this makes sense. The model under predicts some values at a low DMEA loading and this may be due to the influence of relatively high Specflex Activ 2306 level at low DMEA loadings, however if this is the case it is not statistically significant.

4.4.2.2. *Physical Properties*

Density

Density data did not fit a normal distribution; this was specifically due to the foam samples that had collapsed due to insufficient surfactant. These foams had substantially high density (>50 kg.m^{-3}). Setting a threshold at 50 kg.m^{-3} and excluding data above this value, improved the distribution to the point that the data passed a goodness of fit test for a normal distribution. Figure 4.10 shows the density distribution before and after removal of points with density greater than the threshold.

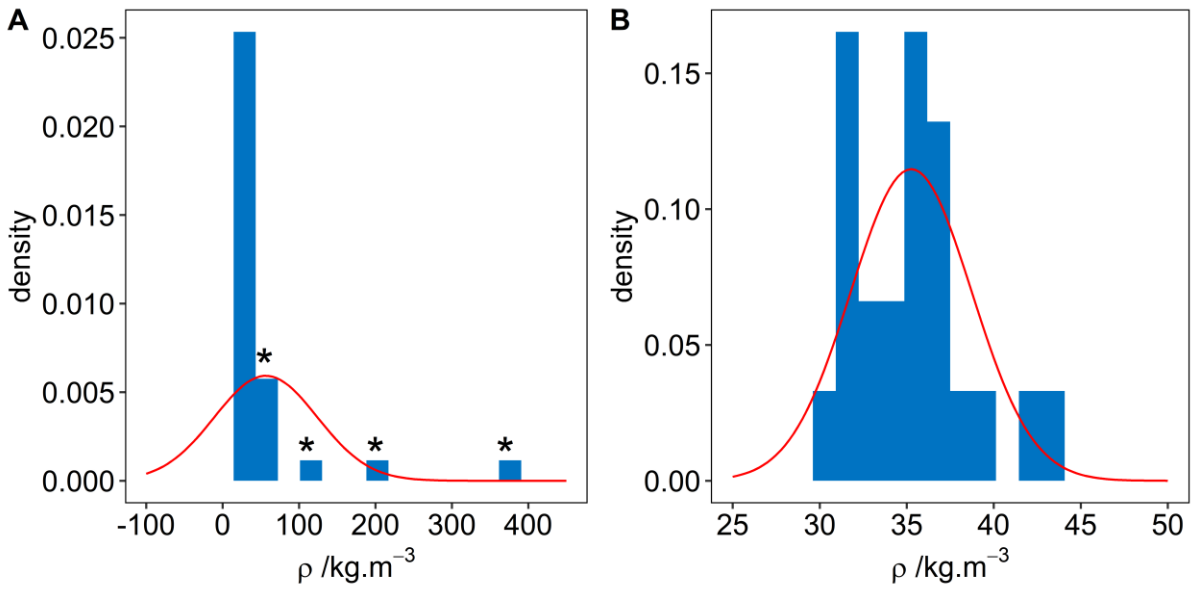

Figure 4.10: (A) The full density data set, which does not follow a normal distribution, with asterisks to indicate threshold data points that were removed and (B) a reduced density data set with threshold data removed, which passes a goodness of fit test for normal distribution.

The removal of these points with a density above the threshold means that some important information is lost, as these were not due to experimental error and the density data at low surfactant loading holds important insight into the minimum amount of surfactant required to make a stable foam. This needs to be taken into consideration when developing a model to predict density. We can also look further into the excluded data to determine a minimum surfactant loading to produce a stable foam.

A nominal logistic regression approach was used to determine which factors are influencing the likelihood of producing a stable foam. Data is categorised into foams that were stable and those that collapsed. Only x_4 (Tegostab 8476) had a significant effect on the production of stable fPUF (p = .0047) and this can be plotted in terms of a logistic plot, shown in Figure 4.11 which gives the probability of producing a stable foam at different x_4 mass percentage. This follows closely our model for predicting foam height, indicating again that Tegostab 8476 is a much stronger surfactant concerning cell wall stabilisation. We can use this probability curve to guide us to producing stable foams in future fPUF formulations.

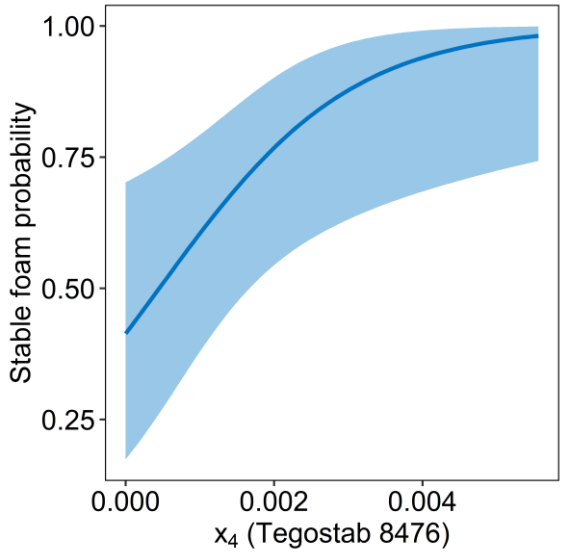

Figure 4.11: Logistic plot showing the probability of generating a fPUF foam as a function of the mass fraction Tegostab 8476.

The remaining data was used to generate a model for predicting density, shown in *Equation 4.8*. Table 4.4 gives the ANOVA table for the density of foams. The model for density is the least robust of the physical properties with an r^2 = 0.57. The low r value and low model robustness may be due to experimental error being introduced during mixing of reagents. Several foams reacted rapidly and required transferring to the reaction vessel before receiving the full 6 seconds of mixing at 3000 RPM. Repeat reactions of the same formulation may be necessary to improve the density models.

$$y_5 = -16.6x_1 - 64.3x_2 - 57.1x_3 + -80500(x_3 - 0.00230)^2 + 0.762 \qquad 4.8$$

This variability is also visible in the predicted and actual density values shown in Figure 4.12. Combining the t-ratio tests and the information gathered from the omitted data we can conclude that a minimum amount of surfactant, specifically Tegostab 8476 is required to produce stable foams, and once that threshold is exceeded, the density is a function of primarily the catalysts and remaining surfactant, which all reduce the density with an increase in loading.

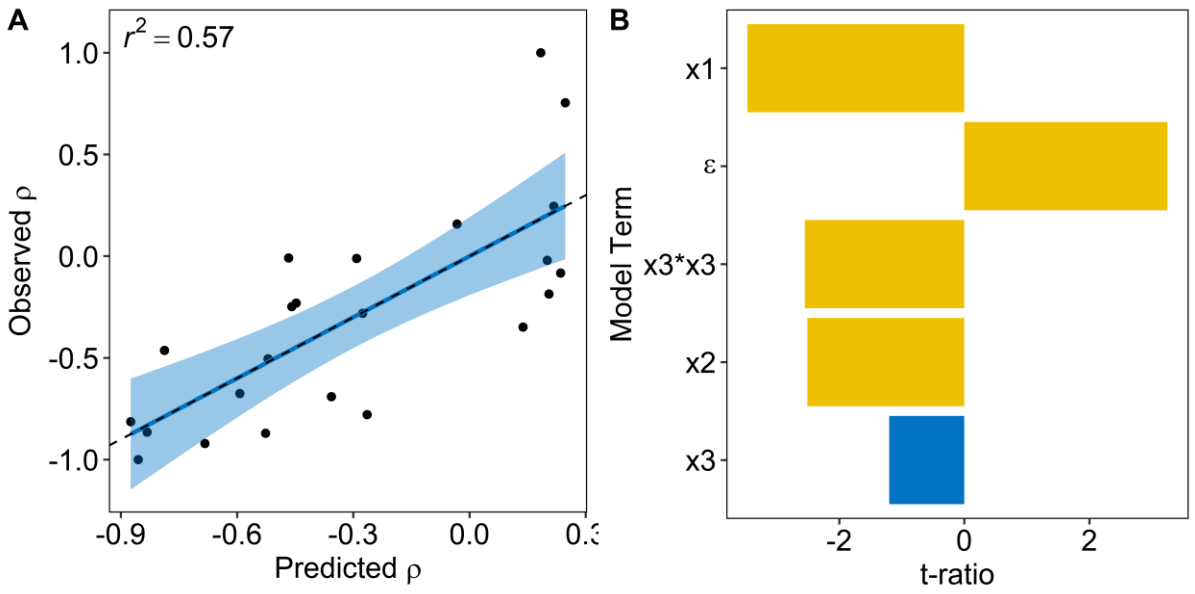

Figure 4.12: (A) predicted and observed density with the blue line indicating the fit and confidence interval and the dashed line indicating the y = x line and (B) t-ratio for density terms. x_1 is the Specflex Activ 2306 mass fraction, x_2 is the DMEA mass fraction and x_3 is the Tegostab BF2470 mass fraction.

Table 4.4: ANOVA table for the models used for fitting physical properties of fPUF.

Property	complexity	r^2	Kfold r^2	d.f.	F	*p*
Density*	5	0.57	0.27	4,18	6.00	.0030
Cell Size	5	0.63	0.47	4,20	8.46	.0004
WHC	9	0.89	0.66	8,17	17.6	<.0001
Log_{10}(WDPT)**	6	0.76	0.48	5,19	11.7	<.0001

**Subset of data with high density samples removed to ensure normality.*

***Data log transformed, due to lack of normal distribution.*

Cell Size

The equation for the model for the fPUF cell diameter is shown in *Equation 4.9*. Table 4.4 gives the ANOVA table for this model. Figure 4.13 (A) shows the predicted final cell size against the observed cell size, (B) shows the t-ratio for each of the model terms and (C) shows the contour plot for predicting cell size of fPUF formulations.

$$y_6 = -202x_3 - 159x_4 + 54400(x_3-0.00266)(x_4 - 0.00260) + 53634(x_3 - 0.00266)^2 + 0.612 \quad 4.9$$

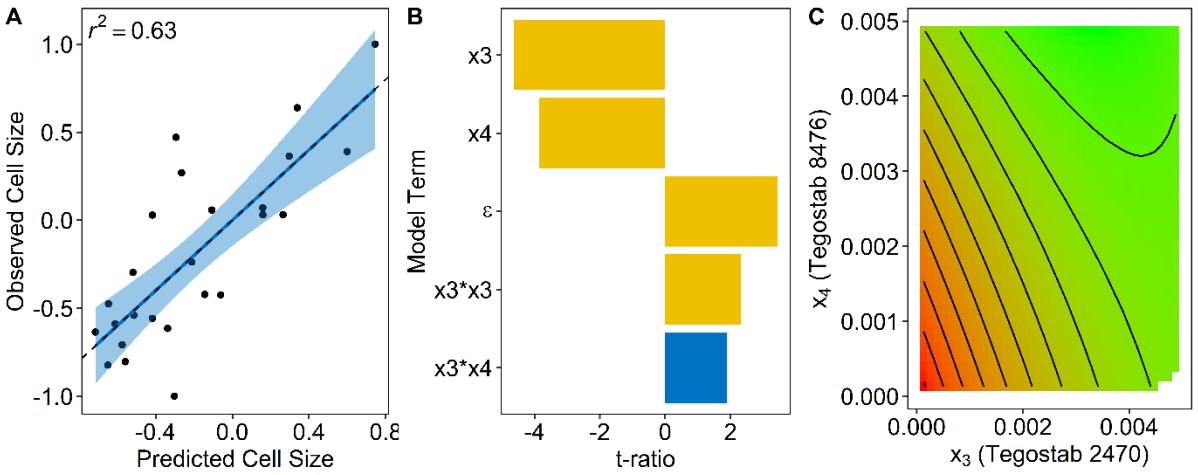

Figure 4.13: (A) predicted and observed cell size with the blue line indicating the fit and confidence interval and the dashed line indicating the y = x line, (b) t-ratio for cell size terms and (c) contour plot showing the influence of the two surfactants on the cell size of the foams, with green indicating smaller cell size and red indicating larger cell size. x_3 is the Tegostab BF2470 mass fraction and x_4 is the Tegostab 8476 mass fraction.

From Figure 4.13 (B) the only factors, which had a significant effect on the cell size of the fPUF, the amount of surfactant in the formulation (x_3 and x_4). Silicone surfactants increase bubble nucleation during the mixing of foam components, and this dictates the eventual cell size. It is therefore an expected result. The curvature and interaction term indicated that there is a saturation point, whereby the addition of any further surfactants no longer decreases the cell size of the foams. The model for cell size has a relatively low $r^2 = 0.63$ and p = .0004 indicating that surfactant level does not explain all the variation of cell size. It is well known that the foam cell size is related to the

way in which the reactants are mixed and experimental error that was introduced during mixing may account for the low model fit parameters.

Water Holding Capacity (WHC)

The equation for the model for the fPUF water holding capacity (WHC) is shown in *Equation 4.10*. Table 4.4 gives the ANOVA table for this model. Figure 4.14 (A) gives the predicted WHC against the actual WHC and (B) gives the t-ratio for all the model terms. The model for the WHC of the foam is the most complex of the physical property models, requiring nine terms to achieve a satisfactory and robust fit. This complexity stems from the fact that fPUF can take up water by two separate mechanisms, physical adsorption where capillary action fills the cell voids and chemical absorption where the water dissolves and swells the polymer. The first mechanism for water uptake would be the adsorption of water into the cell voids, which would be dependent on the cell size, the density and the percentage open and closed cells of the fPUF. The second mechanism of absorption would be into the polymer material itself. This is dependent on the amount of ethylene oxide (EO) and propylene oxide (PO) in the soft segment of the foam.

$$y_7 = -4.84x_1 + 66.9x_2 + 125x_3 + 127x_4 - 5300(x_1 - 0.0251)(x_4 - 0.00273) - 11000(x_2 - 0.00439)^2 - 92200(x_3 - 0.00256)^2 - 51800(x_4 - 0.00273)^2 - 0.132 \quad \textit{4.10}$$

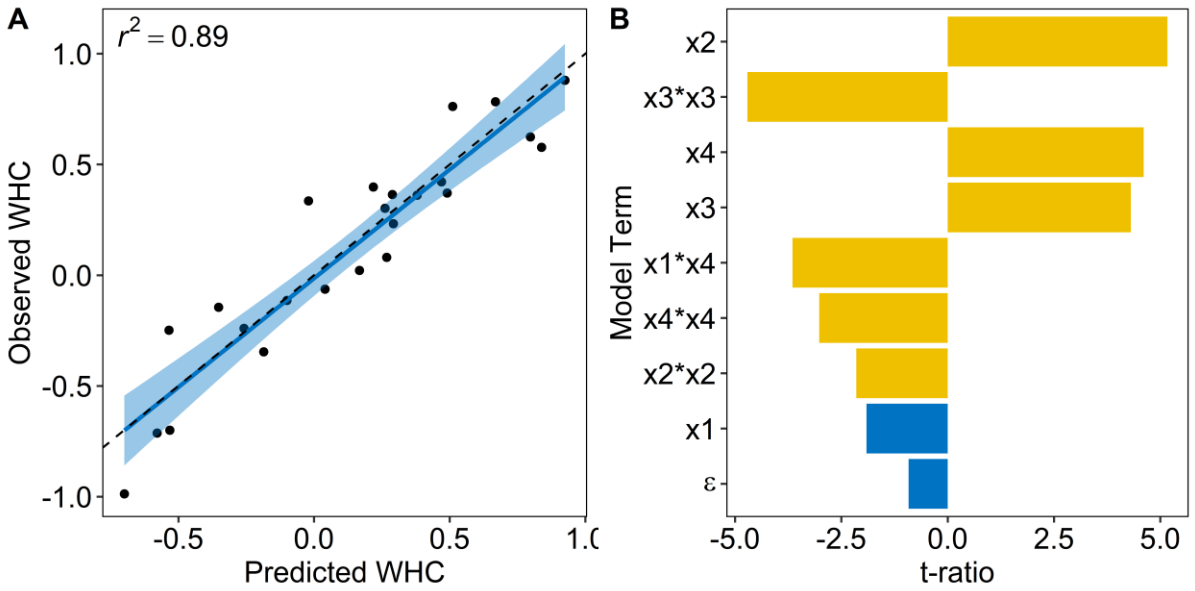

Figure 4.14: (A) predicted and observed WHC with the blue line indicating the fit and confidence interval and the dashed line indicating the y = x line , (B) t-ratio for WHC model terms. x_1 is the Specflex Activ 2306 mass fraction, x_2 is the DMEA mass fraction, x_3 is the Tegostab BF2470 mass fraction and x_4 is the Tegostab 8476 loading.

The terms, which increase the water holding capacity, are x_2 (DMEA loading) and the two surfactant loadings x_3 and x_4. The significant curvature terms of the two surfactants, indicate that there is a maximum WHC after which the addition of any further surfactant causes a decrease in WHC. This is shown in a static prediction profiler taken from JMP shown in Figure 4.15. This curvature may indicate the point where cell walls become over-stabilised and lead to a foam with a higher proportion of closed cells, decreasing the WHC of the fPUF.

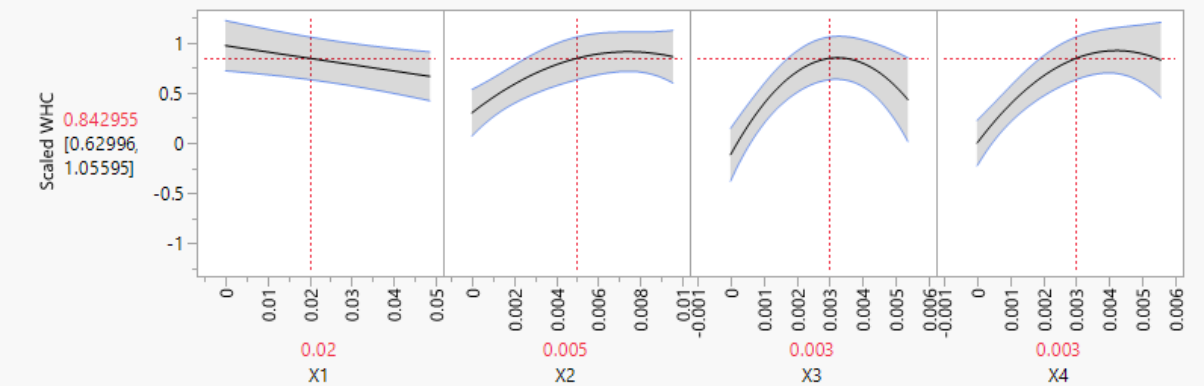

Figure 4.15: Prediction profiler for WHC from JMP at a static formulation showing the predicted scaled WHC response as a function of the mass fraction of each factor. x_1 is the Specflex Activ 2306 mass fraction, x_2 is the DMEA mass fraction, x_3 is the Tegostab BF2470 mass fraction and x_4 is the Tegostab 8476 loading.

Water Drop Penetration Time (WDPT)

The equation for the model for the fPUF water drop penetration time (WDPT) is shown in *Equation 4.11*. Table 4.4 gives the ANOVA table for this model. Figure 4.16 (A) gives the predicted WDPT against the actual WDPT and (B) gives the t-ratio for all the model terms. WDPT data was log transformed to ensure that the data was normally distributed. This occurred as some samples had high WDPT times taking several thousand seconds for the droplet to be absorbed, indicating highly hydrophobic foams.

$$y_8 = 2.80x_1 - 108x_3 + 183x_4 - 5150(x_1 - 0.0242)(x_3 - 0.00247) - 56800(x_3 - 0.00247)(x_4 - 0.00268) - 0.418 \quad 4.11$$

The Tegostab 8476 loading (x_4) was the most significant term, with an increase in loading, increasing the WDPT. The second surfactant Tegostab BF2470 (x_3) had a more expected result, with an increase in surfactant loading, decreasing the WDPT. The Tegostab 8476 may be over stabilising the cell walls and leading to closed cells, an affect more noticeable in the WDPT test when compared to the WHC models, as the foams are soaked for 24 hours in the WHC test allowing sufficient time for water to penetrate all the void spaces within the foam, possibly due to the transfer via the absorption process.

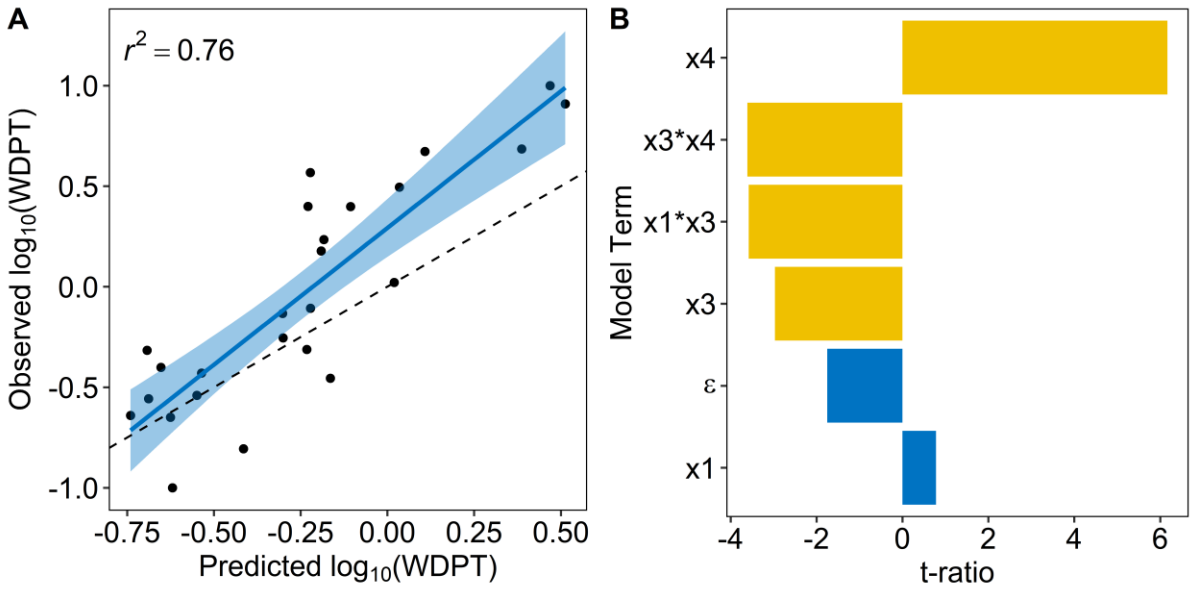

Figure 4.16: (A) predicted and observed WDPT with the blue line indicating the fit and confidence interval and the dashed line indicating the y = x line and (B) t-ratio for WDPT terms. x_1 is the Specflex Activ 2306 mass fraction, x_3 is the Tegostab BF2470 mass fraction and x_4 is the Tegostab 8476 loading.

4.5. Conclusions and recommendations

Statistical DOE was used to test the effect of two catalysts and two surfactants on the reaction kinetics and physical properties of fPUF. 32 formulations were tested and four reaction kinetic properties (isocyanate conversion, foam height, time until maximum reaction temperature and time until maximum height) and four physical properties (density, cell size, water holding capacity and water drop penetration time) were studied. A generalised model was used for all responses, which were reduced, using k-fold cross validation and elastic net regression.

The loading of the two catalysts had the greatest significance on the isocyanate conversion, with a saturation point being reached, after which the addition of any further catalysts had little to no effect on the isocyanate conversion. At these high catalyst loadings the isocyanate conversion also neared 100 %. DMEA was the more significant of the two catalysts. The time to maximum temperature again indicated high significance of the DMEA loading. The larger error term in the time to maximum temperature indicates that there may be experimental error being introduced, possibly

due to disparities in mixing times and speeds between samples. The final height model for the foams was a function of all the four factors, explained by the fact that both catalysts can act as blowing catalysts and surfactants are required to stop the foam from collapsing. The time until maximum height model was only a function of the DMEA loading.

The high significance of the DMEA catalyst in all four kinetic reaction responses measured indicates that it is the more catalytically active (per unit mass) of the two catalysts. This is likely the case due to the DMEA having a much lower equivalent weight (total molar mass divided by the number of tertiary amine groups) than the Specflex Activ 2306 catalytic polyol.

Physical properties were also modelled using the same methodology. A subset of density data needed to be removed to ensure that the data was normally distributed. The data excluded from the density analysis was from collapsed foams having significantly higher density. However, the collapsed foam data was used to produce a logistic plot indicating the probability of producing a stable foam at different Tegostab 8476 loadings. This plot is useful for ensuring that future formulations are likely to produce stable foams. The density model is the least robust of the physical property models, likely due to mixing effects. Cell size was modelled using the loading of the two surfactants, both reducing the cell size with an increase in loading until a saturation point was reached and the addition of any further surfactant had little effect on the cell size of the foams. WHC was the most complex of the models, requiring 9 terms for an acceptable and robust fit. The most significant terms were the DMEA loading and the surfactant loadings. All three components increasing the WHC with an increase in loading. However, interaction and curvature terms indicated that increasing the surfactants above a certain point decreased the WHC capacity of the foam. This is likely due to over stabilisation of the cell walls leading to an increase in the formation of closed cells. A similar result was seen in the WDPT model; however, this indicated that the increase in loading of the stronger surfactant Tegostab 8476 would increase the WDPT. Tegostab 8476 is often the catalyst of choice for applications requiring closed cell foams and our results are in agreement that this surfactant likely increases the number of closed cells in our system.

All reaction kinetic responses and physical properties were successfully modelled and the models are able to predict formulations for the generation of a range of foams with varying properties whilst ensuring complete chemical reaction. Mixing effects may be reduced by the use of a more consistent or automated mixer, either static or impingement. The addition of a method and model for determining the ratio of open to closed cell foams would complement this work, giving further insight into some of the inflection points seen in the WHC and WDPT data specifically.

Chapter 5:
Optimising fPUF Physical Properties for Plant Growth

5.1. DOE and Model Choice for fPUF Physical Properties

Models for predicting four fPUF physical properties (density, cell size, WHC and WDPT) from the catalyst and surfactant loadings were developed in Chapter 4. These physical property models in conjunction with the models developed for ensuring complete isocyanate conversion are capable of developing a new set of foams with varying physical properties. This serves two purposes. It allows for an assessment of the predictive performance of the physical property models, and the generation of foams with a range of different physical properties to determine a fPUF formulation that would optimise plant growth in a hydroponic system.

5.1.1. **DOE**

The same design of experiment process was followed as that in Chapter 4. We are interested here in understanding which physical properties of a fPUF foam influence the growth of plants in a hydroponic system, and in optimising these properties for producing maximum yield.

The chosen response variables are growth (AUC determined by calculating the area under the plant height curve), shoot dry mass (m_d), total chlorophyll (c_t) as a measure of plant health, phosphorus (P) content in leaf matter and nitrogen (N) content in leaf matter as shown in Table 5.1. Plant survivability was also measured however no model was developed for predicting survivability. The plants root mass was also of interest, however due to the nature of the fPUF media, recovery of roots was not possible.

Table 5.1: List of the selected response variables for modelling plant growth using DoE techniques.

Property	Response
AUC	z_1
m_d	z_2
c_t	z_3
N	z_4
P	z_5

The WHC and WDPT models developed in Chapter 4 showed significant curvature, with an increase in surfactant increasing the WHC to a maximum and further addition of surfactant reducing the WHC. The WDPT model revealed that the strong cell stabilising surfactant Tegostab 8476 increased the WDPT. These unexpected results were explained by the surfactants over stabilising the cells and leading to a higher ratio of closed cells compared to open cells. A new technique was developed for measuring the airflow through the foam to help understand this behaviour. The method described in Chapter 2.2.8 for measuring airflow (indirectly the ratio of open to closed cells) was used. The open cells ratio was suspected of influencing plant root development and plant growth. For this reason, it was included as a DOE factor. Table 5.2 lists the factors used for the plant growth DOE.

Table 5.2: List of the fPUF physical property factors used for the modelling of plant growth.

Property	Factor
Density	α_1
Cell Size	α_2
WDPT	α_3
WHC	α_4
Airflow	α_5

The models developed in Chapter 4 would dictate the ranges of the factors and the predicted values are in the unitless rescaled range.

Due to the practical limits of a growth trial, simpler empirical models were required for predicting plant responses. A quadratic model with no interaction terms, *Equation 5.1* was chosen. This model with five factors has 11 terms, the five main effects, the five curvature effects and the error term. The minimum number of experiments required is therefore twelve. The maximum number of formulations that could be trialled using the hydroponic setup available was fifteen and therefore fifteen formulations were trialled.

$$z_i = \sum_{1 \le i \le q} \beta_i \alpha_i + \sum_{1 \le i \le q} \beta_{ii} \alpha_i^2 + \in \qquad 5.1$$

Constraints were put on the experimental design to limit formulations to those that had over 90 % isocyanate conversion to ensure complete reaction of reagents. This section of experimental space is shown as the hatched region in Figure 5.1.

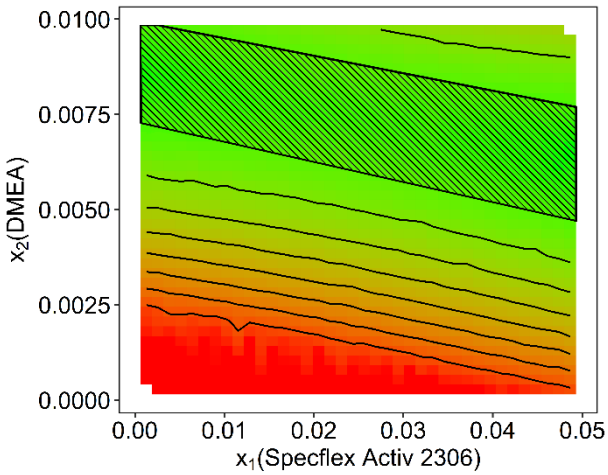

Figure 5.1: The isocyanate conversion as a function of the DMEA and Specflex Activ 2306 catalyst loadings. The hatched region indicates the region where isocyanate conversion is greater than 90 %.

Conventional experimental design techniques assume that you can control each of the factors independently, which is not the case for this experimental dataset. Chapter 4 clearly demonstrated that a change in loading of any of the catalysts or surfactants was unlikely to only change a single property and more likely to influence several physical properties at once.

An alternative method for selecting the experimental factor points was required. To determine the location of the experimental points the models developed in Chapter 4 were used to predict the extreme points (minimum and maximum) as well as the midpoint of the predictable values of each of the four physical properties (density, cell size, WHC and WDPT) separately, whilst not controlling for the other three factors. An example of this is shown in Figure 5.2. The maximum (triangle), minimum (inverted triangle) and midpoint (square) predictions for the cell size are shown on the scaled predicted figure and the paired predicted properties for the other three properties (cell size, WDPT and WHC) are also shown. The points shown in Figure 5.2 for the remaining three physical properties were predicted using their corresponding models

from Chapter 4. This process was repeated for the other three properties to generate twelve formulations.

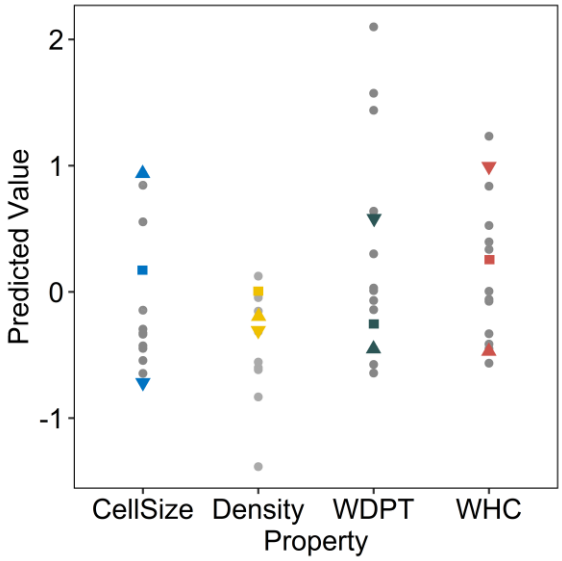

Figure 5.2: An example of the predicted minimum (inverted triangle), maximum (triangle) and midpoint (square) of the cell size data used for selecting three formulations for the growth trial. The paired predictions for the other physical properties are also shown.

The remaining three formulations were selected by plotting the physical property predictions for the first twelve formulations and filling in any obvious gaps in the experimental space. Figure 5.3 shows the predicted physical properties for all fifteen formulations. Experimental points were selected using the first four factors and not airflow, as we did not have a model was yet to be developed for airflow.

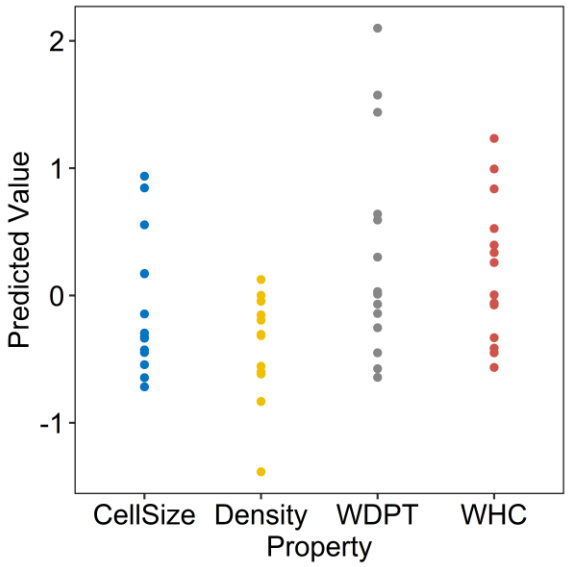

Figure 5.3: Predicted foam properties for the fifteen formulations used for the plant growth DoE trial.

5.1.2. **fPUF physical properties**

The fifteen foam formulations were made by reacting them directly into six plant pots (five growth repetitions and one for measuring physical properties) with a 15 cm diameter and a total volume of 1400 ml. Fourteen of the formulations made stable foams with one collapsing. The nominal logistic plot in Figure 4.11 predicted that this formulation had a 51 % chance of producing a stable foam so it was not completly unexpected that this foam collapsed. The physical properties responses of remaining foams was measured.

5.1.2.1. *Airflow*

A model was developed for the airflow of the foams using the same methods used in Chapter 4. *Equation 5.2* shows the model for the airflow. A simple linear model of each of the four formulation factors fitted the data with an r^2 = 0.93. Table 5.3 shows the ANOVA table for the model and Figure 5.4 (A) shows the fitted and observed values and (B) shows the t-ratio test for each of the terms.

$$y_9 = - 25.7x_1 - 229.0x_2 + 98.0x_3 - 155x_4 + 2.16 \qquad 5.2$$

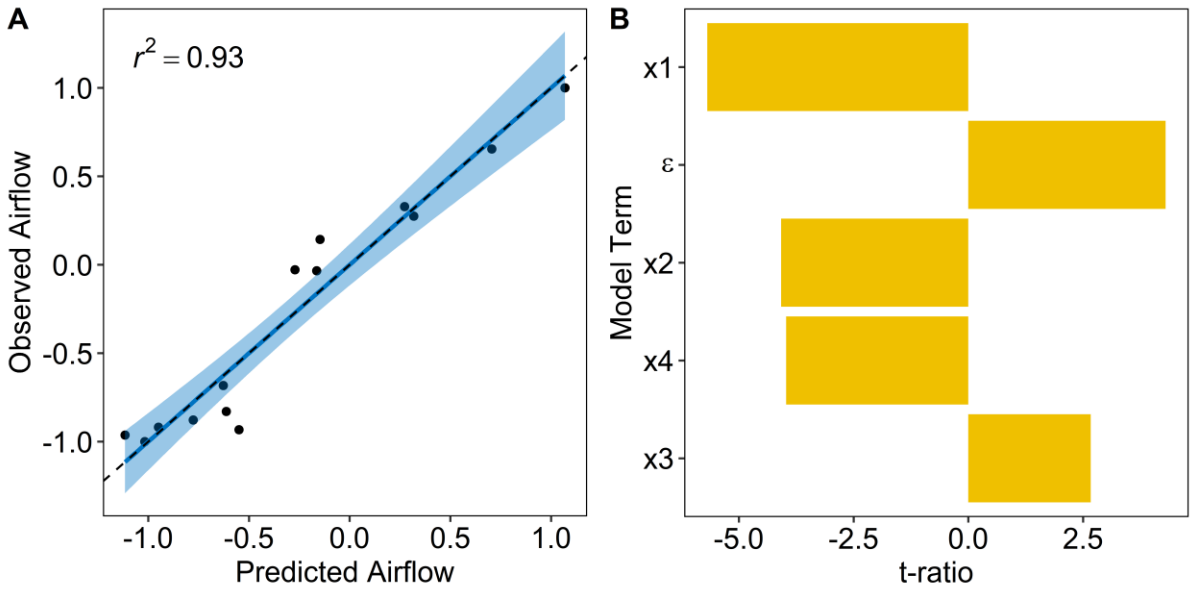

Figure 5.4: (A) predicted and actual airflow, (B) t-ratio for isocyanate airflow terms.

Table 5.3: ANOVA table for model fitting the airflow.

Property	complexity	r^2	Kfold r^2	d.f.	F	*p*
Airflow	5	0.93	0.88	4, 9	31.8	<.0001

The model agrees with some of our results in Chapter 4, especially the behaviour of the two surfactants. The Tegostab 8476 has a negative term, suggesting that it tends to stabilise cell walls promoting closed cells, when compared to the Tegostab BF2470 which has a positive term. The two catalysts also have a negative term suggesting that an increase in either decreases the airflow in the foam. This is unexpected, especially the decrease in airflow with increase in DMEA loading. This may be due to the high significance and value of the ϵ term, which indicates that even at zero loading of all catalysts and surfactants the foam would have near maximum airflow.

5.1.2.2. *Assessing Performance of Physical Property Models*

The predictive ability of the remaining four physical properties was assessed by plotting the observed against predicted graphs, doing a one way ANOVA on the regression between the predicted and observed and determining whether the predicted observed line differed significantly from the x=y line. Figure 5.5 shows the

fitted lines for the four physical properties and Table 5.4 shows the r^2 for each physical property as well as the results from the one way ANOVA.

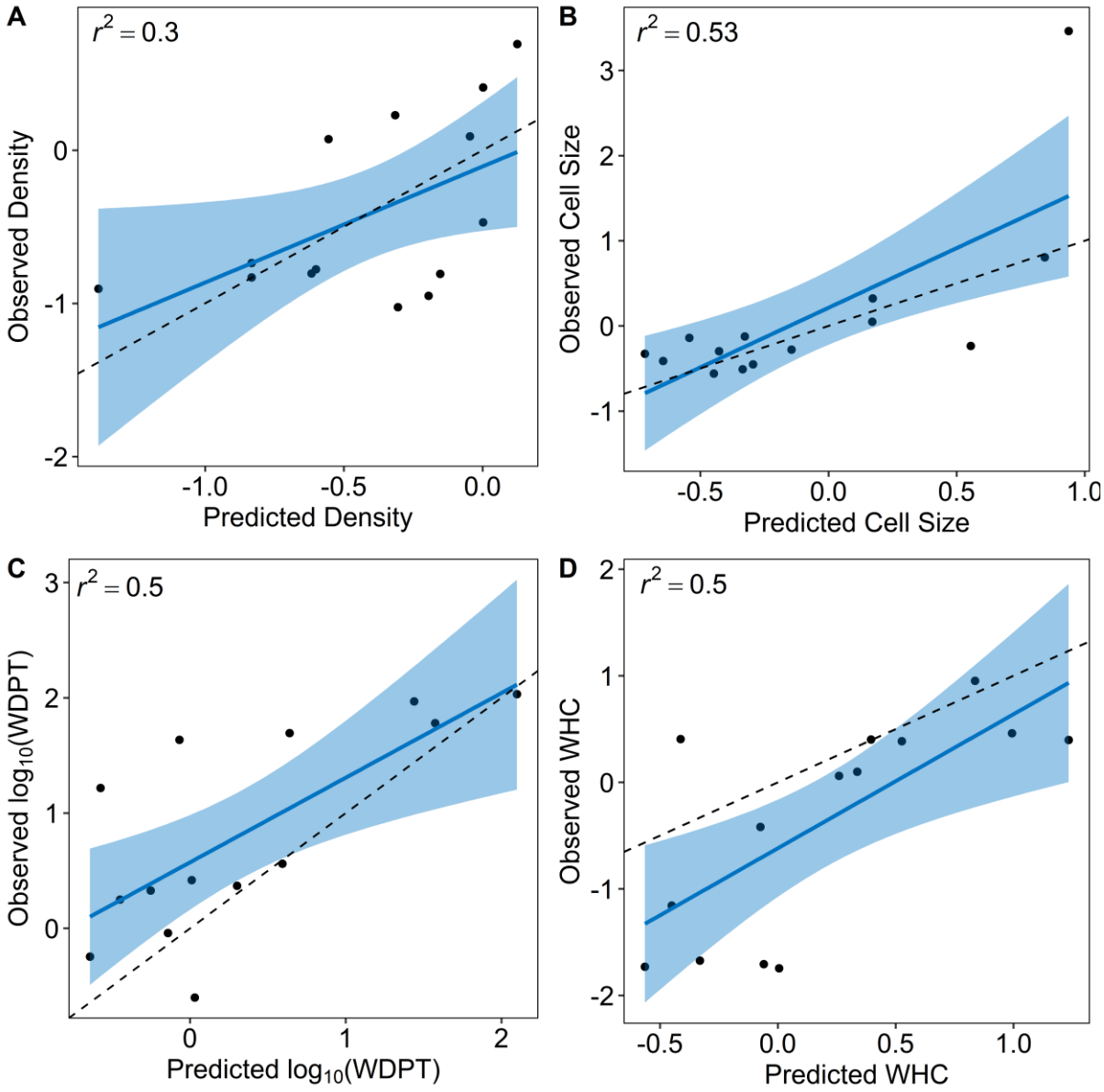

Figure 5.5: The observed and predicted physical property models, with the blue line indicating the linear regression line with confidence interval and the dashed line indicating the x = y line for (A) density, (B) Cell size, (C) log_{10}(WDPT) and (D) WHC.

Table 5.4: Results for the linear regression for physical property models.

Property	r^2	f	d.f	*p*
Density	0.30	5.09	1,12	.0430
Cell Size	0.53	13.7	1,12	.00301
log_{10}(WDPT)	0.50	11.8	1,12	.00498
WHC	0.50	12.0	1,12	.00474

The density was the worst performing of the models, which agrees with our findings from Chapter 4 which indicated that there was a large amount of variance not explained by the model. The other three physical property models all performed similarly, although with lower than expected r^2 values. ANOVA indicated that the linear regression fit was significant for all four models, at a significance of $p < .05$ for the density model and $p < .005$ for the remaining models. The observed r^2 are nearly identical to the k-fold cross validation r^2 values used to select the models in Chapter 4. This shows the importance of the k-fold cross validation technique when selecting the best performing models, more complex models would have increased the overall r^2 of the original model, however this would also have increased the model validation error and therefore led to models with less robust prediction capabilities.

There is one sample (formulation 5) where the cell size model massively under predicted the actual cell size. This sample was barely classed as a stable foam having much larger cell size and very different mechanical properties (very hard, not very flexible, crumbles on compression).

From Figure 5.5 we can also see that the regression fit for the log_{10}(WDPT) as well as the WHC differs from the x = y line. The log_{10}(WDPT) model appears to over predict the log_{10}(WDPT) at low values but predicts more correctly at higher values. The WHC model appears to under predict the actual WHC at all values.

All physical property data from the growth trial foams was fed back into JMP software to refine the physical property models for all further foam development.

5.2. Growth Trial

This plant growth study was carried out in a temperature controlled greenhouse at the Arthur Willis Environmental Centre (AWEC) at the University of Sheffield with a day/ night regime of 12 h at 20 °C / 12 h at 15 °C from 2019/05/15 until 2019/07/16 (8 weeks). Supplementary lighting was used to achieve a minimum solar irradiation of 1000 $W.m^{-2}$ (Phillips Mastercolour CDM-T Elite MW 315W/942 1CT). Pots with a diameter of a 15 cm and a volume of 1400 ml were used. Spring onion (*Allium sepa)* seeds of the variety White Lisbon (Premier Seeds Direct, Wiltshire, UK) were pre-germinated and transplanted to Grodan rockwool starter cubes on 2019/04/23. These seedlings were transplanted into foam on 2019/05/15. Five seedlings were planted per pot with five replicates for each formulation for a total of 350 plants. Plants were supplied with Long Ashton solution[139] via a dripper feed delivering 2 l. hr^{-1}. The drippers were on a timer supplying the plants with nutrient solution for 15 minutes each day. The solution was changed every two weeks and the concentration sequentially increased from 20 %, to 40 % and to 60 % strength over the 8 week growth period. pH of the nutrient solution was maintained between 6 and 6.5 and was adjusted using a 10 % phosphoric acid solution.

Plant height was measured twice a week and the number of surviving plants was also checked twice a week. Plants were photographed once a week to determine the total amount of chlorophyll as a measure of plant health.

5.3. Plant Response Models

5.3.1. **Scatter Plot Matrix**

The same approach for analysis of plant response models was taken as that used for the fPUF physical properties models. A scatter plot matrix identifies any obvious bivariate relationships. The Pearson's correlation coefficient further explores these relationships. Figure 5.6 shows the scatter plot matrix for the plant responses as well as the fPUF physical properties factors. All modelling was done on the mean value of the plant response data to minimise the effects of biological variation.

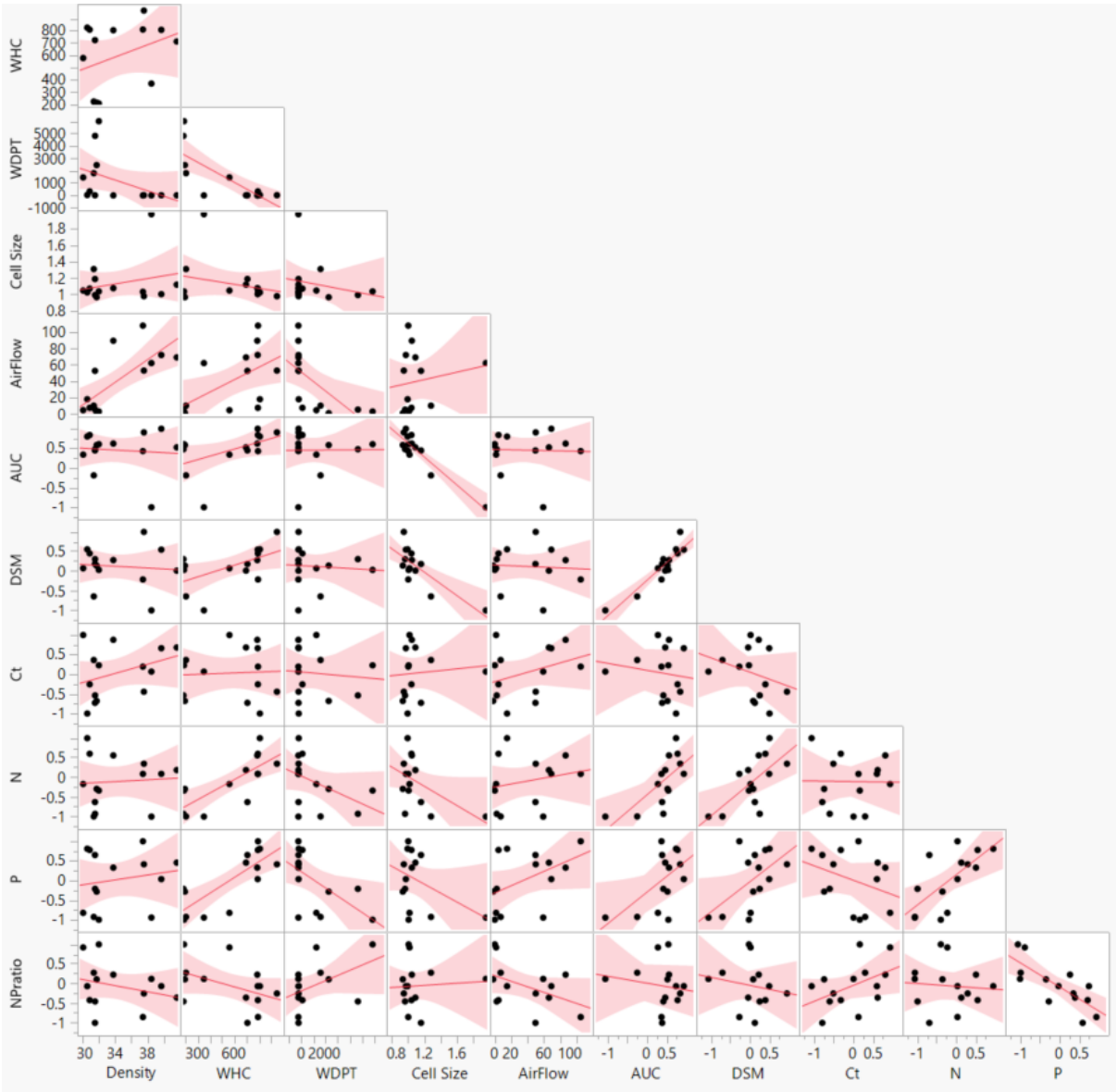

Figure 5.6: Scatterplot matrix of the plant growth factors and responses from JMP software.

Figure 5.7 shows the bivariate relationships between several plant growth responses and fPUF physical properties. It is clear from Figure 5.7 (A) and (B) that cell size has a major influence on the plant growth responses, with it being highly correlated to the area under plant height curves AUC (r = -0.92) and highly correlated to the plant dry shoot mass m_d (r = -0.78). The point at cell size ~ 1.9 mm is a highly influential point, indicating that a choice of models may be highly influenced by this point, and this formulation (5) will be investigated further in the following sections. The negative value of both these coefficients indicates that a larger fPUF cell size reduces the plant growth responses. Figure 5.7 (C) shows that there is a correlation between the AUC and m_d (0.92). This high correlation coefficient is expected as both the dry shoot mass and the

area under curve measurement are observations of the same variable, plant growth. This also explains the similar correlation of both responses to the cell size of the fPUF. It is expected that similar models will explain both responses. From Figure 5.7 (D) and (E) is clear that water holding capacity is the most important factor with regards to plant shoot nutrient content. The WHC is highly, positively correlated to both the shoot nitrogen (r = 0.77) and the phosphorus content (r = 0.79), indicating that a higher water holding capacity results in higher N and P content of plant shoots. Figure 5.7 (F) shows a positive correlation between the N and P content of the plant shoots (r = 0.68). Considering the nutrient and watering regime for all samples was the same, this indicates that fPUF physical properties are influencing the absorption of nutrients through plant roots and the WHC is the most correlated of these physical properties.

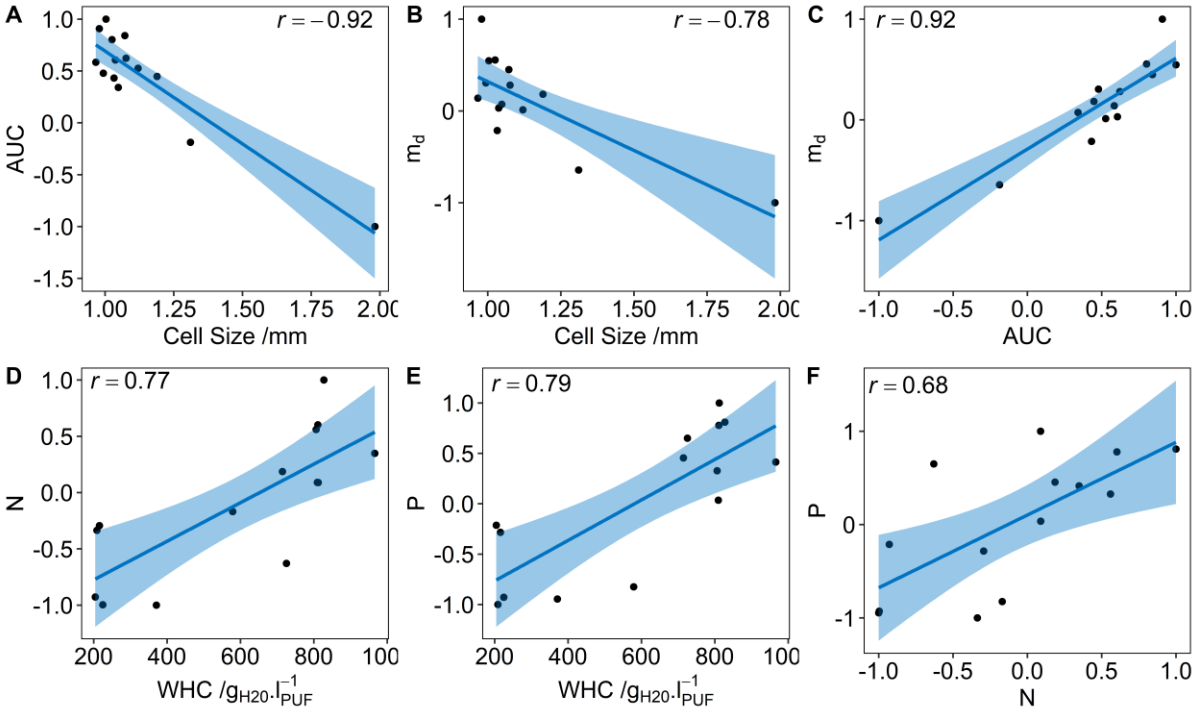

Figure 5.7: Bivariate relationships between (A) area under plant height curve and fPUF cell size, (B) the dry shoot mass and fPUF cell size (C) the dry shoot mass and the area under plant height curve, (D) plant shoot nitrogen content and the fPUF water holding capacity, (E) the plant shoot phosphorus content and the fPUF water holding capacity and (F) the plant shoot nitrogen and phosphorus content. r is the Pearsons correlation coefficient for each of the relationships

Curvature in these relationships is not obvious, however the use of the more complex general model suggested in *Equation 5.1*, would lead to models that are more accurate and improve the fit when compared to the linear bivariate models.

5.3.2. **Survivability**

The Kaplan-Meier survivability curve is shown in Figure 5.8, with two formulations differing significantly from the no-death curve according to the log-rank test. The first and most significant of these is formulation 5 with only 3 (9 %) of the plants surviving until the end of the trial. This formulation has previously been mentioned, having vastly different foam properties from the other formulations. Figure 5.9 shows the optical microscope image used for determining cell size of (A) formulation 5 as well as (B) formulation 7, a sample with a more representative cell structure. All of these plants appeared to die due to lack of water, which is highly likely as the cell size as well as mechanical properties were not conducive to transporting water equally throughout the foam. The other formulation which was significantly different was formulation 6, with 20 (80 %) of the plants surviving until the end of the trial. Diagnosis for this formulation is not as straightforward as none of the physical properties were significantly different from the other formulations. The plants, which did not survive, appeared to die due to lack of water. It was anecdotally observed that formulation 6 interacted in a different manner to the other formulations. This formulation had vastly different hydrodynamic behaviour, with water not wicking horizontally from the irrigation point. The water instead travelled down through the foam and drained out the bottom without wetting the outer edges of the foam. A test on the capillary action of the different foams or the generation of water retention curves may help understand this behaviour.

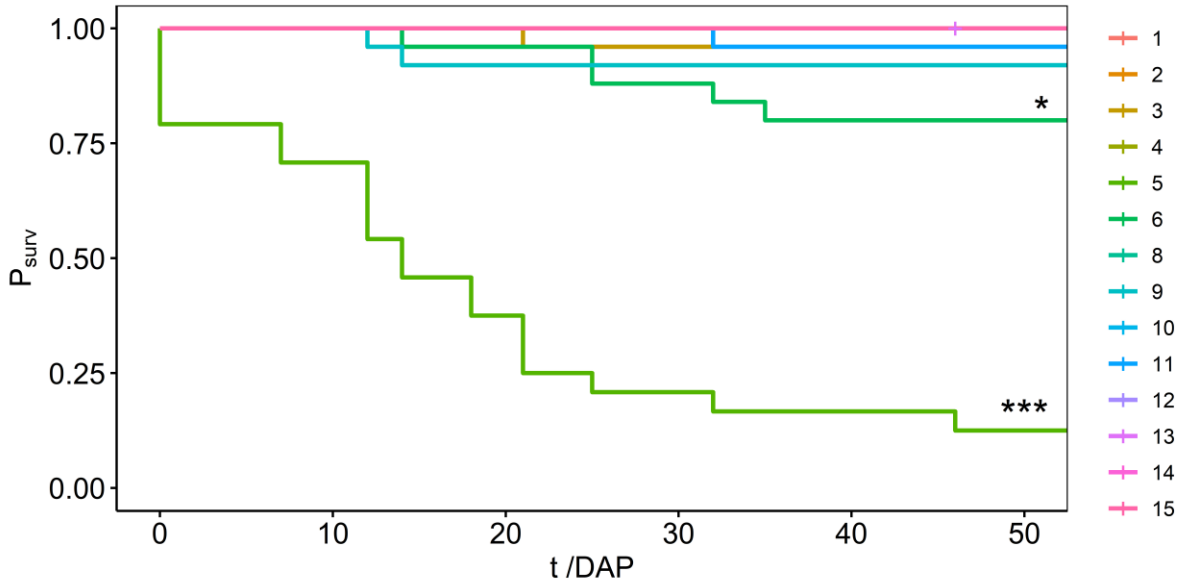

*Figure 5.8: Kaplan-Meier survivability curve for different foam formulations. Asterisks indicate significant differences from zero deaths, *p < .05, ***p < .001 (log rank test).*

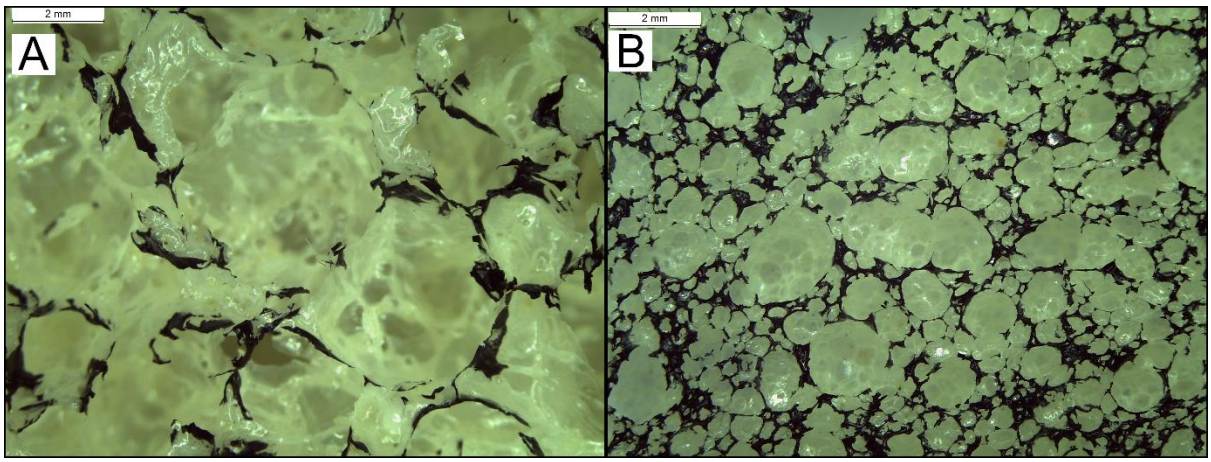

Figure 5.9: OM photograph of (A) formulation 5 and (B) formulation 7 for cell size comparison.

5.3.3. **Plant Height**

The mean plant heights as well as the curves fitted to this are shown in Figure 5.10. These curves are used to calculate the area under the curve (AUC) of the plant height data as a measure of plant growth. From Figure 5.10 it is clear that the exponential growth curve was a good fit for the data set, with the only exception being formulation five.

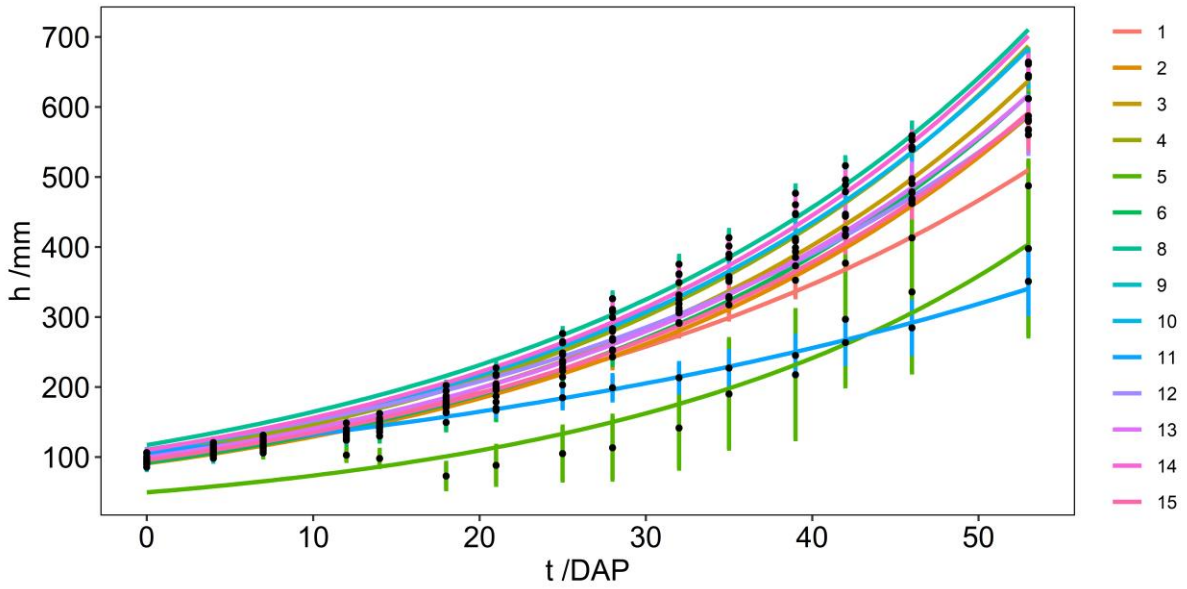

Figure 5.10: Plant height curve for different foam formulations with fitted curves used to calculate AUC. Error bars represent ± 1 standard error.

The model used to fit the AUC is shown in *Equation 5.3* and Table 5.5 shows the ANOVA results for the fitted model. Figure 5.11 shows the (A) predicted and observed values of the AUC, (B) the t-ratio for the model terms and the (C) contour plot showing the influence of the cell size (α_2) and the WHC (α_4) on the plant growth with the green indicating a high AUC value and red indicating a low AUC value.

$$z_1 = - 1.65\alpha_2 + 0.000502\alpha_4 + 2.02 \qquad 5.3$$

The cell size of the foam and the WHC of the foam are the only two factors which influence the growth of spring onions in fPUF in terms of the AUC response. This simple linear model explains a large portion of the total variance with a r^2 of 0.91. The cell size has a negative term, indicating that smaller cell sizes improve plant growth. The WHC has a positive term, indicating that the higher WHC of foams improves plant growth under this watering regime.

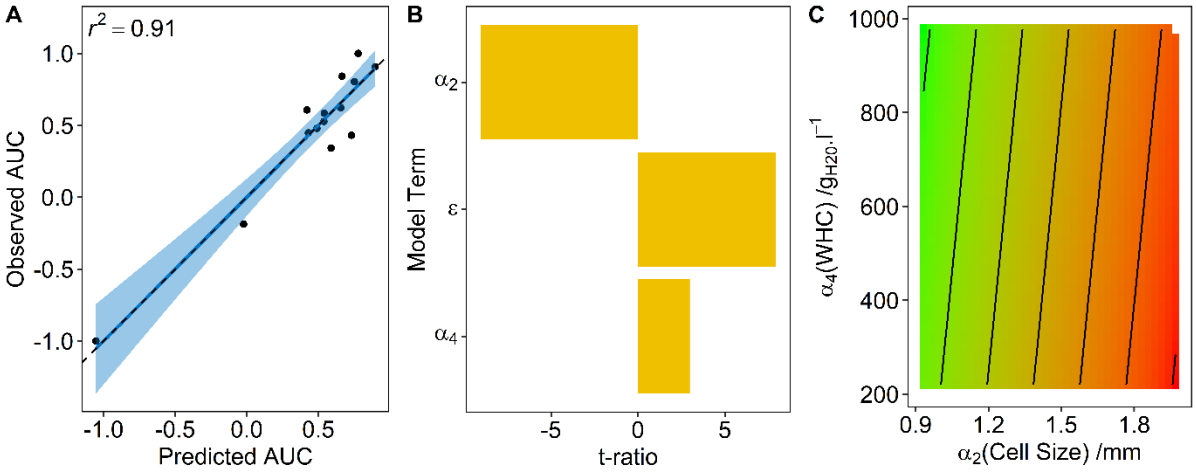

Figure 5.11: (A) Predicted and observed AUC with the blue line indicating the fit and confidence interval and the dashed line indicating the y = x line, (B) t-ratio for AUC model terms and (C) contour plot showing the influence of the cell size and WHC on the AUC with green indicating high AUC values and red indicating low AUC values. α_2 is the cell size and α_4 is the WHC.

Table 5.5: ANOVA results for the plant response models.

Property	complexity	r^2	Kfold r^2	d.f.	F	*p*
AUC	3	0.91	0.80	2,11	56.1	<.0001
m_d	6	0.96	0.76	5, 8	35.2	<.0001
C_t^*	-	-		-	-	-
N	3	0.69	0.37	2, 11	12.4	.0015
P	3	0.67	0.41	2, 11	11.2	.0022

**Did not reach statistical significance in an one way ANOVA test.*

5.3.4. **Dry Plant Shoot Mass (m_d)**

The dry plant shoot mass model is shown in *Equation 5.4* and the results from the ANOVA analysis is shown in Table 5.5. Figure 5.12 shows the (A) predicted and observed values for the m_d model and (B) the f-ratio for the model terms. The plant dry mass is reported on a dry mass per plant basis.

$$z_2 = -2.90\alpha_2 + 0.000653\alpha_4 + 0.000549\alpha_5 + 2.02(\alpha_2 - 1.13)^2 - 0.000188(\alpha_5 - 39.7)^2 + 3.10 \qquad 5.4$$

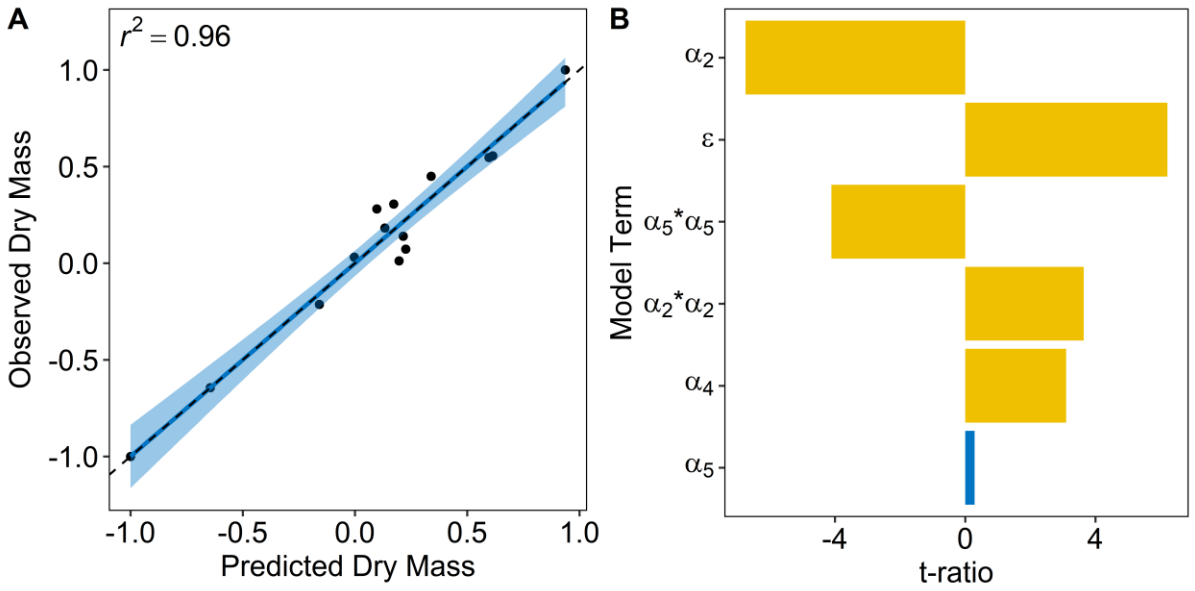

Figure 5.12: (A) Predicted and observed dry mass (m_d) with the blue line indicating the fit and confidence interval and the dashed line indicating the y = x line and (B) t-ratio for m_d model terms. α_2 is the cell size, α_3 is the airflow and α_4 is the WHC.

The m_d model includes all the terms that were used in the AUC model, which is expected as the two growth parameters are correlated as shown in Figure 5.7. The model also includes airflow as a factor as well as a curvature term for the cell size and the airflow. Although the airflow term alone does not reach significance, the curvature term is significant. The linear WHC term indicates that plant mass increases with an increase in WHC. The cell size has a negative term again, indicating that plant mass decreases with an increase in cell size however the curvature term shows that after a critical cell size (~1.8 mm), plant growth is no longer affected. The airflow terms show that an increase in airflow, increases the plant mass, however there is a maximum, where if airflow is increased beyond this point, plant mass decreases. Figure 5.13 shows a static image from the dynamic profiler in JMP showing this curvature. This decrease in plant mass at high airflow and therefore ratio of open cells, may be due to the nutrient solution draining from the media too quickly, before the plant has absorbed the optimum amount of water and nutrients.

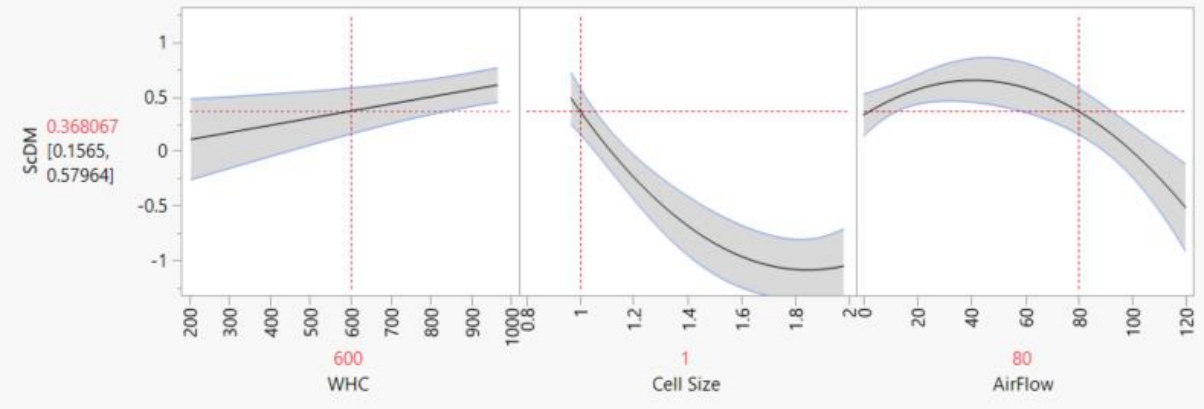

Figure 5.13: Static image from the dynamic prediction profiler in the JMP software showing the scaled plant shoot dry mass as a function of WHC, cell size and airflow.

The differences in WHC between the foam samples meant that not all foam pots were able to retain all of the nutrient solution at each watering event. This would mean that even though each pot was supplied the same amount of nutrient solution, every plant would not necessarily receive the same amount of nutrient solution. This would explain the high significance of the WHC term in both the AUC and the m_d models.

5.3.5. **Chlorophyll Content**

The total chlorophyll content was determined using photographs and the colourimetric method developed in Chapter 2.4.4. The difference in total chlorophyll between the different formulations did not reach significance in a one way ANOVA, with the results summarised in Table 5.6. This lack of significant variation between the different formulations meant no further modelling was done.

Table 5.6: Summary of the one way ANOVA for C_t response.

Property	d.f.	F	*p*
C_t	13,344	1.416	0.149

The lack of significance indicates that although the different formulations affect plant growth, the differences in the physical properties have no significant effect on the total chlorophyll content of the plants under these experimental conditions.

5.3.6. **Shoot Nitrogen Content (N)**

The model for plant shoot nitrogen content is shown in *Equation 5.5* and Table 5.5 shows the ANOVA table for the response. Figure 5.14 (A) shows the observed N shoot content and the predicted N content, (B) shows the t-ratio test for the model terms and (C) shows the contour plot for WHC and cell size of fPUF and their influence on plant N shoot content, with green indicating high N content and red indicating how N content.

$$z_4 = -0.800\alpha_2 + 0.00152\alpha_4 - 0.100 \qquad 5.5$$

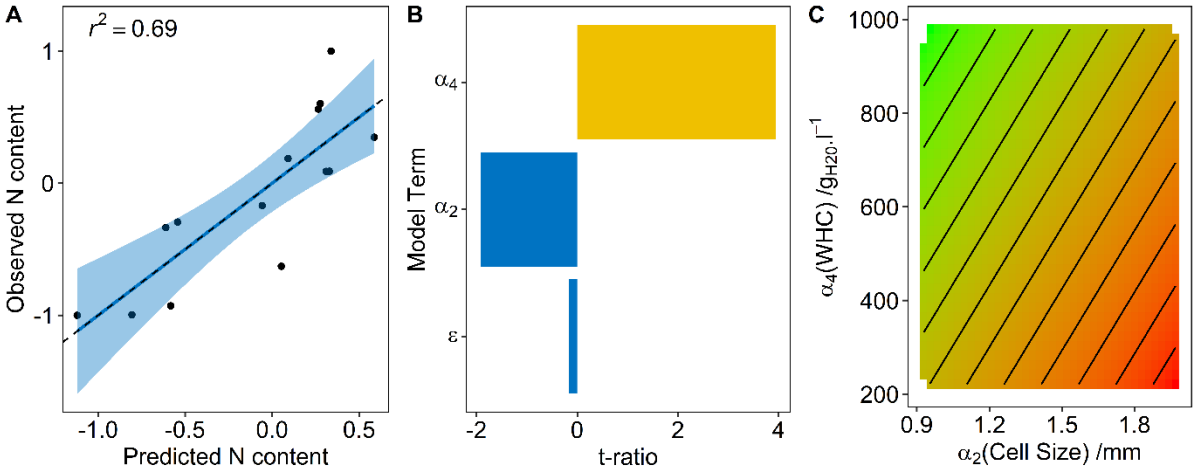

Figure 5.14: (A) Predicted and observed N content with the blue line indicating the fit and confidence interval and the dashed line indicating the y = x line, (B) t-ratio for N content model terms and (C) contour plot showing the influence of the cell size and WHC on the N content with green indicating high N values and red indicating low N values. α_2 is the cell size and α_4 is the WHC.

The N model includes only the main effect terms for the two factors, the fPUF cell size and WHC. This WHC is the most significant of the terms, in agreement with the linear bivariate models and Pearson's correlation coefficient. The WHC has a positive term indicating that an increase in WHC increases the amount of P in the plant shoots. The cell size is negatively correlated, indicating that an increase in cell size causes a reduction in nitrogen uptake.

5.3.7. **Shoot Phosphorus Content (P)**

The model for plant shoot phosphorus content is shown in *Equation 5.6* and Table 5.5 shows the ANOVA table for the response. Figure 5.15 (A) shows the observed shoot P content and the predicted P content, (B) shows the t-ratio test for the model terms and (C) shows the contour plot for WHC and cell size of fPUF and their influence on plant P shoot content, with green indicating high P content and red indicating low P content.

$$z_5 = - 0.617\alpha_2 + 0.00186\alpha_4 - 0.381 \qquad 5.6$$

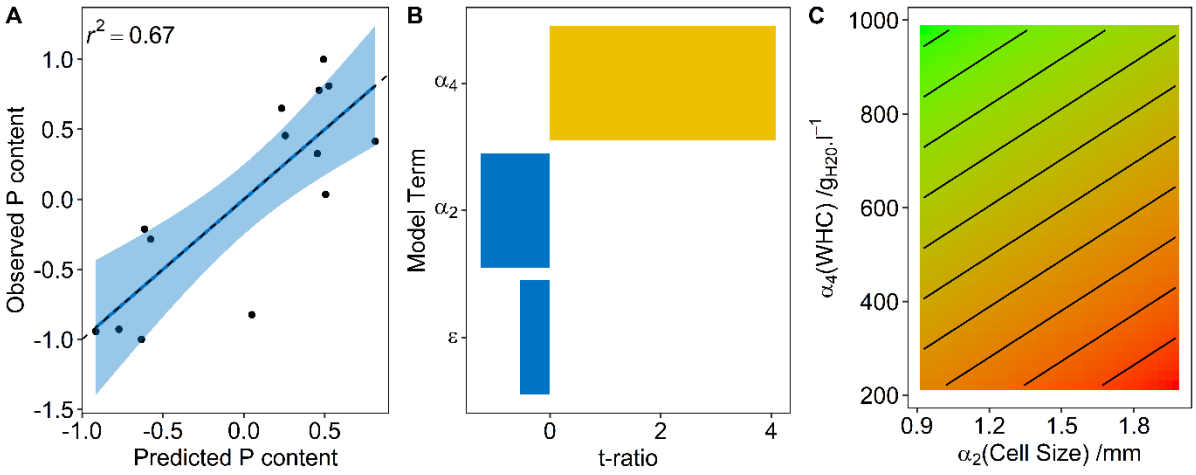

Figure 5.15: (A) Predicted and observed P content with the blue line indicating the fit and confidence interval and the dashed line indicating the y = x line, (B) t-ratio for P content model terms and (C) contour plot showing the influence of the cell size and WHC on the P content with green indicating high P values and red indicating low P values. α_2 is the cell size and α_4 is the WHC.

The P model is similar to the N model, with the same terms in the model and the same signs, with only the β coefficients varying between the two models. This is not unexpected, as the scatter plot matrix and Pearson's correlation coefficient revealed that the N content and P content were significantly correlated. The WHC is again the most significant term influencing P content of the shoot.

Both the simple linear regression models and the nutrient models showed that the WHC was the most significant factor influencing the nutrient amounts in the shoots. Even though all foam samples were under the same fertigation regime, the large difference in WHC between the foam samples likely meant that plants were receiving different amounts of water and therefore nutrients. This would explain the high correlation between the WHC and the N and P amounts in the shoot.

The r^2 value for the N (0.69) and P (0.67) models is significantly lower than that of the plant growth responses (AUC and m_d), and the fact that the slope and intercept of the y = x is the same as the observed:predicted line indicates that the errors in prediction are due to unexplained variance[155]. This unexplained variance is likely due to biological variance between plant samples.

5.4. Optimum fPUF formulation

The development of these plant growth response models, influenced by the physical properties of a fPUF can be used to develop a formulation for optimum growth of spring onions (*Allium sepa)* under the chosen watering regime. An example of the use of plant response models for development of an optimised fPUF formulation follows.

Plant shoot dry mass (m_d) is the selected response maximised, in this example, as an analogue for maximising yield. If other responses were favoured for optimisation, for example in the case where high nutritional content was required, the appropriate model could be selected. The model, *Equation 5.4* has one maximum, as seen in the prediction profiler from JMP, Figure 5.13. Table 5.7 shows the physical properties of the fPUF that maximise plant yield.

Table 5.7: Properties that predict spring onion dry shoot mass and the values of these properties optimising for maximum yield.

Property	Value	Scaled Value
WHC	966 $g_{H2O}.l^{-1}_{fPUF}$	0.951
Cell Size	0.966 mm	-0.560
Airflow	44.6 CFM	-0.185

The physical property models developed in Chapter 4 and Chapter 5.1.2.1 are then used to determine the optimised formulation. The models for cell size, WHC and airflow are shown below as *Equations 4.9*, *Equation 4.10* and *Equation 5.2.*

$$y_6 = -202x_3 - 159x_4 + 54400(x_3-0.00266)(x_4 - 0.00260) + 53634(x_3 - 0.00266)^2 + 0.612 \quad 4.9$$

$$y_7 = -4.84x_1 + 66.9x_2 + 125x_3 + 127x_4 - 5300(x_1 - 0.0251)(x_4 - 0.00273) - 11000(x_2 - 0.00439)^2 - 92200(x_3 - 0.00256)^2 - 51800(x_4 - 0.00273)^2 - 0.132 \quad 4.10$$

$$y_9 = -25.7x_1 - 229.0x_2 + 98.0x_3 - 155x_4 + 2.16 \quad 5.2$$

It is not possible to meet the exact values shown in Table 5.7, as the models have the same factors determining their response, therefore giving an explicit value to one will vary the other two physical properties. A formulation that minimises this difference between the predicted properties and required properties is therefore required. There is a further requirement that we have complete conversion of the reagents. Therefore any formulation would also need to meet the minimum requirements of 90 % isocyanate conversion occurring during the reaction time. *Equation 4.4* shows the model for isocyanate conversion.

$$y_1 = 6.43x_1 + 138x_2 - 1910(x_1 - 0.0248)(x_2 - 0.00409) - 20800(x_2-0.00409)^2 - 0.128 \quad 4.4$$

These equations are solved simultaneously using the Microsoft Excel Solver add in, using the GRG nonlinear solving method. Table 5.8 shows the suggested optimised fPUF formulation. The optimised foam has a loading of 0.0350 PPHP of the reactive polyol Specflex Activ 2306, which is insignificant and for ease of future formulations can be set to zero. Changing this to zero has little effect on the predicted conversion or resulting physical properties. Table 5.9 shows the isocyanate conversion and the predicted physical properties for the plant yield optimised fPUF foam, these properties are with the amount of Specflex Activ 2306 set to zero.

Table 5.8: fPUF formulation optimising for plant yield using the physical property models.

Component	Mass fraction	Loading (PPHP)
x_1 (Specflex Activ 2306)	0.000167	0.0350
x_2 (DMEA)	0.00982	2.07
x_3 (Tegostab BF2470)	0.00367	0.779
x_4 (Tegostab 8476)	0.00297	0.625

The predicted values in Table 5.9 are nearly identical to the plant optimum values from by *Equation 5.4*, indicating that the GRG nonlinear solver successfully solved the simultaneous equations, and in this case, the formulation optimised for all three physical properties whilst ensuring a predicted conversion of 99.1 %. This fPUF foam formulation was made and Table 5.9 shows the actual values of the physical properties of this fPUF formulation. The cell size and WHC were accurately predicted, however the model under predicted the airflow and therefore ratio of open cells within the foam. This higher airflow reduces the m_t from the maximum point; this reduction in m_t is from 8.82 g to 8.77 g (a 0.5 % reduction in m_t). This decrease in predicted m_t is minimal and therefore this formulation is accepted as the optimum formulation for the growth of spring onions (*Allium sepa)* under the chosen watering regime.

Table 5.9: Predicted isocyanate conversion and physical properties for the plant yield optimised fPUF foam as well as the optimum foams actual values.

Property	Predicted	Actual Value	Plant Optimum
Conversion	99.1 %	95.4 %	>90 %
WHC	966 $g_{H2O}.l^{-1}_{fPUF}$	960 $g_{H2O}.l^{-1}_{fPUF}$	966 $g_{H2O}.l^{-1}_{fPUF}$
Cell Size	0.966 mm	0.979 mm	0.966 mm
Airflow	44.3 CFM	53.0 CFM	44.6 CFM

5.5. Summary and Conclusions

fPUF physical property models developed in Chapter 4 were used to formulate a new set of fPUF with varying physical properties for optimising properties for plant growth. The models performed as expected with observed and predicted values having r^2 values similar to the k-fold cross validation r^2 of the models. The density model was

the worst performing of the models, having a r^2 value of 0.3. The models were able to generate a set of foams with a wide range of selected physical properties (density, cell size, WHC and WDPT).

Novel 3d printed open-source airflow equipment was developed as a proxy for determining the ratio of open to closed cells within the fPUF. This equipment characterised the plant growth foams and a model was developed using the same techniques as in Chapter 4. A model with no curvature or interaction terms was found to best fit the data with a $r^2 = 0.93$ (k-fold $r^2 = 0.88$). The airflow property was included in the physical properties used to develop plant response models.

A drip irrigation hydroponic setup was designed for the growth of Spring onion (*Allium sepa)* of the variety White Lisbon and plant growth parameters (plant survivability, height and greenness) were measured during an eight week growth trial. Yield (dry shoot mass) was determined at the end of the experiment as well as nitrogen and phosphorus content of the shoot material. Recovery of roots was not possible due to the nature of the fPUF growing media.

Two formulations recorded plant deaths that were significantly different from the no death curve. Formulation 5 had drastically different properties to the rest of the foams with a large cell size, unexpected for stable foams. The second formulation recording a high number of deaths (formulation 6) had no obvious difference in properties, however the foam appeared to have different hydrodynamic properties, with water not absorbing throughout the foam, resulting in areas of dry foam. A test on the capillary action of the foams would help understand whether this is the case.

All models indicated that foams with high water holding and small cell size were beneficial to plant growth under these conditions. The cell size was the most significant factor affecting plant growth whilst the WHC was the most significant factor affecting N and P uptake. The high influence of the WHC on plant growth and N and P uptake indicated that although foam pots were all on the same nutrient solution supply, formulations with lower WHC were not able to hold all of the supplied nutrient solution. This led to different amounts of nutrient solution available to plants in different foam formulations. The model for plant yield (m_d) indicated that the ratio of open cells is also

an important factor, with a curvature term indicating that there is a ratio of open to closed cells, beyond that yield is reduced. This is likely due to a change in hydrodynamics with a fPUF containing a high number of open cells not retaining water for long enough for the plant to obtain the optimum amount of water and nutrients.

The dry shoot mass (m_d) model was then used as an example for selecting an optimised foam formulation. This model predicted the ideal WHC, cell size and airflow for a foam. Physical property models predicted the chemical formulation required to generate a fPUF foam with physical properties as near to the optimum as possible. This foam was characterised and the physical properties were sufficiently similar to the optimum for it to be selected as the optimum foam for growing spring onions in a drip hydroponic setup.

It is important to note that the models developed are only valid under the nutrient schedule and experimental condition tested, and that different crop varieties may require different physical properties to optimise growth. However, the methods used for developing these optimised formulations can be implemented for any crop and nutrient schedule.

Chapter 6:
Summary, Conclusions
and
Suggestions for Future Work

6.1. Summary and Conclusions

The expanding use of controlled environment agriculture (CEA) and urbanisation of food production means there will be an estimated 42 million $m^3.yr^{-1}$ gap in the market for novel growing media. This market gap is compounded by pressure to move towards more environmentally friendly growing media in CEA agriculture and has led to the development and use of novel growing media such as polyurethane foams. The aim of this work was to design a fPUF for the use as a synthetic growing media in controlled environment agriculture, using hydroponic technology. Although polyurethane foams have been used for horticultural applications, there has been little work published on the methodology required for designing and optimising a foam for this application. The diverse nature of fPUF allows for complete control over the physical and chemical properties of the resulting foam, however the cross-disciplinary nature of this work meant that several new techniques were required to design and characterise fPUF for this application.

In order to deliver the research a number of new measurement and analysis methods were developed. New fPUF formulations were generated to make the substrate more amenable to being a synthetic soil, and the materials development was undertaken in via a design of experiments process given the large number of input and output variables. Model predictions were validated throughout and led to a clear understanding of the interrelationships between the formulation and foam properties. A series of foams were used test the growth of a model crop. This growth trial was enabled by the experimental and statistical methods developed specifically for this thesis and led to the production of a foam optimised for spring onion productivity.

6.1.1. **Development and Adaption of Characterisation Techniques**

Research into PUF reaction kinetics by the adiabatic temperature rise technique was used as a basis for developing the FoamPi, a low cost open source equipment able to monitor the fPUF reaction, logging temperature change, height change as well as sample mass throughout the reaction. Temperature change was used to determine

isocyanate conversion, and mass loss was used to normalise height data. Complete reagent conversion is important for horticultural applications as any leached reagents are in direct contact with crops and present a potential food safety hazard. The use of the FoamPi proved useful in ensuring complete isocyanate conversion. Further methods for characterising physical and chemical properties were adapted from literature, specifically for characterising density, cell size, water holding capacity, water drop penetration time and airflow. Properties identified as likely to affect plant growth and plant health. A low cost open source 3d printed airflow meter was also built to determine airflow through foams as an analogue for ratio of open to closed fPUF cells.

Two methods were identified for characterising plant growth. Height over time was used and an exponential growth curve was fitted to determine the area under curve (AUC). Dry shoot mass was also used as a method for quantifying plant growth. Root mass was also of interest however due to the nature of the fPUF, roots were not recoverable. Nitrogen and phosphorus content of the shoots was also determined using standard spectrophotometric methods. A novel automated method for determining plant chlorophyll levels of spring onion (*Allium cepa*) using a digital camera was developed following the methodology described by Liang *et al*[111] for a*rabidopsis*. RGB colour data extracted from the colour corrected and threshold image was fitted to the total chlorophyll ($r^2 = 0.75$).

6.1.2. **Formulation Development**

The application of using a fPUF as a growing media put specific constraints on the appropriate formulation required, with emphasis being on reducing the leaching of any dangerous components whilst providing the optimum media properties. A standard fPUF formulation was screened and reduction of the stannous octoate catalyst led to an incomplete conversion of isocyanate. A different catalyst package was therefore required. A reactive tertiary amine, DMEA, and an autocatalytic polyol, Specflex Activ 2306 were identified and both these catalysts were appropriate for our formulation. The standard formulation led to foams with hydrophobic qualities, not appropriate for a horticultural application. Two approaches were taken to increase the hydrophilicity of the fPUFs. The addition of a functional filler, sodium bentonite to increase the WHC of the foams and the use of hydrophilic polyols, with higher ethylene oxide content.

The addition of sodium bentonite affected all the foam properties, increasing density, WHC and CEC whilst decreasing the mechanical properties and WDPT. These foams were used to grow tomatoes during their vegetative growth cycle and bentonite at a loading of 10 PPHP increased the plant growth, both in terms of the AUC of the plant height and the dry shoot mass (m_d).

Polyethylene glycol (PEG) of varying molecular mass was added to the formulation and models were developed for WHC and WDPT to determine the polyol compositions that would lead to hydrophilic foams. PEG with higher MW and at higher loadings led to more hydrophilic foams, with higher WHC and lower WDPT. This was attributed to the increase in EO content of the foam as well as the higher molecular mass PEG requiring less isocyanate and therefore ensuring a higher mass percentage of the hydrophilic soft segment in the PU matrix. Voranol 1447 was identified as a high EO content polyol with properties likely to result in a hydrophilic fPUF through communication with Dow Polyurethanes. A polyol composition of 75:25 Voranol 1447 to Voranol 3322 had an EO content of 58.2 %, greater than the predicted 30 % requirement for a hydrophilic foam.

6.1.3. **fPUF Physical Property Models**

Due to the large number of experimental factors and expected complex interactions between components in a polyurethane formulation an experimental design approach was used to optimise the fPUF for plant growth. The surfactant and catalyst package were selected as design factors. A complex 15 term general model was selected for modelling the responses of the foam. Kinetic responses (isocyanate conversion, time until maximum temperature, final foam height and time until maximum height) and physical foam property responses (density, cell size ,WHC and WDPT) were selected as response variables. 32 formulations were trialled and models were fitted, reduced and optimised using k-fold cross validation and elastic net regression.

The two catalysts, DMEA a reactive blowing catalyst and Specflex Activ 2306 a catalytic polyol, accounted for the majority of the variance in the kinetic responses, with the DMEA loading being the most significant factor for the isocyanate conversion

and the time until maximum height. The surfactant loadings were important factors in influencing the final foam height, with stable foams requiring a minimum loading of surfactants. The physical property models showed the complexity of fPUF formulations with all four factors influencing the properties. Cell size was determined solely by the surfactant loadings with cell size, decreasing with increase in surfactant until a saturation point was reached after which further surfactant addition had little effect. The density model was the least robust with a large amount of unexplained variance, likely introduced due to mixing effects during the PU reaction. The selected catalysts and surfactants succeeded in generating a set of foams with physical properties that varied significantly. Foams with densities ranging between 30 – 42 $kg.m^{-3}$, cell sizes ranging between 0.85 – 1.36 mm, WHC ranging between 415 – 979 $g_{water}.l_{foam}^{-1}$ and WDPT of 0.12 – 152 s were generated. These large ranges in physical properties allow significantly different foams to be tested in plant growth trials to determine which foam physical properties affect plant growth.

6.1.4. **Optimisation of fPUF Properties for Plant Growth**

These physical property models were used to generate a new set of foams with a range of physical properties for a growth trial experimental trial. Airflow through the foam was determined and a model was developed for predicting airflow based on the fPUF formulation. Spring onions (A*llium cepa*) were selected as the model crop and a drip fed hydroponic system was designed. WHC and cell size were the most important factors in determining plant growth with high WHC and small cell size leading to improved growth and nutrient uptake.

The physical properties required to maximise growth and yield of spring onions (A*llium cepa*), in a drip irrigation hydroponic system, were determined using the developed plant response models. Physical property models dictated the formulation of the foam that closely delivered this set of optimised properties. This foam with optimised properties, dictated by the physical property and plant growth models was generated and the physical properties were measured for validation of the models. The water holding capacity was 960 $g_{water}.l_{foam}^{-1}$ and the predicted optimum WHC was 966 $g_{water}.l_{foam}^{-1}$. The cell size was 0.98 mm and the predicted optimum was 0.97 mm. The airflow was the property that varied the most from the predicted value. The foam

had an airflow value of 53 CFM, whilst the predicted optimum was 44 CFM. This difference in airflow was translated to a difference in open cells of roughly 4 %. As differences between this generated foams physical properties and the predicted optimised foam were slight, the formulation was selected as the optimised formulation.

6.2. Suggestions for Future Work

6.2.1. **Improvements to Work Presented**

Adaptation to some of the techniques used for synthesising and characterising fPUFs could improve the accuracy and robustness of the kinetic and physical property models. Additional testing methods may also improve the amount of variance explained by plant growth models. These are discussed in more detail in the following subsections.

6.2.1.1. *fPUF reactions*

The use of DMEA, which leads to foams with short reaction times makes consistent mixing difficult. These mixing effects are suspected of leading to low r^2 values for the density model. A replacement catalyst, which increases the time between mixing and expansion of the foam (cream time), but leads to fPUFs with similar resulting physical property may be a more appropriate catalyst. A set of screening experiments with different catalysts and the use of the FoamPi would help identify an appropriate catalyst. An alternative approach would be to use dual syringe system with a static mixing head for the reactions, or even commercial-scale high-pressure moulded foam machines. This type of system would allow for reduction in the error introduced during the mixing of reagents by having identical mixing times and conditions for all formulations.

6.2.1.2. *Dynamic Water Behaviour*

The physical properties explain a large portion of the variance in our samples, however there were a few experiments that indicated that the hydrodynamic behaviour of the

fPUF may also help explain the results. The death of several plants in formulation 6, which anecdotally had very different hydrodynamic behaviour as well as the curvature seen through the effects of porosity (the airflow term) when describing the shoot dry mass may be more fully explained with a complementary test. A test for the capillary action of the fPUF would be beneficial, and although not as fast as the water holding capacity test used in this study, a full soil-water retention curve may help explain some of these results[156]. Due to the time required to produce a full water retention curve it may be optimum to only do this test on a subset of foams that are identified as having abnormal hydraulic properties.

6.2.2. **Complementary Work**

6.2.2.1. *Optimum fPUF Formulation Growth Trial*

A growth trial to validate the foam optimised using Chapter 4 and Chapter 5 was meant to be done as part of this thesis. A comparative study between the optimised fPUF media and rockwool would have led to an understanding of the similarities and differences between the novel substrate developed here and the industry standard media for hydroponics. This may have also given insight into the possible need for different watering and fustigation schemes for the two substrates. This was planned for the date of March 2020 – July 2020. However due to the Covid-19 pandemic, this experiment was shut down shortly after starting. The completion of such a growth trial will validate the work in optimising a foam formulation and is suggested as the most important complementary work to this thesis.

6.2.2.2. *Scaling up Foam Production for Greenhouse Scale Trial*

This study was focused on laboratory scale synthesis of fPUF and pot scale plant growth trials, however if a fPUF growing media is to be scaled to commercial levels several adaptations will be required.

All of the polyols, isocyanate, catalysts and surfactants are commercial samples and available at a scale required for commercial production of fPUF. The sodium bentonite used in this study was purchased from a chemical supplier, and this would not be

feasible at production scale. Three different bentonite clays were identified from the supplier BYK Additives & Instruments. Cloisite 116 is a micorgranulated clay based on a natural mineral with optimised cation composition, Cloisite Na+ is a natural sodium form of bentonite and Cloisite Ca++ is a natural calcium form of bentonite.

The CEC of these clays was determined using the method described in Chapter 2.3.1. The clays were incorporated into the optimum fPUF formulation developed in Chapter 5 and the resulting foams physical properties were characterised. Figure 6.1 (A) shows the CEC of the three new clays as well as the lab grade sodium bentonite, and (B) – (F) show the physical properties of the resulting foam. The CEC of both the Cloisite Na+ and Cloisite 116 were the same or greater than the lab grade sodium bentonite. These two samples also resulted in foams with physical properties most similar to the optimum foam. Cloisite 116, at a loading of 30 PPHP, appears to be the best substitute for the lab grade sodium bentonite.

Several commercial foam manufacturers were approached with the formulation, however the short reaction times would not allow for sufficient mixing in a batch mixing machine, and longer cream times are required for this type of commercial manufacture. Screening tests for an appropriate replacement catalyst as suggested in Chapter 6.2.1.1 would lead to foam formulation with more appropriate reaction times for commercial foam equipment.

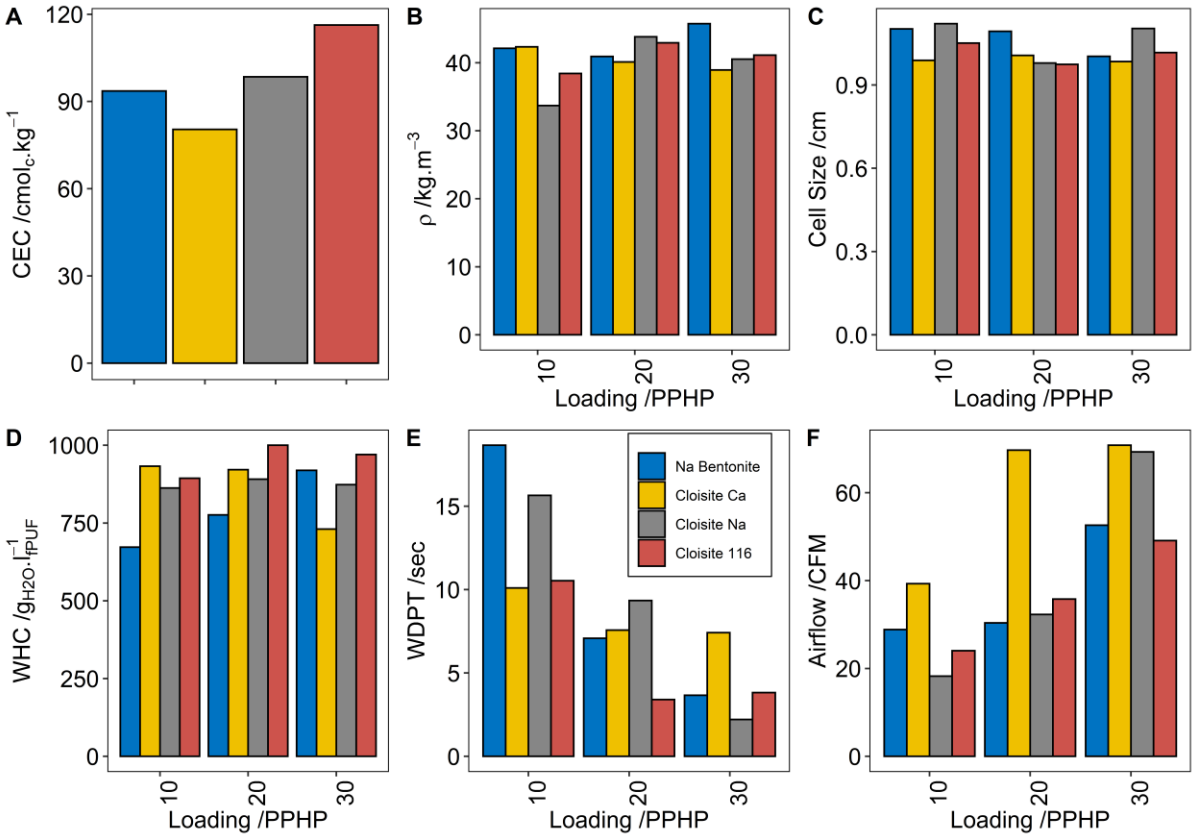

Figure 6.1: (A) Cation exchange capacity for three additive replacements for lab grade sodium bentonite and physical properties of fPUF containing replacement additives at several loadings. (B) Density, (C) Cell size, (D) WHC (E) WDPT and (F) airflow.

6.2.2.3. *Inoculation of Beneficial Bacteria*

The physical and chemical properties of fPUF were explored and optimised in this study. However, the biological properties of the foam were not. All growth trial experiments were under biologically sterile conditions. Chapter 1.2.1.3 highlighted some of the problems with biological sterile hydroponic systems. The lack of biological life means any pathogens which enter the system have no competition, and plants do not benefit from any disease resistance induced by beneficial bacteria or fungi.

Research exploring the types of bacteria in recirculating tilapia aquaponics (a combination aquaculture and hydroponics system) found that 41 % of the isolated bacteria was plant growth promoting (PGPB)[157]. A recirculating tilapia aquaponics system was in use at the University of Sheffield for a separate research project and an experiment was setup to determine the effect the bacteria in this system would

have on plant growth of spring onions in a drip fed hydroponics system using the optimised fPUF, developed herein, as the growing media.

The foam was inoculated by placing the pots with media into the aquaponics grow bed for two weeks prior to the start of the hydroponic growth trial. Figure 6.2 (A) shows the amount of DNA in the fPUF after the inoculation period, indicating that the foam was successfully inoculated with the aquaponic bacteria. Unfortunately due to mechanical action within the aquaponics grow beds, the foam was repeatedly crushed by the mass of the aquaponics growing media, changing the foams physical properties and reducing the volume of foam in the pots. The growth trials were still completed under the same conditions as Chapter 5.2 however, the change in physical properties meant it was not feasible to determine which factors were influencing plant growth. Figure 6.3 (A) shows the plant height over time and (B) the dry shoot mass at harvest. The heights over time as well as the final mass of the inoculated foams were less than the foams that were not inoculated. It was also of interest to determine whether the inoculated bacteria was priming the plant for disease resistance. Callose synthesis within the plant has been used as an effective tool for determining the plant resistance to pathogens and callose synthesis is elicited by submerging shoot material in a chitosan solution[158]. Callose is quantified by determining the percentage of fluorescent pixels in samples stained with methyl blue under UV light[159]. Figure 6.2 (B) shows the percentage of fluorescent pixels for the spring onion samples at different chitosan loadings. At low chitosan spiking there is no difference between inoculated and non-inoculated samples, however at a chitosan loading of 0.05 % the inoculated samples show a higher number of fluorescent pixels.

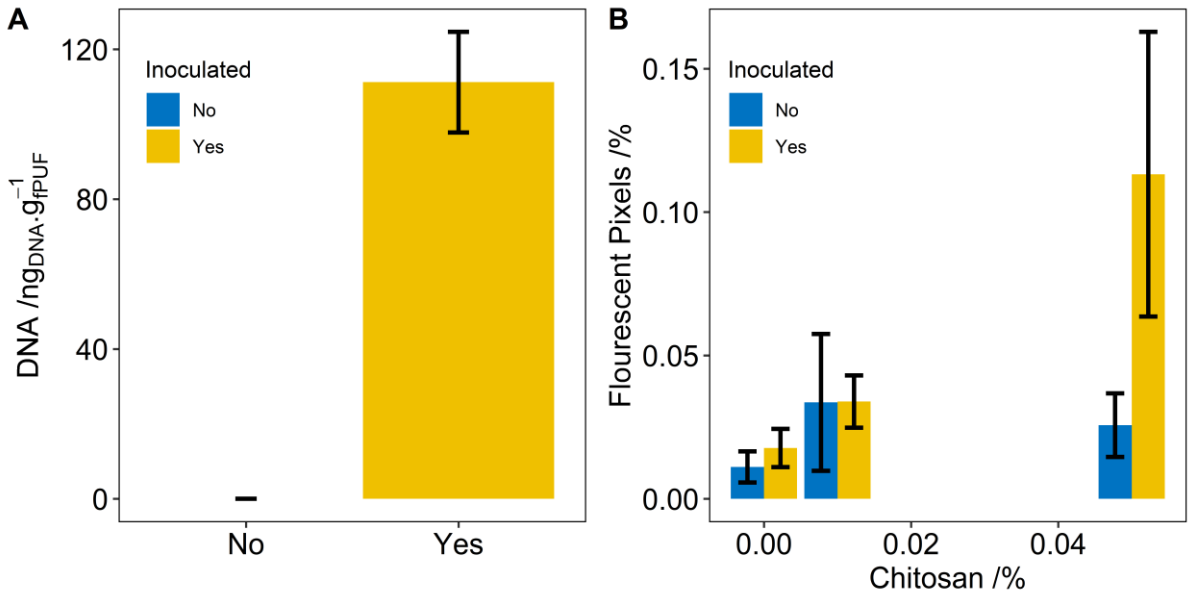

Figure 6.2: (A) The amount of DNA extracted from the fPUF inoculated with aquaponic bacteria and the non-inoculated fPUF and (B) The percentage of fluorescent pixels of spring inion leaves identified as an indication of callose production in response to chitosan.

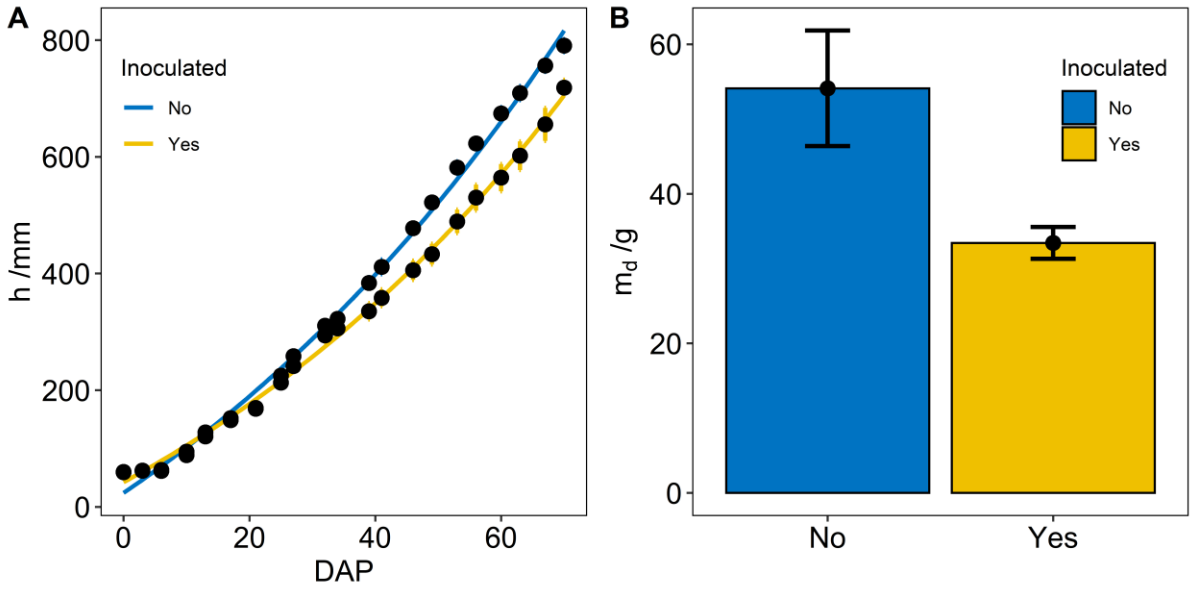

Figure 6.3: (A) Plant height curves with exponential fit for the fPUF inoculated with aquaponic bacteria and the non-inoculated fPUF and (B) plant shoot dry mass for the same two foams.

This experiment revealed that the bacteria in a tilapia-based recirculating aquaponics system may help induce resistance to pathogens in a hydroponic system, however

further experimental work with careful controls, due to the experimental difficulties encountered in this experiment, is needed to confirm this.

Further experiments using more carefully selected bacteria cultures and inoculation methods could add significantly to the scientific understanding of bacteria in hydroponic systems, and may have commercial benefits as well, as increasing pathogen and disease resistance in hydroponic systems can reduce crop losses as well as reduce food safety concerns within these types of systems.

6.2.2.4. *Incorporation of Renewable Materials*

The selection of PU as a possible alternative to the currently available growing media was because PU can have an environmental benefit when compared to more conventional media such as rockwool. This environmental advantage could be further enhanced by incorporating raw materials from renewable resources into the formulation.

Helling and Russell[160] used life cycle analysis (LCA), a tool that measures the environmental impact of a service or a product, to quantify the environmental sustainability of castor and soy-based polyols and found that the bio-based products used 33 – 64 % of fossil fuel resources compared to petroleum-based polyols. They also found that the bio-based polyols generated much lower greenhouse gas emissions. Another study into the use of soy-based polyols found that the bio-based polyol was better for the environment in all impact categories, except Ozone Depletion Potential[161]. LCA also shows that the main downfall of the bio-based polyols is the amount of water used in their production, mainly due to the agricultural component of their synthesis.

A screening experiment was completed during experiments reducing stannous octoate to determine the feasibility of swapping fossil fuel based polyols for bio based ones. Figure 6.4 shows images of three different bio-based polyols, Agrol 2 and 4 (soy-based polyols) as well as castor oil, at several loadings in a fPUF formulation. The significant change to physical properties meant that no further work was done on these formulations at that time.

The understanding of fPUF physical properties and their effect on plant growth gained in this study make it feasible to revaluate these bio-based polyols in future trials.

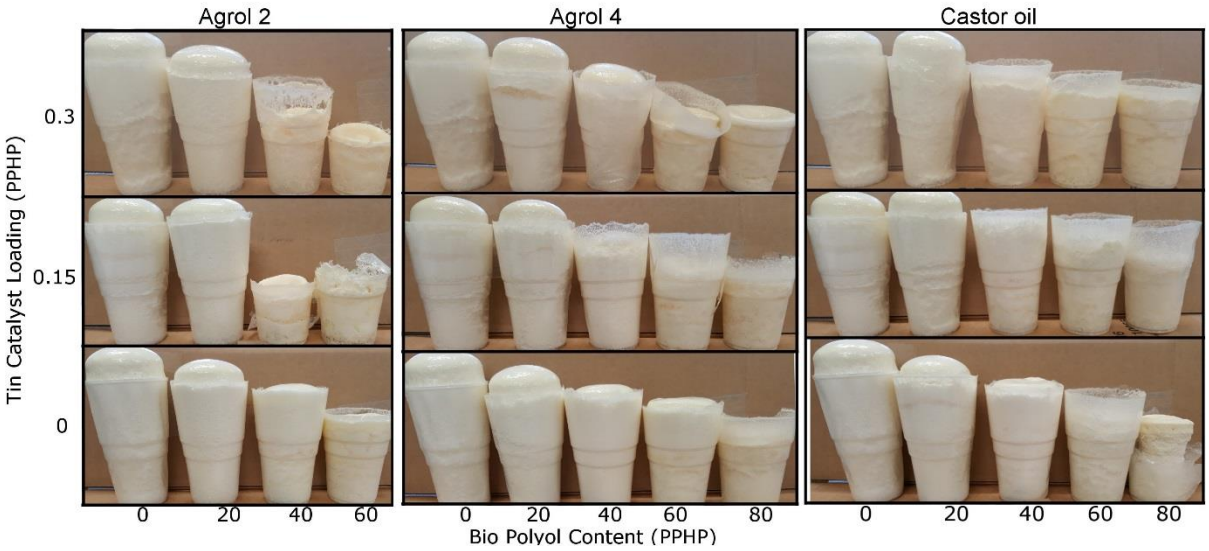

Figure 6.4: Photos of foams with carrying amount of three different bio-based polyols at three different loadings of stannous octoate catalyst.

6.2.2.5. *Recycling at End of Life*

Reuse of current growing media is possible, although it is rarely done due to the expense and difficulty of steam cleaning media between uses to ensure sterility[162]. It can be assumed that although fPUF media is easily reusable, in practice these same limitations in reuse would be encountered. fPUF benefits from being easily mechanically recycled by shredding the polymer and rebinding with an isocyanate capped polyol to make a rebonded foam. Exploring the use of these techniques to generate a second use foam, with application in horticulture or green roof and green wall applications would be an interesting topic of research with possible commercial applications.

6.2.2.6. *Crop and Technique Optimised foam*

The fPUF optimised in this study, was optimised under one watering regime and for one crop. The experimental procedure described in Chapter 5 can be used for any crop and any hydroponic technique, allowing for the development of crop specific and technique optimised foams.

References

1 IPCC, eds. P. R. Shukla, J. Skea, E. Calvo Buendia, V. Masson-Delmotte, H. O. Pörtner, D. C. Roberts, P. Zhai, R. Slade, S. Connors, R. van Diemen, M. Ferrat, E. Haughey, S. Luz, S. Neogi, M. Pathak, J. Petzold, J. Portugal Pereira, P. Vyas, H. E, K. Kissick, M. Belkacemi and J. Malley, 2019, pp. 437–550.

2 UN, Our growing population, https://www.un.org/en/sections/issues-depth/population/, (accessed 10 February 2021).

3 P. M. Kopittke, N. W. Menzies, P. Wang, B. A. McKenna and E. Lombi, *Environ. Int.*, 2019, **132**, 105078.

4 R. R. Shamshiri, F. Kalantari, K. C. Ting, K. R. Thorp, I. A. Hameed, C. Weltzien, D. Ahmad and Z. Shad, *Int. J. Agric. Biol. Eng.*, 2018, **11**, 1–22.

5 D. G. Dalrymple, *Controlled Environment Agriculture: A Global Review of Greenhouse Food Production*, 1973.

6 D. D. Despommier, *The vertical farm : feeding the world in the 21st century*, Thomas Dunn Books, New York, 1st edn., 2010.

7 C. Gómez, C. J. Currey, R. W. Dickson, H. J. Kim, R. Hernández, N. C. Sabeh, R. E. Raudales, R. G. Brumfield, A. Laury-Shaw, A. K. Wilke, R. G. Lopez and S. E. Burnett, *HortScience*, 2019, **54**, 1448–1458.

8 G. L. Barbosa, F. D. Almeida Gadelha, N. Kublik, A. Proctor, L. Reichelm, E. Weissinger, G. M. Wohlleb and R. U. Halden, *Int. J. Environ. Res. Public Health*, 2015, **12**, 6879–6891.

9 M. H. Jensen, *HortScience*, 1997, **32**, 1018–1021.

10 G. De Rijck and E. Schrevens, *Sci. Hortic. (Amsterdam).*, 1998, **72**, 277–285.

11 A. C. Bunt, *Modern Potting Composts*, Springer Netherlands, Dordrecht, 1988.

12 W. T. Bussell and S. Mckennie, *New Zeal. J. Crop Hortic. Sci.*, 2004, **32**, 29–37.

13 N. Engler and M. Krarti, .

14 B. F. Daley and R. K. Dumroese, *Tropical Nursery Manual*, USDA, 1st edn., 2014.

15 F. Lemaire, *Acta Hort*, 1995, 396, 273–284.

16 T. E. Bilderback, S. L. Warren, J. S. Owen and J. P. Albano, *Horttechnology*, 2005, **15**, 747–751.

17 H. Resh, *Hydroponic Food Production*, CRC Press, 2012.

18 M. R. Ashman and G. Puri, *Essential soil science: a clear and concise introduction to soil science*, Blackwell Science, Oxford, 2002.

19 A. Silber, in *Soilless Culture*, eds. M. Raviv and J. H. Lieth, Elsevier, Amsterdam, 2008, pp. 209–244.

20 J. S. Owen, North Carolina State University, 2006.

21 T. Witzke, L. Torres-Dorante, F. Bullerjahn and H. Pollmann, in *Minerals as Advanced Materials II*, ed. S. V. Krivovichev, Springer Berlin Heidelberg, Berlin, 1st edn., 2012, pp. 131–145.

22 J. Vallance, F. Déniel, G. Le Floch, L. Guérin-Dubrana, D. Blancard and P. Rey, *Sustain. Agric.*, 2009, **2**, 711–726.

23 M. E. Stanghellini and S. L. Rasmussen, *Plant Dis.*, 1994, **78**, 1129–1138.

24 G. Buyanovsky, J. Gale and N. Degani, *Plant Soil*, 1981, **60**, 131–136.

25 J. Postma, in *Recent Developments in Management of Plant Diseases*, eds. U. Gisi, I. Chet and M. L. Gullino, Springer Netherlands, Dordrecht, 2009, pp. 133–146.

26 D. M. Weller, J. M. Raaijmakers, B. B. McSpadden Gardener and L. S. Thomashow, *Annu. Rev. Phytopathol.*, 2002, **40**, 309–348.

27 S. Lee and J. Lee, *Sci. Hortic. (Amsterdam).*, 2015, **195**, 206–215.

28 V. Gravel, H. Antoun and R. J. Tweddell, *Soil Biol. Biochem.*, 2007, **39**, 1968–1977.

29 F. K, A. Gül and Y. Tüzel, 2009, 475–480.

30 M. C. Brundrett, *New Phytol.*, 2002, **154**, 275–304.

31 K. Shuhada, M. W. Puteri Edaroyati and O. Radziah, *J. Trop. Plant Physiol.*, 2013, **5**, 42–60.

32 Ö. Ikiz, K. Abak, H. Y. Daşgan and I. Ortaş, *Acta Hortic.*, 2009, **807**, 533–540.

33 H. Y. Dasgan, S. Kusvuran and I. Ortas, *African J. Biotechnol.*, 2008, **7**, 3606–3613.

34 M. M. Maboko, I. Bertling and C. P. Du Plooy, *Acta Agric. Scand. Sect. B–Soil Plant Sci.*, 2013, **63**, 261–270.

35 G. E. Barrett, P. D. Alexander, J. S. Robinson and N. C. Bragg, *Sci. Hortic. (Amsterdam).*, 2016, **212**, 220–234.

36 P. Wallace, S. Homes, R. Alexander, J. England and R. Gaze, *Review of growing media use and dominant materials (peat and alternatives) for growing media in other countries (European and international).*, 2010.

37 J. Benton, *Complete Guide for Growing Plants Hydroponically*, CRC Press, 2014.
38 D. Dannehl, J. Suhl, C. Ulrichs and U. Schmidt, *J. Appl. Bot. Food Qual.*, 2015, **88**, 68–77.
39 3979198, 1976, 7.
40 F. Benoit and N. Ceustermans, *Soil. Cult.*, 1988, **2**, 2–9.
41 F. Benoit and N. Ceustermans, *Acta Hortic.*, 1995, 17–30.
42 M. Hardgrave, *Acta Hortic.*, 1995, 201–208.
43 J. J. Huber, Y. Zheng and M. A. Dixon, *Acta Hortic.*, 2005, **697**, 139–145.
44 Y. Zheng, J. Huber, P. Zhang and M. Dixon, *Acta Hortic.*, 2009, **819**, 435–442.
45 EUROPUR, *Flexible Polyurethane (PU) Foam*, 2015.
46 W. Yang, Q. Dong, S. Liu, H. Xie, L. Liu and J. Li, *Procedia Environ. Sci.*, 2012, **16**, 167–175.
47 M. Szycher, *Szycher's handbook of polyurethanes*, CRC Press, Boca Raton, FL, 2nd edn., 2013.
48 M. F. Sonnenschein, *Polyurethanes: Science, Technology, Markets and Trends*, John Wiley & Sons, Inc, 1st edn., 2014.
49 Plastics Europe, *Plastics – the Facts 2014/2015 An analysis of European plastics production, demand and waste data 1*, 2013.
50 *Polyurethane (Flexible Foam, Rigid Foam, Coatings, Adhesives, Sealants, and Elastomers) Market for Furniture, Building & Construction, Electronics, Automotive, Footwear, Packaging, Other Applications - Global Industry Perspective, Comprehensive Analysis,* , 2016.
51 F. Zafar, Ed., *Polyurethane*, InTech, 2012.
52 K. Ashida, *Polyurethane and Related Foams*, CRC Press, 2006.
53 R. B. Seymour and G. B. Kauffman, *J. Chem. Educ.*, 1992, **69**, 909.
54 J. Bicerano, R. D. Daussin, M. J. A. Elwell, H. R. van der Wal, P. Berthevas, M. Brown, F. Casati, W. Farrissey, J. Fosnaugh, R. de Genova, R. Herrington, J. Hicks, K. Hinze, K. Hock, D. Hunter, L. Jeng, D. Laycock, W. Lidy, H. Mispreuve, R. Moore, L. Nafziger, M. Norton, D. Parrish, R. Priester, K. Skaggs, L. Stahler, F. Sweet, R. Thomas, R. Turner, G. Wiltz, T. Woods, C. P. Christenson and A. K. Schrock, in *Polymeric Foams*, eds. S. T. Lee and N. S. Ramesh, CRC Press, 1st edn., 2004.
55 L. D. Artavia and C. W. Macosko, in *Low density cellular plastics*, Springer

Netherlands, Dordrecht, 1994, pp. 22–55.

56 J. K. Fink, in *Reactive Polymers Fundamentals and Applications*, Elsevier, 2005, pp. 69–138.

57 J. G. Hanna and S. Siggia, *J. Polym. Sci.*, 1962, **56**, 297–304.

58 Z. T. Ossefort and P. B. Testroet, *Rubber Chem. Technol.*, 1966, **39**, 1308–1327.

59 S. Li and M. Vert, in *Degradable Polymers*, Springer Netherlands, Dordrecht, 2002, pp. 71–131.

60 Y. Li, X. Luo and S. Hu, *Bio-based Polyols and Polyurethanes*, Springer International Publishing, Cham, 2015.

61 Z. Petrovic, *Polym. Rev.*, 2008, **48**, 109–155.

62 A. Prociak, in *Biofoams: Science and Applications of Bio-Based Cellular and Porous Materials*, eds. S. Iannace and C. B. Park, CRC Press, 1st edn., 2015, pp. 267–286.

63 D. A. Babb, in *Synthetic Biodegardable Polymers*, eds. B. Rieger, A. Kunkel, G. W. Coates, R. Reichardt, E. Dinjus and T. A. Zevaco, Springer Berlin Heidelberg, Berlin, 1st edn., 2012, pp. 315–360.

64 L. Bengtström, M. Salden and A. A. Stec, *Fire Sci. Rev.*, 2016, **5**, 4.

65 D. Rosu, L. Rosu and C. N. Cascaval, *Polym. Degrad. Stab.*, 2009, **94**, 591–596.

66 US Pat, US6924321B2, 2005.

67 S. Huo, C. Jin, G. Liu, J. Chen, G. Wu and Z. Kong, *Polym. Degrad. Stab.*, 2019, **159**, 62–69.

68 European Patent Office, EP 2 725 046 B1, 2016, 1, 1–35.

69 C. Defonseka, *Practical Guide to Flexible Polyurethane Foams*, Smithers Rapra Technology, Shropshire, 1st edn., 2013.

70 S. A. Snow and R. E. Stevens, in *Silicone Surfactants*, ed. R. M. Hill, CRC Press, 1st edn., 1999, pp. 137–154.

71 A. Aneja, Virginia Polytechnic Institute and State University, 2002.

72 R. Herrington, K. Hock and R. Autenrieth, *Flexible polyurethane foams*, Dow Chemical, Midland, 1997.

73 C. Scheutz, M. H. Jensen and P. Kjeldsen, *Environ. Sci. Technol.*, 2001, **35**, 209–216.

74 A. L. Silva and J. C. Bordado, *Catal. Rev.*, 2004, **46**, 31–51.

75 Y. Zhao, University of Missouri-Columbia, 2015.

76 R. Van Maris, Y. Tamano, H. Yoshimura and K. M. Gay, *J. Cell. Plast.*, 2005, **41**, 305–322.

77 M. J. Elwell, A. J. Ryan, H. J. M. Grünbauer and H. C. Van Lieshout, *Macromolecules*, 1996, **29**, 2960–2968.

78 W. Li, A. J. Ryan and I. K. Meier, *Macromolecules*, 2002, **35**, 5034–5042.

79 K. Yasunaga, R. A. Neff, X. D. Zhang and C. W. Macosko, *J. Cell. Plast.*, 1996, **32**, 427–448.

80 J. L. Edmondson, H. Cunningham, D. O. Densley Tingley, M. C. Dobson, D. R. Grafius, J. R. Leake, N. McHugh, J. Nickles, G. K. Phoenix, A. J. Ryan, V. Stovin, N. Taylor Buck, P. H. Warren and D. D. Cameron, *Nat. Food*, 2020, **1**, 155–159.

81 Chris Blok, in *Acta Horticulturae*, 2020.

82 S. D. Lipshitz and C. W. Macosko, *J. Appl. Polym. Sci.*, 1977, **21**, 2029–2039.

83 A. J. Rojas, J. Borrajo and R. J. J. Williams, *Polym. Eng. Sci.*, 1981, **21**, 1122–1127.

84 S. A. Baser and D. V. Khakhar, *Polym. Eng. Sci.*, 1994, **34**, 632–641.

85 Y. Zhao, M. J. Gordon, A. Tekeei, F. H. Hsieh and G. J. Suppes, *J. Appl. Polym. Sci.*, 2013, **130**, 1131–1138.

86 S. Tan, T. Abraham, D. Ference and C. W. MacOsko, *Polymer (Guildf).*, 2011, **52**, 2840–2846.

87 C. W. Macosko, *RIM, Fundamentals of reaction injection molding*, Hanser, Vienna, Munich, New York, 1st edn., 1989.

88 A. Van Thuyne and B. Zeegers, *J. Cell. Plast.*, 1978, **14**, 150–160.

89 L. Shen, Y. Zhao, A. Tekeei, F.-H. Hsieh and G. J. Suppes, *Polym. Eng. Sci.*, 2014, **54**, 1503–1511.

90 G. Van Rossum and F. L. Drake, *Python 3 Reference Manual*, CreateSpace, Scotts Valley, CA, 2009.

91 R. Herrington and K. Hock, *Flexible Polyurethane Foams*, The Dow Chem Co, 2nd edn., 1998.

92 ASTM Standard D3574-11, *Standard Test Methods for Flexible Cellular Materials—Slab, Bonded, and Molded Urethane Foams*, West Conshohocken, 2012.

93 ASTM Standard D3576-15, *Standard Test Method for Cell Size of Rigid Cellular Plastics*, West Conshohocken, 2014.

94 S. H. Doerr, *Earth Surf. Process. Landforms*, 1998, **23**, 663–668.
95 R Core Team, 2013.
96 L. Ammann, F. Bergaya and G. Lagaly, *Clay Miner.*, 2005, **40**, 441–453.
97 J. P. Reganold and J. B. Harsh, *J. Agron. Educ.*, 1985, **14**, 84–90.
98 E. L. Kaplan and P. Meier, *J. ASA*, 1958, **73**, 457–481.
99 D. Pavlovic, B. Nikolic, S. Djurovic, H. Waisi, A. Andjelkovic and D. Marisavljevic, *Pestic. i fitomedicina*, 2014, **29**, 21–34.
100 H. K. Lichtenthaler, *J. Plant Physiol.*, 1996, **148**, 4–14.
101 F. Florina, V. Giancarla, P. Cerasela and P. Sofia, *J. Hortic. For. Biotechnol.*, 2013, **17**, 363–367.
102 A. Nankishore and A. D. Farrell, *J. Plant Physiol.*, 2016, **202**, 75–82.
103 H. M. Kalaji, P. Dąbrowski, M. D. Cetner, I. A. Samborska, I. Łukasik, M. Brestic, M. Zivcak, H. Tomasz, J. Mojski, H. Kociel and B. M. Panchal, *J. Plant Nutr.*, 2017, **40**, 1024–1034.
104 C. M. Giletto and H. E. Echeverría, *Am. J. Potato Res.*, 2013, **90**, 313–323.
105 L. Prost and M. H. Jeuffroy, *Agron. Sustain. Dev.*, 2007, **27**, 321–330.
106 J. Uddling, J. Gelang-Alfredsson, K. Piikki and H. Pleijel, *Photosynth. Res.*, 2007, **91**, 37–46.
107 Z. Yuan, Q. Cao, K. Zhang, S. T. Ata-Ul-Karim, Y. Tan, Y. Zhu, W. Cao and X. Liu, *Front. Plant Sci.*, 2016, **7**, 1–10.
108 S. P. Yadav, Y. Ibaraki and S. D. Gupta, *Plant Cell. Tissue Organ Cult.*, 2010, **100**, 183–188.
109 F. J. Adamsen, P. J. Pinter, E. M. Barnes, R. L. LaMorte, G. W. Wall, S. W. Leavitt and B. A. Kimball, *Crop Sci.*, 1999, **39**, 719–724.
110 M. Riccardi, G. Mele, C. Pulvento, A. Lavini, R. D'Andria and S. E. Jacobsen, *Photosynth. Res.*, 2014, **120**, 263–272.
111 Y. Liang, D. Urano, K. L. Liao, T. L. Hedrick, Y. Gao and A. M. Jones, *Plant Methods*, 2017, **13**, 1–10.
112 T. Mansencal and M. Leonhardt, Colour - Checker Detection, https://github.com/colour-science/colour-checker-detection, (accessed 8 September 2020).
113 P. Menesatti, C. Angelini, F. Pallottino, F. Antonucci, J. Aguzzi and C. Costa, *Sensors (Switzerland)*, 2012, **12**, 7063–7079.
114 D. M. Woebbecke, G. E. Meyer, K. Von Bargen and D. A. Mortensen, *Trans.*

Am. Soc. Agric. Eng., 1995, **38**, 259–269.

115 G. E. Meyer and J. C. Neto, *Comput. Electron. Agric.*, 2008, **63**, 282–293.

116 H. K. Lichtenthaler and C. Buschmann, *Curr. Protoc. Food Anal. Chem.*, 2001, **1**, F4.2.1-F4.2.6.

117 A. R. Wellburn, *J. Plant Physiol.*, 1994, **144**, 307–313.

118 J. Murphy and J. P. Riley, *Anal. Chim. Acta*, 1962, **27**, 31–36.

119 J. R. Leake, University of Sheffield, 1988.

120 M. K. John, *Soil Sci.*, 1970, **109**, 214–220.

121 S. H. Yuen and A. G. Pollard, *J. Sci. Food Agric.*, 1954, **5**, 364–369.

122 M. D. Krom, *Analyst*, 1980, **105**, 305.

123 ASTM Standard D4274-16, *Standard Test Method for Testing Polyurethane Raw Materials: Determination of Hydroxyl Numbers of Polyols*, West Conshohocken, 2016.

124 ASTM Standard D4875-11, *Standard Test Methods of Polyurethane Raw Materials : Determination of the Polymerized Ethylene Oxide Content of Polyether Polyols 1*, West Conshohocken, 2015.

125 A. L. Silva and J. C. Bordado, *Catal. Rev.*, 2004, **46**, 31–51.

126 M. a Ashraf, M. J. Maah and I. Yusoff, *Int. J. Environ. Sci. Technol.*, 2011, **8**, 401–416.

127 M. C. Tanzi, P. Verderio, M. G. Lampugnani, M. Resnati, E. Dejana and E. Sturani, *J. Mater. Sci. Mater. Med.*, 1994, **5**, 393–396.

128 R. Wheeler, S. Schwartzkopf, T. W. Tibbitts and R. W. Langhans, *HortScience*, 1985, **20**, 448–449.

129 M. S. Islam, S. Khan, T. Ito, T. Maruo and Y. Shinohara, *J. Hortic. Sci. Biotechnol.*, 2002, **77**, 143–148.

130 J. Y. Kang, H. H. Lee and K. H. Kim, *Acta Hortic.*, 2004, **644**, 231–235.

131 M. Abad, F. Fornes, C. Carrión, V. Noguera, P. Noguera, Á. Maquieira and R. Puchades, *HortScience*, 2005, **40**, 2138–2144.

132 The Perlite Institute, 2018, 1–2.

133 F. Kakoei and H. Salehi, *J. Cent. Eur. Agric.*, 2013, **14**, 140–148.

134 S. D. J. Inglethorpe, D. J. Morgan, D. E. Highley and A. . Bloodworth, *J. Math.*, 1993, 124.

135 H. H. Murray, in *Developments in Clay Science*, 2nd edn., 2006, pp. 111–130.

136 G. Harikrishnan, T. U. Patro and D. V. Khakhar, *Ind. Eng. Chem. Res.*, 2006,

45, 7126–7134.

137 H. Rastin, Z. Ahmadi, M. R. Saeb and K. Formela, *J. Vinyl Addit. Technol.*, 2016, **22**, 415–422.

138 D. Schwarz, A. J. Thompson and H.-P. Kläring, *Front. Plant Sci.*, 2014, **5**, 625.

139 E. J. Hewitt, *Sand and water culture methods used in the study of plant nutrition*, Commonwealth Agricultural Bureaux, 1966.

140 C. R. E. Mansur, C. M. F. Oliveira, G. González and E. F. Lucas, *J. Appl. Polym. Sci.*, 1997, **66**, 1767–1772.

141 O. J. Kwon, S. T. Oh, S. Do Lee, N. R. Lee, C. H. Shin and J. S. Park, *Fibers Polym.*, 2007, **8**, 347–355.

142 W. F. Smith, *Experimental Design for Formulation*, Society for Industrial and Applied Mathematics, Alexandria, Philadelphia, 1st edn., 2005.

143 D. C. Montgomery, *Design and Analysis of Experiments*, John Wiley & Sons, Inc, 9th edn., 2017.

144 R. H. Fechter, C. Sandrock, I. Kühnert and F. J. W. J. Labuschagné, *J. Vinyl Addit. Technol.*, 2019, **25**, E44–E58.

145 H. Lim, S. H. Kim and B. K. Kim, *Express Polym. Lett.*, 2008, **2**, 194–200.

146 NIST/SEMATECH, e-Handbook of Statistical Methods, http://www.itl.nist.gov/div898/handbook/, (accessed 14 August 2020).

147 T. P. Ryan, *Modern Experimental Design*, John Wiley & Sons, Inc., Hoboken, NJ, USA, 2007, vol. 49.

148 F. E. Harrell, *Regression Modeling Strategies*, Springer International Publishing, Cham, 2015, vol. 45.

149 J. Fox and S. Weisberg, in *JMP, A Business Unit of SAS*, 2011, pp. 246–279.

150 A. E. Hoerl and R. W. Kennard, *Technometrics*, 2000, **42**, 80–86.

151 R. Tibshirani, *J. R. Stat. Soc. Ser. B*, 1996, **58**, 267–288.

152 H. Zou and T. Hastie, *J. R. Stat. Soc. Ser. B (Statistical Methodol.*, 2005, **67**, 301–320.

153 T.-T. Wong and N.-Y. Yang, *IEEE Trans. Knowl. Data Eng.*, 2017, **29**, 2417–2427.

154 D. B. Carr, R. J. Littlefield, W. L. Nicholson and J. S. Littlefield, *J. Am. Stat. Assoc.*, 1987, **82**, 424–436.

155 G. Piñeiro, S. Perelman, J. P. Guerschman and J. M. Paruelo, *Ecol. Modell.*, 2008, **216**, 316–322.

156 P. A. Londra, *HortScience*, 2010, **45**, 1106–1112.

157 F. A. Sanchez, V. R. Vivian-Rogers and H. Urakawa, *Aquac. Res.*, 2019, 1–12.

158 F. Franco and M. Iriti, *Caryologia*, 2007, **60**, 121–124.

159 L. Scalschi, E. Llorens, G. Camanes, V. Pastor, E. Fernandez-Crespo, V. Flors, P. Garcia-Agustin and B. Vicedo, *BIO-PROTOCOL*, , DOI:10.21769/BioProtoc.1610.

160 R. K. Helling and D. A. Russell, *Green Chem.*, 2009, **11**, 380–389.

161 Omni Tech International, *Life Cycle Impact of Soybean Production and Soy Industrial Products*, 2010.

162 W. T. Bussell and S. Mckennie, *New Zeal. J. Crop Hortic. Sci.*, 2004, **32**, 29–37.

Appendix

Desert Garden Project

During my time completing this thesis I was privileged to be part of a team of researchers from the University of Sheffield that worked on the Desert Garden project. The Desert Garden project was a project started by Professor Tony Ryan to reuse polyurethane mattress foam as a growing media in low-tech hydroponic systems in Za'atari refugee camp in Jordan in 2017.

Za'atari refugee camp is home to 80 000 Syrian refugees who left their home due to civil war. The camp is 5.2 km^2 and is located 10 km east of Mafraq in Jordan. It is the worlds largest refugee camp for Syrian refugees and was setup in 2012. Since then the camp has turned into a more permanent settlement, with a piped water distribution network as well as a piped sewerage network completed in 2019 by UNICEF. Each family member in the camp is supplied with 35 l of potable water a day. To put this in perspective the average person in the United Kingdom uses 142 l water per day. Many of the residents were farmers in Syria, either as a primary occupation or as subsistence farmers supplementing their diet with homegrown produce. However the heavy water restrictions, poor soil quality as well as legislation that does not allow for permanent structures (including plants in the ground) means that residents are unable to continue their agricultural practices.

Over the course of my PhD I visited Jordan and Za'atari Refugee camp on four occasions for a week at a time. My role was in supporting the refugees in their development of low tech nutrient film technique (NFT) hydroponic setups, as well as simple deep water systems, which both relied on the reused fPUF as the substrate, giving the plants physical support. The NFT systems has a nutrient tank buried underground to keep the nutrient solution cool, this is then pumped to a secondary buffer tank on top of the system. Water then trickles through reused drain pipes in contact with plant roots inside the pipes and circulates back to the nutrient tank. The buffer tank ensures watering of the plants can continue even if there is a power outage.

(A) (B)

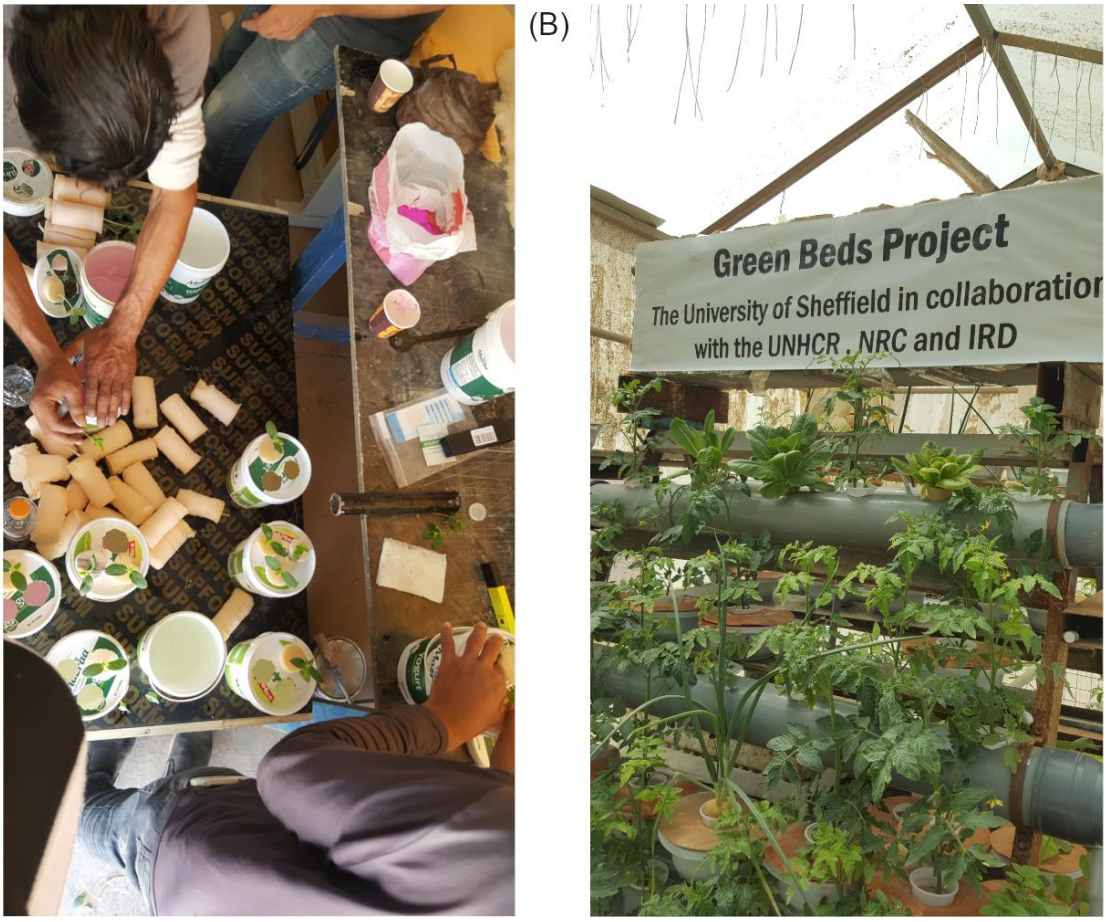

Figure I: (A) Yogurt tubs being reused as deep water hydroponic systems and (B) a NFT hydroponic system installed inside Za'atari camp.

My other role was in training refugees in techniques required in hydroponics, including making up nutrient solutions, using pH meters and adjusting the pH of the nutrient solution.

A large variety of crops have now been grown in these systems including herbs like basil, coriander and mint, leafy greens such as spinach and lettuce as well as soft fruit such as cucumbers, chillis, tomatoes and okra.

Since my final trip in April 2019, the Desert Garden Project has taken off with enormous success. An appeal on the JustGiving website has raised over £230 000, enough to keep the project funded for three years. Training inside the camp undertaken by volunteers as well as trained refugees have trained over 1000 people in the use of hydroponic techniques and this project is now being implemented in Azraq camp as well as in the urban refugee regions in Jordan.

Although the small scale hydroponic systems may not have a major calorific benefit to the refugees growing produce at home, the mental health benefits of having a green plant growing on your windowsill, countertop or porch are momentous especially to the backdrop of a brown desert.

I believe my most significant contributions resulting from this thesis were not achieved in a lab or greenhouse in Sheffield, but rather in a desert in Jordan.

An article based on this work has been published in Nature reviews earth and environment:

Al Meselmani, M.A., Wright, H.C., Cameron, D.D. and Ryan A.J. How scientists and refugees brought green to the Desert Garden. *Nat Rev Earth Environ* **1,** 439 (2020).